Advanced Methodologies for Measuring and Manipulating Zebrafish Behavior and Physiology

Dissertation

der Mathematisch-Naturwissenschaftlichen Fakultät

der Eberhard Karls Universität Tübingen

zur Erlangung des Grades eines

Doktors der Naturwissenschaften

(Dr. rer. nat.)

vorgelegt von

David-Samuel Burkhardt

aus Filderstadt

Tübingen

2026

Gedruckt mit Genehmigung der Mathematisch-Naturwissenschaftlichen Fakultät der Eberhard Karls Universität Tübingen.

Tag der mündlichen Qualifikation:	14.07.2026
Dekan:	Prof. Dr. Thilo Stehle
1. Berichterstatter/-in:	Prof. Dr. Aristides Arrenberg
2. Berichterstatter/-in:	Prof. Dr. Thomas Euler

"The progress of science is the progress of instruments."

Raymond Thayer Birge

1940 Nobel Prize in Physics Ceremony Speech

Erklärung / Declaration

Ich erkläre, dass ich die zur Promotion eingereichte Arbeit mit dem Titel

Advanced Methodologies for Measuring and Manipulating Zebrafish Behavior and Physiology

selbständig verfasst, nur die angegebenen Quellen und Hilfsmittel benutzt und wörtlich oder inhaltlich übernommene Stellen als solche gekennzeichnet habe. Ich versichere an Eides statt, dass diese Angaben wahr sind und dass ich nichts verschwiegen habe. Mir ist bekannt, dass die falsche Abgabe einer Versicherung an Eides statt mit Freiheitsstrafe bis zu drei Jahren oder mit Geldstrafe bestraft wird.

I hereby declare that I have produced the work entitled

Advanced Methodologies for Measuring and Manipulating Zebrafish Behavior and Physiology

submitted for the award of a doctorate, on my own (without external help), have used only the sources and aids indicated and have marked passages included from other works, whether verbatim or in content, as such. I swear upon oath that these statements are true and that I have not concealed anything. I am aware that making a false declaration under oath is punishable by a term of imprisonment of up to three years or by a fine.

Tübingen, den ....

Datum / Date Unterschrift / Signature

Acknowledgements

With this page, I would like to thank all the people who accompanied and supported me during the process of this PhD thesis.

First and foremost, I would like to thank Prof. Dr. Arrenberg for the opportunity to do my PhD in his amazing lab. I felt welcome from the very first day, even though I turned out to be the only engineer in the lab - surrounded by a whole bunch of biologists and neuroscientists who kept asking biology questions! The atmosphere you created in the lab was just right for me: an excellent mixture of high-class scientific research, great equipment and advanced methodologies, but also funny lab activities, relaxed colleagues, and (oh my god!) several coffee breaks per day with great and sometimes wonderfully random, non-scientific discussions. I also want to thank you for giving me the freedom and space to further develop myself - by allowing me to create an entirely new lecture series together with Christian, supervise multiple bachelor's and master's students, and represent you and your lab during meetings and lectures. I truly appreciate that.

My thanks also go to my second supervisor, Prof. Dr. Thomas Euler, who was always there when I had a question and who pointed me toward some very important directions during our advisory board meetings. Thanks a lot for that!

Next, I want to thank the "core team" of the Arrenberg Lab: Tim, Giulia, Carina, Yunyi, Claire, Christian, Florian and Nash. Together with Lidia and Michael, you were the best company I could have wished for. You make the Arrenberg Lab what it is. I will remember the (sometimes challenging) but always fruitful interdisciplinary work with you in the lab. Having five different perspectives on one problem can be confusing, but it always enables you to solve it comprehensively. I found that to be a core strength of the Arrenberg Lab.

I also want to thank my fiancé, Mona, who supported me throughout my entire PhD. You always had an open ear for me when I brought home some fish-talk - even though sometimes I had no idea what I was actually talking about. Thank you for always being there. Finally, I want to thank my parents, Irina and Oliver, for raising me to be who I am today and for laying the foundation that allowed me to study and now complete my PhD.

Thank you all!

List of Content

Abbreviations

dpf	days post fertilization
AC	alternating current
DC	direct current
PDC	pulsed direct current
vOKR	vertical optokinetic response
hOKR	horizontal optokinetic response
vVOR	vertical vestibulo-ocular reflex
OMR	optomotor response
rr	repetition rate
DS	direction selective
RCCB	residual-current circuit breaker
IR	infrared
PSD	power spectral density
ROI	region of interest
CW	clockwise
CCW	counter-clockwise
STA	stimulus-triggered average
MAE	motion after effect
SD	spreading depolarization

List of Figures

1. Summary

1.1 Abstract

Larval zebrafish offer unique advantages for systems neuroscience, including optical transparency, genetic accessibility, and conserved vertebrate brain organization. However, essential behavioral tools and methods remain underdeveloped, while sophisticated imaging techniques such as two-photon calcium imaging drives research forward. This study aims to provide advanced but easy to implement methodological solutions for behavioral research addressing two critical methodological gaps: the lack of humane, standardized euthanasia protocols, and the limited ability to measure eye movements in all degrees of freedom during visuomotor behavior.

First, an open-source and modular platform for electrical stunning of zebrafish larvae was developed. Using controlled alternating current (AC) electrical fields, immediate loss of behavioral responsiveness and complete suppression of stimulus-evoked neuronal activity were achieved, as confirmed by two-photon calcium imaging in the optic tectum. Unlike mostly used methods such as MS-222 overdose, electrical stunning avoids aversive reactions or inconsistent efficacy, offering a rapid, reproducible, and ethically refined euthanasia protocol.

Second, both single- and dual-camera eye-tracking systems were established to simultaneously record vertical and horizontal eye movements in agarose-embedded larvae during both visual and vestibular stimulation. This enabled characterization of the vertical optokinetic response (vOKR) and the vertical vestibulo-ocular reflex (vVOR) - previously unexplored in larval zebrafish. vOKR exhibited distinct dynamic properties compared to its horizontal counterpart, including delayed plateauing of eye positions, no resetting saccades and frequency-dependent phase shifts. Moreover, during vOKR, spontaneous saccades occurred in both vertical and horizontal planes, suggesting a more complex oculomotor repertoire than previously recognized.

These methodological advances aim to expand the zebrafish neuroscience toolkit, enabling more comprehensive analysis of sensorimotor processing and behavior as well es refinement with regard to animal welfare. The tools are designed for compatibility with high-resolution imaging and scalable behavioral experiments and are accessible to laboratories without specialized engineering infrastructure.

1.2 Zusammenfassung

Larvale Zebrafische sind aufgrund ihrer optischen Transparenz, genetischen Zugänglichkeit und der konservierten Organisation des Wirbeltiergehirns ein zentrales Modellsystem der systemischen Neurowissenschaften. Während hochauflösende bildgebende Verfahren wie 2-Photonen-Calcium-Imaging neuronale Aktivität im gesamten Gehirn zugänglich machen, bleibt die quantitative Analyse des Verhaltens methodisch limitiert. In dieser Arbeit werden experimentelle Ansätze vorgestellt, die zwei zentrale methodische Herausforderungen adressieren: das Fehlen standardisierter und tierschonender Euthanasieverfahren für frühe Entwicklungsstadien sowie die eingeschränkte Erfassung mehrdimensionaler Augenbewegungen in visuomotorischen Experimenten.

Hierfür wurde eine offene und modulare Plattform zur elektrischen Durchströmung larvaler Zebrafische entwickelt. Das kontrollierte Anlegen von Wechselstromfeldern führte zu einem unmittelbaren Verlust der Verhaltensaktivität sowie zu einer vollständigen Unterdrückung stimulusinduzierter neuronaler Aktivität. Im Gegensatz zur Überdosierung des gebräuchlichen Anästhetikums MS-222 traten dabei keine aversiven Verhaltensreaktionen auf. Elektrische Durchströmung stellt somit ein schnelles, reproduzierbares und nicht-aversives Verfahren zur Euthanasie dar.

Zusätzlich wurden ein- und zweikamerabasierte Eye-Tracking-Setups entwickelt, die eine simultane Messung horizontaler und vertikaler Augenbewegungen bei in Agarose immobilisierten Larven während visueller und vestibulärer Stimulation ermöglichen. Diese Ansätze erlaubten erstmals eine systematische Charakterisierung der vertikalen optokinetischen Antwort (vOKR) sowie des vertikalen vestibulo-okulären Reflexes (vVOR) im larvalen Zebrafisch. Dabei zeigte die vOKR deutliche Unterschiede zur horizontalen OKR, darunter ein verzögertes Erreichen einer stationären Augenposition, das Fehlen ausgeprägter Rückstellbewegungen sowie frequenzabhängige Phasenverschiebungen. Darüber hinaus wurden spontane Sakkaden sowohl in der vertikalen als auch in der horizontalen Ebene beobachtet, was auf ein bislang unterschätztes okulomotorisches Repertoire hinweist.

Die vorgestellten Methoden liefern neue experimentelle Werkzeuge zur präzisen und umfassenden Verhaltensanalyse larvaler Zebrafische und ermöglichen gleichzeitig Verbesserungen im Hinblick auf das Tierwohl in der wissenschaftlichen Forschung.

Die experimentellen Aufbauten sind so konzipiert, dass sie mit hochauflösender Bildgebung und skalierbaren Verhaltensexperimenten kompatibel sind, und stehen auch Laboren ohne spezielle technische Infrastruktur zur Verfügung.

2. Publications

2.1 List of Publications

Burkhardt, D.-S., Leyden, C., Thomas, C, Brysch, C, Dehmelt, F. A., Arrenberg, A. B. (2025). Behavioral and neurophysiological effects of electrical stunning on zebrafish larvae. *Lab Animal* 54, 50-58. DOI: https://doi.org/10.1038/s41684-024-01505-0

Burkhardt, D.-S.*, Möller, G.*, Deligand, L., Fichtner, C., Hladnik, T. C., Arrenberg, A. B. (2026). Vertical Optokinetic Eye Movements in the Larval Zebrafish. *J Exp Biol*. DOI: https://doi.org/10.1242/jeb.251770

2.2 Statement of Contributions

Publication 1: Behavioral and Neurophysiological Effects of Electrical Stunning on Zebrafish Larvae
A.B.A. (50%), D.-S.B. (40%) and F.A.D. (10%) did the conceptualization of the project
D.-S.B. (70%), C.L. (15%) and A.B.A. (15%) designed and constructed the experimental setups
D.-S.B. (80%) and C.L. (20%) conducted all experiments and recorded all data
D.-S.B. (100%) analyzed all data
A.B.A. (100%) provided all resources
D.-S.B. (70%), C.T. (20%) and A.B.A. (10%) made the figures
D.-S.B. (70%) and A.B.A. (20%) wrote the manuscript with the help of F.A.D. (5%) and C.B. (5%)
D.-S.B. (40%), A.B.A. (40%) and F.A.D. (20%) acquired funding

Publication 2: Vertical Optokinetic Eye Movements in the Larval Zebrafish
D.-S.B. (80%) and T.C.H. (20%) developed and constructed the setups
D.-S.B. (50%), G.M. (30%) and A.B.A. (20%) developed the methodologies
G.M. (70%), D.-S.B. (10%), L.D. (10%) and C.F. (10%) recorded all data
G.M. (60%) and D.-S.B. (40%) analyzed all data
D.-S.B. (70%), A.B.A. (20%) and G.M. (10%) wrote the manuscript
D.-S.B. (50%) and A.B.A (50%) supervised the project

3. Introduction

3.1 The Model Organism Zebrafish (*Danio Rerio*)

Model organisms are fundamental tools in biological and biomedical research, allowing scientists to explore complex physiological processes, developmental pathways, and disease mechanisms in experimentally accessible systems. The zebrafish, a 4 to 6 cm long tropical teleost native to the northern Indian subcontinent, has emerged as an important vertebrate model organism in biology and biomedical research within the last few decades (Bilotta and Saszik, 2001; Fetcho and Liu, 1998; Grunwald and Eisen, 2002; Rinkwitz et al., 2011; Tavares and Lopes, 2013). Especially at the larval stage, the zebrafish offers a unique combination of vertebrate complexity and optical transparency. With a brain consisting of only ~100,000 neurons, its optical transparency allows for almost whole-brain imaging of neuronal activity at single-cell resolution, using approaches like two-photon calcium imaging and light sheet microscopy (Ahrens et al., 2013; Feierstein et al., 2015; Renninger and Orger, 2013). Zebrafish larvae develop externally in optically transparent eggs and rapidly, with the major organs forming within the first 24-48 hours (Kimmel et al., 1995). At young age (4 – 6 days post-fertilization), they already display a diverse behavioral repertoire (Budick and O'Malley, 2000; Marques et al., 2018). These behaviors - such as the optokinetic response, optomotor response, and vestibulo-ocular reflex - are amenable to quantitative analysis and offer entry points for dissecting sensorimotor processing (Beck et al., 2004; Dehmelt et al., 2021; Huang, 2008; Kist and Portugues, 2019; Lim et al., 2024; Rinner et al., 2005). Another advantage is their high fecundity. A single breeding pair can produce hundreds of embryos per week, allowing for statistically robust experimental designs.

Today, zebrafish are used in various research fields, serving as models for different aspects of biology and disease. For example, in developmental biology, zebrafish are used to study vertebrate embryogenesis (Haddon and Lewis, 1996; Kimmel et al., 1995); in neurobiology, they are used for study and modeling brain function and disorders (Naumann et al., 2016; Portugues et al., 2014); and in toxicology and pharmacology, they are used for high-throughput drug screening and environmental hazard assessments (Deeti et al., 2014; Lopez-Luna et al., 2017). Additionally,

zebrafish models are increasingly applied in cancer biology, cardiovascular research, and regenerative medicine (Chico et al., 2008; Feitsma and Cuppen, 2008; Mione and Trede, 2010; Poon and Brand, 2013; Zhao et al., 2015), making them a valuable system for translational biomedical studies (Stewart et al., 2014), also because about 70% of the zebrafish' genes are orthologous to humans (Amores et al., 2011; Howe et al., 2013).

While the zebrafish provides a powerful and versatile model system, it is important to acknowledge that no single organism can fully address the vast range of biological questions. A comprehensive understanding of complex biological systems necessitates not only the selection of an appropriate model but also the application of suitable experimental tools and technologies specifically tailored to the research objectives.

3.2 A Young Field of Research – Need for Behavioral Measuring and Manipulation Methods

Originally, zebrafish were established as a model organism in developmental biology to study vertebrate embryogenesis (Kimmel et al., 1995), pattern formation, and organ development (Driever et al., 1996; Haffter et al., 1996) during early life stages. Their transparency and ex utero development enabled visual observation of various developmental processes (He et al., 2014), while their small size and rapid development facilitated high-throughput methods. Over the past 20 years, the role and importance of the zebrafish as a model organism have expanded and shifted. As new methods and techniques advanced the field of neurobiology - and population-level recording techniques such as large-scale electrophysiology and optical imaging shifted focus from single-neuron measurements to circuit- and brain-wide dynamics (Ahrens et al., 2013) - the zebrafish's unique characteristics enabled it to enter this field as well. However, this field is still relatively young, with many experimental tools and protocols in early stages of development compared to those for other model organisms. For example, stable, precise, and fast 3D eye-tracking has been available in monkeys since the last century using search coils - tiny wire coils embedded in soft contact lenses - that precisely measure the eye's position as the monkey moves its head within

a magnetic field (Bartl et al., 1996; Hess et al., 1992; Kenyon, 1985; Tweed et al., 1990). Due to the tiny eyes of larval zebrafish and the fact that they move underwater, search coils cannot be used to track eye movements, leaving video recording as the only viable option for tracking body and eye motion. In zebrafish larvae behavioral tracking of swimming and eye movements is frequently restricted to a single plane of observation. In many experimental setups, larvae are embedded in agarose or placed in shallow water, and movements are recorded from either above, front or the side (Bianco et al., 2011; Dehmelt et al., 2018; Easter Jr. and Nicola, 1997; Huang, 2008; Lin and Huang, 2023; Müller and van Leeuwen, 2004). This simplification might be useful for addressing distinct research questions like understanding the OKR in only a single plane, but for a more comprehensive understanding of behavior, methods that take multiple dimensions into account are needed.

On the other hand, as a young field, zebrafish neuroscience is characterized by rapid innovation and adaptation, especially with regard to different imaging methods. Sophisticated tools such as light-sheet microscopy, whole-brain calcium imaging, and optogenetics have been successfully applied to zebrafish larvae, enabling unprecedented access to brain-wide activity patterns at single-cell resolution (Ahrens et al., 2013; dal Maschio et al., 2017; Feierstein et al., 2015; Renninger and Orger, 2013). These advanced methods represent a major strength of the model and have accelerated our understanding of neural circuit function. However, they also tend to be complex, resource-intensive, and technically demanding. Paradoxically, while imaging technologies have evolved rapidly, some essential behavioral measurement techniques - such as eye tracking - remain underdeveloped or overly simplistic. This mismatch highlights a critical gap in the zebrafish neuroscience toolkit: the need for comprehensive, scalable and standardized behavioral research tools that are also simple, accessible, and compatible with existing experimental pipelines. Whereas in more established fields, such as mouse research, standardized behavioral apparatuses like the rotarod - a device for measuring motor coordination, balance, and motor learning (Favre-Guilmard et al., 2009; Korhonen et al., 2008; Marino et al., 2009) - or the Morris water maze - a circular water tank with a hidden platform used to study, e.g. learning, memory, and spatial navigation (Anisman and McIntyre, 2002; Arqué et al., 2008; CHO et al., 2006; Ruiz-Medina et al., 2008) - are widely distributed and even professionally manufactured (“Behavioral Research,” 2026), the zebrafish research community lacks such standardized behavioral measurement and manipulation tools.

Ideally, these tools should allow researchers to capture more complete behavioral repertoires while maintaining alignment with real-time brain activity measurements, like calcium imaging. Two examples of behavioral methods which are currently simplistic or even missing are the method of (1) measuring combined horizontal and vertical eye movements and (2) the method of electrical stunning to immobilize, anesthetize or even euthanize larval zebrafish.

(1) As previously mentioned, eye movement measurements in zebrafish often focus on only a single plane. This likely arises from the historical development of OKR assays, where the OKR in larval zebrafish was mainly used as a readout for investigating visual function (Brockerhoff et al., 1997; Neuhauss et al., 1999) and tracking horizontal eye movements in larvae is relatively easy. However, the OKR has now become more important for studying zebrafish ocular behavior itself (Matsuda and Kubo, 2021). Consequently, simply tracking purely horizontal eye movements is no longer sufficient. There are valid reasons for primarily studying horizontal eye movements, such as the OKR, in zebrafish: in their natural habitat, they mostly move in the horizontal plane, making horizontal compensation of retinal slip crucial for stable image processing. Nevertheless, zebrafish are also capable of vertical and torsional eye movements, as they possess the same six eye muscles as all other vertebrates (Land, 2015). Some studies have already partially described either vertical or torsional eye movements in zebrafish and goldfish, most often elicited by vestibular stimuli (Bianco et al., 2012; Migault et al., 2024; Sugioka et al., 2023; Tadokoro et al., 2025; Takabayashi et al., 2003). However, combined recordings of, for example, vertical and horizontal movements during OKR stimuli have not been published so far.

(2) Electrical stunning is a method used to anesthetize or euthanize fish through the controlled application of an electrical field. This approach might be more humane and reliable for euthanasia compared to currently used methods such as overdoses of the anesthetic MS-222 or hypothermia (Leyden et al., 2022; Readman et al., 2013; Rombough, 2007; Strykowski and Schech, 2015; Wallace et al., 2018). Although electrical stunning is already recognized as a legal euthanasia method by the EU (Directive 2010/63/EU), it is not currently implemented because reliable parameters are largely unknown, and adequate equipment is not readily available (Köhler et al., 2017; Lidster et al., 2017).

In this thesis, I address this specific gap by developing technical solutions for combined eye tracking of vertical and horizontal movements using a dual-camera setup, as well as 3D-printable setups for controlled application of electrical fields alongside two-photon calcium imaging to study electrical stunning. This leads to an initial characterization of the vertical vestibulo-ocular reflex (vVOR), the vertical optokinetic reflex (vOKR), and combined eye movements, along with the first assessment of electrical stunning as a humane euthanasia method.

3.3 Electrical Stunning: Towards a Humane Euthanasia Alternative

3.3.1 Pain and Nociception in Fish and the 3R

Why is it necessary to develop alternative anesthesia and euthanasia methods like electrical stunning, which might be more humane than others? The answer is twofold and linked to the ongoing discussion of whether and, if so, in what form fish perceive and suffer pain, as well as to the ethical principle of the 3Rs .

First, it is important to distinguish between nociception, which refers to the sensing of noxious stimuli with the potential to cause damage of various kinds (Tracey, 2017), and pain, which is an unpleasant, subjective sensory and emotional experience that can follow nociception and is always associated with actual or potential tissue damage (Raja et al., 2020). Nociceptors have been found in different mammalian species, vertebrates, and invertebrates, and their presence has also been confirmed in fishes (Sloman et al., 2019; Sneddon, 2018; Sneddon et al., 2014). Notably, their properties are very similar to those underlying pain in mammals (Ashley et al., 2007, 2006; Sneddon, 2003), leading to the assumption that fish might also be capable of experiencing pain. This has been further supported by studies showing changes in brain activity during noxious stimuli (Dunlop and Laming, 2005; Nordgreen et al., 2007; Reilly et al., 2008) and aversive changes in behavior and physiology during noxious treatment (Dunlop et al., 2006; Maximino, 2011; White et al., 2017). In line with that, anesthetics targeting mammalian nociceptors are also suitable for preventing aversive behavior in fish (Lopez-Luna et al., 2017; Nordgreen et al., 2009). However, there are

also good arguments for why, although capable of nociception, fish might not perceive and suffer pain. One argument is their less developed neural system, most prominently their lack of a neocortex (Rose, 2002). In humans, the neocortex is both necessary and sufficient for the feeling of pain (Key, 2016). Also, because pain is thought to be a subjective sensory and emotional experience and cannot be reduced to activity in sensory pathways (Raja et al., 2020), this raises the question of the degree to which fish are even conscious and aware of themselves (Chandroo et al., 2004; Key, 2015). To this day, the scientific community has not ultimately agreed on whether, and if so in what form, fish perceive or suffer pain, and there are commentaries for (Merker, 2016) and against (Key, 2016) pain perception in fish.

So, if it is not clear whether fish are capable of perceiving and suffering pain, is there a need for developing more humane euthanasia methods? One approach could be the following: as long as we are unsure whether fish perceive and suffer pain, we should always look for the least harmful method, accounting for the possibility that fish *might* feel pain. This goes hand in hand with the ethical principle of the 3Rs, first introduced by Russel and Burch (Russel, W. M. S. and Burch, R. L., 1959). Good scientific practice alone already requires well-designed and planned animal experiments which is further reinforced by an increasing awareness of the use of animals for scientific research in society (Clemence and Leaman, 2016). In Germany, the legal basis for this is the EU Directive 2010/63/EU, which is implemented in the German Animal Welfare Act (Tierschutzgesetz) and the German Laboratory Animal Welfare Ordinance (Tierschutz-Versuchstierverordnung). Within these laws, the 3Rs (Replace, Reduce and Refine) are applied. "Replace" refers to the replacement of animal experiments by alternative non-animal methods such as tissue cultures or computational approaches, or the usage of less sentient species, whenever possible. "Reduce" means the overall reduction of animal numbers to a necessary minimum by optimizing statistical analysis and methodological procedures. Last but not least, "Refine" refers to the refinement of existing methods and experimental procedures to keep potential stress and suffering of animals as low as possible. This is also where the investigation of electrical stunning as a “refined” euthanasia alternative comes into play, especially because the method is already foreseen by the relative EU Directive (Directive 2010/63/EU) and the currently used methods like the overdose of the anesthetic MS-222 (Tricain) are not yet ideal from an animal welfare point of view.

3.3.2 Electrical Fields and their Impact on Biological Tissue and Fish

Using electrical fields to manipulate biological tissue is a common method, for example used to transfer substances through cell membrane via electroporation (Hendricks and Jesuthasan, 2007; Kotnik et al., 2019). The overall method is generally the same: two electrodes are placed parallel to each other, with the sample in between, generating a homogeneous electrical field with specific characteristics to achieve the desired effect on the sample. The overall voltage (U) and current (I) needed depend on the desired voltage gradient (E), the distance between the electrodes (d), their surface area (a), and the conductivity of the medium in between (C_m).

$$E = \frac{U}{d}$$

$$I = U * \frac{C_m}{\left(\frac{d}{a^2}\right)}$$

This also applies to using electrical fields to anesthetize or euthanize zebrafish larvae. Two electrodes are placed around one or more fish to generate an electric field with a power density (P_f) sufficient for anesthesia or euthanasia. This power density also depends on the conductivity of the fish (Cf) and, according to Kolz (2006), reaches its maximum when the ratio of C_m and C_f is one (Kolz, 2006).

$$P_f = C_m * E^2 * \frac{\left(4 * \frac{C_f}{C_m}\right)}{\left(1 + \frac{C_f}{C_m}\right)^2}$$

Electric fields, when applied to biological tissue, can elicit a broad range of effects. For example, perturbations in ion homeostasis across cellular plasma membranes which sometimes can be rapidly rectified by ion pumps (Cho et al., 1999). However, electric fields stronger than ~60 V/cm can induce structural changes in membranes and proteins, including conformational changes, potentially resulting in the formation of irreversible pores, as exploited in electroporation (Lee, 2005). In more severe cases, irreversible damage to membranes or the initiation of intracellular pathways due to alterations in ion gradients can lead to cellular death. Larger cells tend to be more

vulnerable than smaller ones, primarily due to their larger trans-membrane gradient (Gaylor et al., 1988). Also, different voltage types (direct current (DC), pulsed direct current (PDC) and alternating current (AC)) and voltage gradients are known to have different effects on fish. For example, injuries such as tissue disruption, vertebral dislocations, and even fractures most likely arising from strong muscle contractions caused by direct electrical stimulation of either muscles or the neuromuscular pathway are directly linked to voltage gradient, type, and frequency (Lines et al., 2003; Nordgreen et al., 2008; Robb et al., 2002). However, findings vary regarding how different types of voltage affect mortality and injuries in fish. According to Reynolds, using DC or reducing the frequency at PDC results in less injury to large food fish, whereas AC is more likely to cause tetany, potentially resulting in injury and mortality (Reynolds, J.B., 1996). Snyder also reported that spinal injuries have mostly been associated with AC (Snyder, D. E., 2003), and numerous reports indicate that non-DC waveforms, together with different frequencies, negatively affect injury and survival rates (Dolan and Miranda, 2004; Lines et al., 2003; Robb et al., 2002; Sharber et al., 1994; Snyder, D. E., 2003). However, this does not seem to be the case for embryos and zebrafish larvae, which are found to be more vulnerable to DC (Bohl et al., 2009; Dwyer and Erdahl, 1995; Henry and Grizzle, 2004; Nguyen et al., 2019).

3.3.3 Euthanasia Methods for Zebrafish within the EU

Within the European Union, the directive 2010/63/EU states the euthanasia methods which are legal for fish (*Directive 2010/63/EU*, 2010). Those are percussive blow to the head, anesthetic overdose, electrical stunning and due to the recently published Commission Delegated Directive (EU) 2024/1262 also hypothermic shock (*Commission Delegated Directive (EU) 2024/1262 of 13 March 2024 amending Directive 2010/63/EU*, 2024). However, as mentioned before, there are uncertainties regarding the application of these methods to zebrafish larvae (Figure 1).

Percussive blows to the head are impractical and unsafe for euthanizing zebrafish larvae due to their small size (only 4mm) (Valentim et al., 2016). An overdose of the anesthetic MS-222, which induces death in adult fish via asphyxiation and hypoxemia by blocking gill ventilation (Soivio et al., 1977), also does not reliably work in larvae. This is because zebrafish larvae primarily rely on cutaneous respiration during early development (Rombough, 2002; Strykowski and Schech, 2015); gill function only

becomes essential for meeting basic respiratory demands by 12–14 dpf (Rombough, 2007). Consequently, despite cardiac arrest occurring at high MS-222 concentrations (900mg/l), larvae can regain consciousness after being transferred to regular tank water (Strykowski and Schech, 2015). Moreover, the use of MS-222 has been associated with aversive reactions in zebrafish, as they can smell the anesthetic even before the onset of the anesthetic effect (Collymore et al., 2016; Readman et al., 2013). These reactions include behaviors such as piping, twitching, and erratic swimming, all indicative of stress (Wilson et al., 2009). Wong et al. showed that zebrafish even prefer to spend significantly more time in a dark environment than in a bright environment containing MS-222, suggesting they would rather undergo discomfort than be exposed to the anesthetic (Wong et al., 2014). Furthermore, the efficacy of MS-222 has proven variable across individuals, making its use unreliable (Rombough, 2007).

Hypothermic shock is a recently added euthanasia method (sometimes also called rapid chilling, rapid cooling or hypothermia). This method involves placing fish in cold water (2-4 °C), with the resulting hypothermic shock thought to slow down cellular activities, eventually leading to cardiac arrest and death (Strykowski and Schech, 2015). The previously feared formation of ice crystals is now considered disproven in zebrafish. Therefore, rapid cooling is mostly considered a more humane euthanasia method than anesthetic overdose, also because the duration of visible distress is much shorter (Chen et al., 2014; Köhler et al., 2017; Wilson et al., 2009). However, zebrafish larvae are highly tolerant of cold water and can survive extended exposure (Mocho et al., 2022). Specifically in larvae, reliable euthanasia requires at least 12 hours of cold exposure (Wallace et al., 2018), necessitating that animals be kept in a freezer overnight to ensure death. Also, a recent study suggests that rapid cooling might have negative effects on zebrafish larvae, as calcium surges in both the pretectum and hindbrain could be observed during gradual cooling (Leyden et al., 2022).

'Animals-remarks/methods	Fish	Amphibians	Reptiles	Birds	Rodents	Rabbits	Dogs, cats, ferrets and foxes	Large mammals	Non-human primates	Cephalopods
Anaesthetic overdose	(1)	(1)	(1)	(1)	(1)	(1)	(1)	(1)	(1)	
Captive bolt			(2)							
Carbon dioxide					(3)					
Cervical dislocation				(4)	(5)	(6)				
Concussion/percussive blow to the head				(7)	(8)	(9)	(10)			
Decapitation				(11)	(12)					
Electrical stunning	(13)	(13)		(13)		(13)	(13)	(13)		
Inert gases (Ar, N_2)								(14)		
Shooting with a free bullet with appropriate rifles, guns and ammunition			(15)				(16)	(15)		
Hypothermic shock	(17)'									

Figure 1: Euthanasia methods for different animals in the EU. Although Electrical Stunning is foreseen by the EU directive 2010/63/EU for killing zebrafish, it is not used because of unknown parameters and unavailable equipment *(*Commission Delegated Directive (EU) 2024/1262 of 13 March 2024 amending Directive 2010/63/EU*, 2024)*.

Electrical stunning is currently not used as a euthanasia method in zebrafish. While the relevant EU directive foresees its use, little is known about the effects of different electrical fields on zebrafish larvae and their relation to death. Furthermore, adequate equipment for applying electrical stunning protocols is not readily available (Köhler et al., 2017). Although some protocols have been established for larger fish, primarily in the context of slaughter (Lines et al., 2003), their applicability to laboratory zebrafish remains poorly studied (Mocho et al., 2022). Critical parameters such as the needed voltage gradient, exposure time, voltage type, water conductivity, and the resulting power density remain unknown (Lidster et al., 2017). While different aspects of electrical stunning have been investigated in various fish species, the electrical parameters were often not systematically varied, and the stunning and euthanasia effects, both behavioral and neurophysiological, were not systematically recorded (Bohl et al., 2010; Mocho et al., 2022; Teulier et al., 2018). Teulier et al. exposed adult zebrafish to electrical fields for 5 seconds at a voltage gradient of 3 V/cm and a

conductivity of 400 µS/cm and found no effect on survival (Teulier et al., 2018). In another study, Russell J. Bohl et al. applied a voltage gradient of 15 V/cm at a conductivity of 60 µS/cm to zebrafish embryos, achieving a mortality rate close to 100% for young developmental stages (Bohl et al., 2009). Gross et al. investigated the effect of different DC voltage gradients on rainbow trout at different developmental stages, also considering the influence of water conductivity. At a conductivity of 220 µS/cm and a voltage gradient of 10 V/cm, a mortality rate of 100% was achieved in 7 dpf larvae (Gross et al., 2015). Nguyen et al. showed that a voltage gradient of 20 V/cm and a resulting power density of 860 µW/cm3 still resulted in a 100% survival rate for 4 dpf zebrafish larvae. However, they hypothesized that mortality rates would increase at higher voltage gradients and power densities (Nguyen et al., 2019). Finally, Mocho et al. demonstrated that pulsed direct current (PDC) with a voltage gradient of 25 V/cm for a 1-minute exposure duration can reliably euthanize zebrafish larvae on a behavioral level (Mocho et al., 2022), but also here parameters were not systematically varied and no correlates of neuronal activity was taken into account to ensure stress-free euthanasia.

3.4 Measuring Combined Vertical and Horizontal Eye Movements

3.4.1 Zebrafish Larvae: Need for Vertical Eye Movement Measurements?

Understanding how neural circuits generate adaptive behavior requires precise and quantitative descriptions of the behaviors themselves. In larval zebrafish, oculomotor behavior has become a central readout for circuit analysis because eye movements are tightly linked to visual and vestibular processing and can be measured easily with good temporal precision (Brysch et al., 2019; Leyden et al., 2021). In the past, most oculomotor studies in zebrafish have focused on horizontal eye movements, particularly the horizontal optokinetic reflex, which stabilizes visual input during locomotion and head motion (Beck et al., 2004; Dehmelt et al., 2021; Easter Jr. and Nicola, 1997; Huang, 2008; Rinner et al., 2005). This reflex minimizes retinal image slip and thereby maintains visual acuity, an essential requirement for prey capture, predator avoidance, and navigation. Horizontal OKR paradigms have therefore

become standard assays to probe visual motion processing and sensorimotor transformations in larval zebrafish. However, zebrafish live and swim in a three-dimensional aquatic environment. During natural behavior, larvae move along both horizontal and vertical axes, encounter water currents, and perform pitch and roll body rotations (Davis et al., 2025; Ehrlich and Schoppik, 2017a; Ravan et al., 2025; Sugioka et al., 2023). These ecological conditions inevitably generate vertical retinal image motion, which to some degree must be compensated by vertical eye movements to stabilize gaze and maintain visual function. Furthermore, zebrafish possess all relevant eye muscles to move their eyes horizontally, vertically, and torsionally (Kasprick et al., 2011), and previous studies have shown direction-selective neurons in the zebrafish optic tectum and pretectum that encode vertical motion (Wang et al., 2019; Zhang et al., 2022). So vertical motion and the ability to encounter for that must be relevant for zebrafish. Yet vertical oculomotor behavior in larval zebrafish has received almost no attention compared with horizontal eye movements, although the need for compensatory eye movements exists. Characterizing vertical oculomotor behavior is therefore essential for several reasons. First, it enables a complete description of the zebrafish oculomotor repertoire, which is necessary for linking neural activity to behavior in circuit-level studies. Second, it provides insight into how zebrafish adapt to ecological challenges such as vertical locomotion and hydrodynamic perturbations. And third, it allows comparison with other vertebrates, where vertical gaze control has been extensively studied, facilitating cross-species understanding of conserved oculomotor mechanisms. Therefore, incorporating vertical eye movements into the study of larval zebrafish oculomotor behavior is a necessary step toward a complete and mechanistic understanding of how neural circuits support adaptive behavior in a three-dimensional environment.

3.4.2 The Oculomotor System in Zebrafish

The larval zebrafish has become an increasingly important model organism in oculomotor research (Orger, 2016; Portugues et al., 2014). Due to the rapid development of their visual system, zebrafish larvae are able to perform several eye movements and visual reflexes, such as the optokinetic response, as early as 4 dpf (Easter and Nicola, 1996). Further visually driven behaviors, like phototaxis, looming escape, hunting behavior, and the optomotor response (OMR), occur at 5 and 6 dpf

(Bilotta and Saszik, 2001; Neuhauss, 2003). At this stage, all extraocular muscles are present, and the neuronal projections to 10 different retinorecipient brain areas are functional (Baier and Wullimann, 2021). Like all vertebrates, zebrafish larvae possess 3 pairs of eye muscles (Figure 2A) which enable them to move their eyes in three orthogonal axes (horizontal, vertical, torsional, see Figure 2B): the medial rectus (MR), responsible for moving the eye temporal-nasally; the lateral rectus (LR), responsible for nasal-temporal movements; the superior rectus (SR), responsible for eye elevation; the inferior rectus (IR), moving the eye downwards; and the inferior and superior oblique (IO, SO), generating torsional eye movements with a certain degree of depression or elevation (Kasprick et al., 2011; Kels et al., 2015).

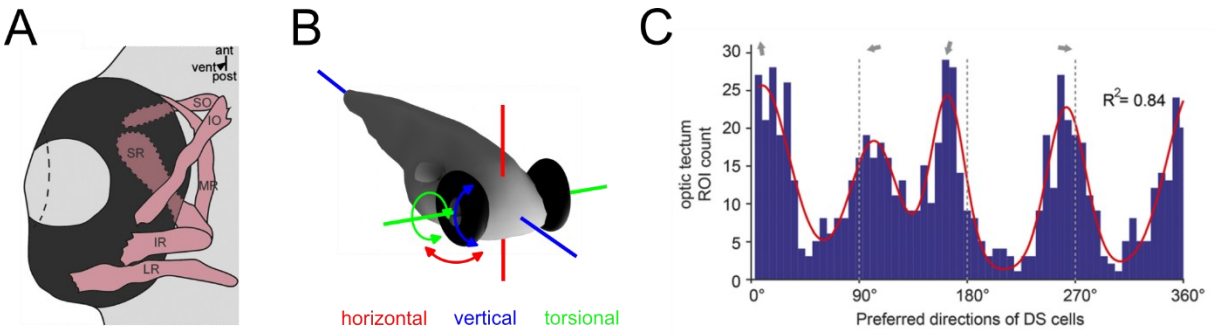

Figure 2: Zebrafish oculomotor system. A) Ventral view of the six extraocular eye muscles of a 96 hpf larvae (adapted from Tulenko and Currie, 2020). B) Rotation axis of the zebrafish eye. C). Distribution of preferred directions of direction-selective neurons in the optic tectum. 0/360°: up, 90°: NT, 180°: down, 270°: TN (adapted from Wang et al., 2019).

All muscles are innervated by three cranial nerves. Their somata comprise three cranial nuclei (nIII, nIV and nVI). The nIII lies in the midbrain and controls the medial rectus, inferior rectus, and the inferior oblique via ipsilateral projections, as well as the superior rectus via contralateral projections. The nIV contralaterally controls the superior oblique, and the nVI, also ipsilaterally, controls the lateral rectus. Both nIV and nVI lie in the hindbrain (Bellegarda et al., 2025; Spencer and Porter, 2006; Tulenko and Currie, 2020).

Zebrafish exhibit a diverse array of eye movements, that can generally be categorized into slow and fast types. In foveated animals, such as primates, rapid eye movements (saccades) facilitate the alignment of objects of interest with the high-acuity region of the retina. Conversely, zebrafish and other lateral-eyed animals lacking a defined fovea primarily utilize eye movements to stabilize the visual field rather than to focus on specific points (Dowell et al., 2024; Robinson, 1981). This stabilization relies on

optic flow mediated self-motion estimation (Britten, 2008; Kubo et al., 2014; Wang et al., 2019; Warren and Hannon, 1988). Optic flow refers to the motion of objects and surfaces within a visual scene, resulting from the relative movements between an observer and the scene (Koenderink and van Doorn, 1987). Through this optic flow, animals can estimate their own locomotion and based on their strategy, actively adjust their trajectory or eye positions. In zebrafish, the optic tectum and pretectum primarily process this optic flow, utilizing a large set of neurons tuned to different directions and motion patterns. Specifically, each direction-selective neuron exhibits a preference for one of four local directions: up, down, temporal-nasal, or nasal-temporal (Gabriel et al., 2012; Hunter et al., 2013; Wang et al., 2019; Zhang et al., 2022). Due to their swimming behavior, zebrafish predominantly experience horizontal motion with only minor vertical shifts (Ehrlich and Schoppik, 2017b). However, the number of direction-selective neurons coding for vertical up and down motion is approximately equal to the number of neurons encoding horizontal motion (Wang et al., 2019; Zhang et al., 2022), see Figure 2C. This suggests that vertical motion, in addition to horizontal motion, is relevant for zebrafish.

3.4.3 The Optokinetic Response and the Vestibulo-Ocular Reflex

Maintaining a stable retinal image is essential for accurate visual perception across all vertebrates. Two principal reflexes mediate this stabilization: the vestibulo-ocular reflex (VOR) and the optokinetic response (OKR). The VOR is activated by vestibular input during head movements and is present in zebrafish as well as in mammals and birds. When vestibular input becomes unreliable - such as during prolonged or low-frequency motion - the OKR provides a visual-based compensatory mechanism to maintain image stability (Robinson, 1981).

The OKR is a fundamental visuomotor behavior that functions to stabilize the image on the retina during whole-body or environmental motion. This reflexive eye movement is elicited by large-field motion across the retina and serves to reduce retinal slip through a combination of smooth pursuit movements (slow phase) and rapid resetting saccades (quick phase) (Beck et al., 2004). The OKR has been evolutionarily conserved across vertebrates, suggesting its critical role in visual perception and motor control. The OKR can be reliably evoked by displaying rotating vertical gratings to the fish, either using a drum or more sophisticated visual stimulation approaches

(Brockerhoff, 2006; Dehmelt et al., 2021). In response to this stimulation, the larval zebrafish will perform the OKR, which, as previously mentioned, consists of two components: the slow and the fast phase (Figure 3A). During the slow phase, the fish visually follows the visual grating with its eyes to compensate for retinal slip until a certain eye deflection is reached. Then, during the fast phase, the eyes quickly move back towards a more neutral position. The OKR is tuned to several angular velocities, spatial frequencies, and contrasts (Mueller and Neuhauss, 2010; Rinner et al., 2005). To quantify this tuning, a gain, which describes the ratio of eye velocity to stimulus velocity and thus how well the animal can compensate for retinal slip, can be calculated. Although the gain increases with age, it is always below one, indicating that the fish never perfectly manages to follow the stimulus and always lags behind (Beck et al., 2004; Dehmelt et al., 2021). Also, the gain is asymmetrical, with higher values for temporal-nasal movements (Qian et al., 2005; Roeser and Baier, 2003).

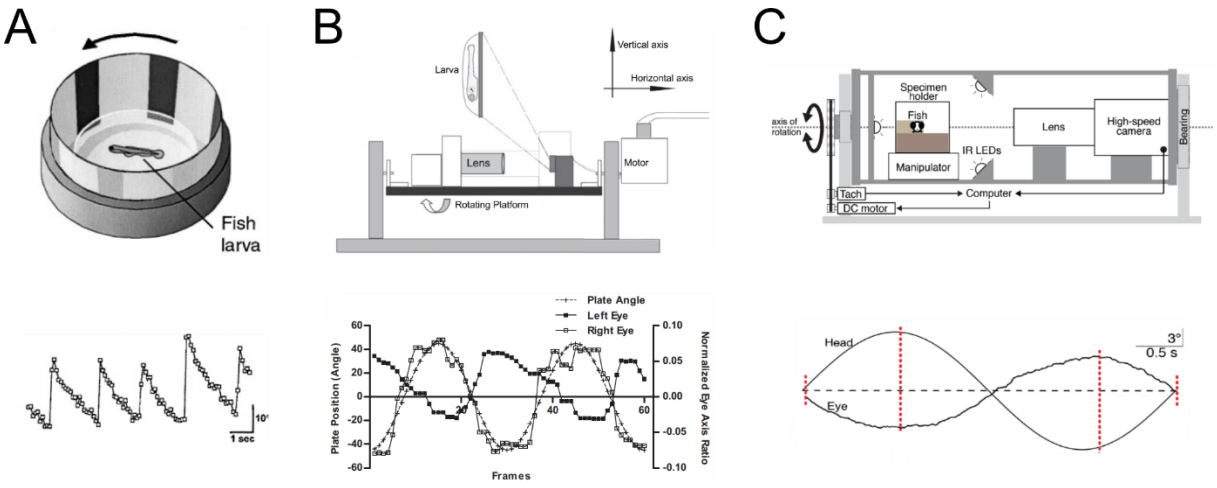

Figure 3: OKR and VOR. A) Visual stimulation setup and exemplary eye trace for the horizontal OKR (adapted from Neuhauss et al., 1999). B) Vestibular stimulation setup and exemplary eye trace for the horizontal VOR (adapted from Mo et al., 2010). C) Vestibular stimulation setup and exemplary eye trace for the torsional VOR (adapted from Bianco et al., 2012).

In zebrafish, the OKR has been extensively characterized in the horizontal domain, whereas the vertical domain remains largely unexplored (Beck et al., 2004; Dehmelt et al., 2021; Easter Jr. and Nicola, 1997; Huang, 2008; Rinner et al., 2005). However, in other species, including primates, cats, and even rabbits - the latter being lateral-eyed animals like zebrafish that lack foveate vision - the vertical OKR is well-described (Collewijn, 1980; Erickson and Barmack, 1980; Kitama et al., 2001; van den Berg and Collewijn, 1988). In rabbits, for example, vertical eye movements are less interrupted

by resetting saccades and can be sustained for more than 10 seconds at their maximum deflection. They also reach higher angles (> 20°) compared to horizontal eye movements (< 15°), and the gain for up-down stimulation is slightly higher than for down-up stimulation (Erickson and Barmack, 1980). Additionally, in goldfish, a recent study has provided evidence for a vOKR that is very similar to the well-known hOKR in its overall pattern (Tadokoro et al., 2025).

The VOR is a reflex mediated by the vestibular system, which detects angular and linear acceleration of the head via the semicircular canals and the otolith organs, respectively (Bagnall and Schoppik, 2018). In contrast to the OKR, which is more effective at slower velocities or in situations involving passive environmental motion, the VOR is tuned to rapid, high-frequency accelerations, such as those that occur during swim bouts (Beck et al., 2004; Masseck and Hoffmann, 2009). However, it should be noted that the angular VOR is thought not to be present in larval zebrafish because the semicircular canals only become functional after one month due to their small size (Lambert et al., 2008). Until that age, zebrafish larvae are presumably only able to perform linear VOR based on vestibular input from the otolith organs. The VOR can be experimentally evoked in zebrafish by rotating the animal in either complete darkness or light, effectively isolating vestibular contributions from visual input (Bianco et al., 2012; Lambert et al., 2008; Lim et al., 2024; Mo et al., 2010; Sun et al., 2018). In response to these stimuli, the eyes perform conjugate compensatory movements by rotating in the counter-stimulus direction. To date, most studies have investigated horizontal eye movements in response to vestibular stimuli (Figure 3B). Depending on the orientation of the larvae within the VOR setup, e.g., horizontal vs. vertical embedding (Beck et al., 2004; Mo et al., 2010), different combinations of vestibular inputs (semicircular vs. otolith) can be examined. Some studies also report a torsional VOR (Bianco et al., 2012; Leary et al., 2025) (Figure 3C), and a few describe vertical eye movements in response to body rotation in zebrafish and goldfish (Sugioka et al., 2023; Tadokoro et al., 2025; Takabayashi et al., 2003).

Altogether, the zebrafish oculomotor system provides a robust model for exploring the neural basis of eye movements. Therefore, it is essential to understand the full behavioral repertoire of the fish. With regard to the OKR and VOR, several aspects, such as the investigation of vOKR and vVOR, are still missing, which is one focus of this study.

4. Aims and Objectives

The aim of this project was to close a critical gap in zebrafish neuroscience research where underdeveloped and sometimes simplistic behavioral technology and tools limit further investigation of zebrafish behavior alongside sophisticated and advanced complex imaging methods by developing comprehensive behavioral research tools that are accessible, modular and compatible with existing experimental pipelines. These tools were then applied to publish previously missing results in the fields of animal welfare and the oculomotor system. The specific objectives were:

1. Electrical Stunning

a. Development of two experimental setups for controlled application of electric fields to i) free swimming larvae alongside camera tracking and ii) agarose-embedded larvae alongside simultaneous visual stimulation and 2-photon calcium imaging
b. Investigation of electrical stunning as an alternative euthanasia method on behavioral and neurophysiological level

2. Vertical Optokinetic Eye Movements

a. Development of an experimental setup for tracking vertical eye movements of agarose-embedded larvae alongside vestibular (and visual) stimulation
b. Further development of an existing visual stimulation arena (Dehmelt et al., 2018) for combined tracking of vertical and horizontal eye movements
c. Characterization of the vVOR and the vOKR and comparison to the hOKR

5. Key Results

5.1 Electrical Stunning

5.1.1 Modular Setups for Application of Electrical Fields alongside Behavioral Tracking, Visual Stimulation and Calcium Imaging

To examine the effects of electrical stunning at both behavioral and neurophysiological levels, two setups were developed and constructed. The first setup allowed for the application of various electrical fields to free-swimming larvae while simultaneously tracking their behavior using an infrared camera. The second setup enabled the same electrical stimulation on single, agarose-embedded, and thus restrained, larvae, coupled with 2-photon calcium imaging and full surround visual stimulation. Both setups were controlled by a programmable power source (GW Instek ASR2050R) and custom-written software (synchASRcontrol, (Burkhardt and Arrenberg, 2024)).

The core of the behavioral setup is a multi-layer exposure chamber, consisting of a 56x36x36 mm polystyrene box. This box has a dielectric strength of 22 – 55 kV/mm at 20 °C to ensure electrical insulation, and it is surrounded by a 3D-printable box that houses the wiring and a snap-action switch-based safety mechanism (MAR 1005.0404, MARQUARDT, Germany). The switch is operable at up to 400 V and only allows electricity to flow when the lid is closed. Inside the polystyrene box, two stainless steel electrodes, covering opposing faces, are held in place by a 3D-printable frame. This frame also features a rigid net cage (PA-405/47, 405µm, Eckert, Waldkirch, Germany) in the middle to ensure that larvae remain centered within the electric field during exposure. Both the lid and the surrounding chamber have a large, transparent window to enable behavioral recording via a camera positioned above, along with diffuse illumination at a 940nm wavelength from below. For protection against leakage currents, a RCCB type B (F200, B Type, ABB Ltd (Asea Brown Boveri), Zürich, Switzerland) was inserted between the chamber and the power source. Video recording was performed using a camera equipped with a 6mm objective (DMK23UV024, The Imaging Source Europe GmbH, Bremen, Germany) and an IR long-pass filter (SCHOTT RG780, Edmund Optics Inc., Barrington, USA), see Figure 4A.

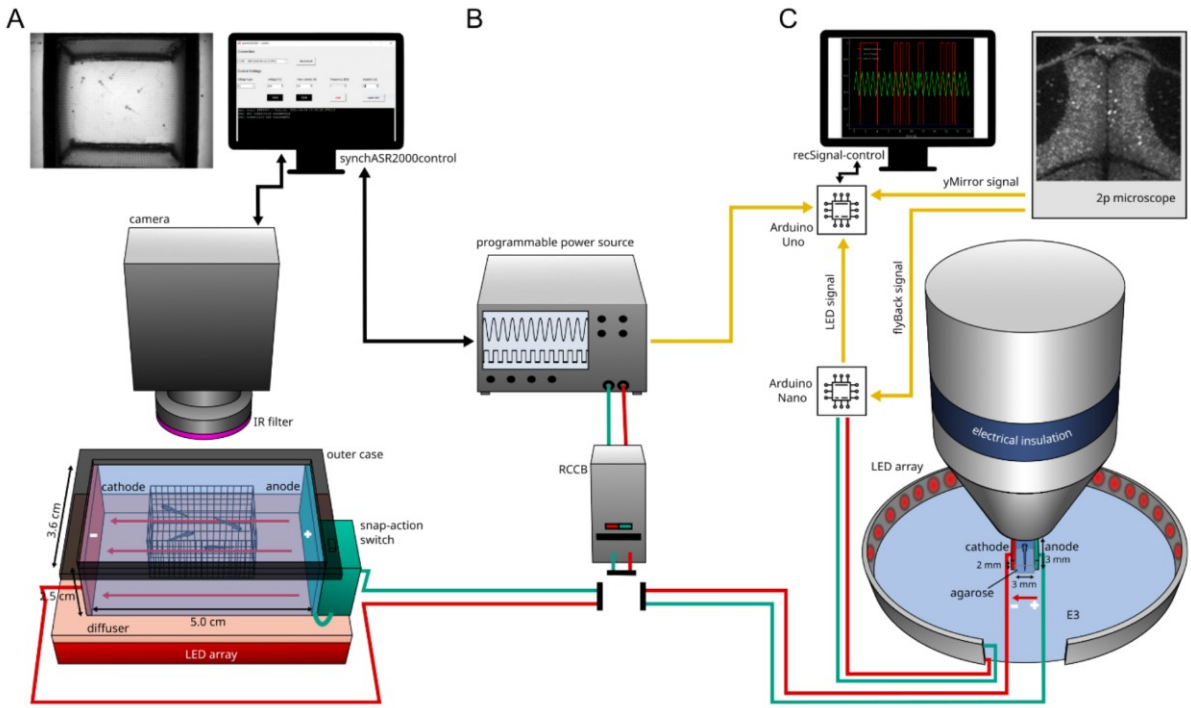

Figure 4: Setups for Investigation of Electrical Stunning. A) Behavioral setup that allows the application of electrical fields on multiple free swimming zebrafish larvae while video-tracking their behavior. B) Programmable power source GW Instek ASR2025R for generation of arbitrary electrical fields. The power source is controlled by the Python written software synchASRcontrol. C) Setup for electrical stunning of single larvae alongside visual stimulation and 2-photon calcium imaging (adapted from Burkhardt et al., 2025).

The electrical stunning setup for 2-photon calcium imaging and visual stimulation of single larvae consisted of two 2x3 mm stainless steel electrodes with a thickness of 0.5mm. These electrodes were placed 3 mm apart in a 50 mm petri dish and held in place by a 3D-printed electrode frame. A 200 µm copper plate was welded onto the back of the electrodes to allow for cable soldering. The electrode frame enclosed the electrodes on three sides to prevent unwanted contact with the microscope objective. A LED array, consisting of 18 650 nm LEDs, enabled 360° visual stimulation, synchronized with the microscope scanning via an Arduino Nano. The microscope and the electrical stunning setups were electrically separated using a modified SM1L05 lens tube containing an insulating polymer insert. Temporal information about the electrical field application and the visual stimulation were recorded using an Arduino Uno and custom-written Python software and were synchronized with the imaging process (Figure 4B). Both setup designs ensure safety and experimental flexibility while remaining straightforward enough to be constructed by laboratories without

specialized engineering infrastructure and therefor meeting the requirements of advanced but still accessible tools needed for zebrafish neuroscience research.

5.1.2 AC Fields evoke Immediate Loss of Behavior and Consciousness

To determine an effective and humane protocol for electrical stunning in zebrafish larvae, a comprehensive evaluation of different electrical parameters was conducted, focusing on the type of current, frequency, voltage gradient, and exposure duration. Zebrafish larvae at 4 dpf were exposed to direct current (DC), alternating current (AC), or pulsed direct current (PDC at 60 Hz or 6 Hz, duty cycle 50%) under controlled laboratory conditions using the previously described behavioral electrical stunning setup. Mortality was assessed by using a multimodal criterion that included loss of equilibrium, absence of spontaneous locomotion, cessation of gill ventilation, and lack of response to tactile stimulation, corresponding to the fourth stage of anesthesia in fish, which describes overdose (Sneddon, 2012). At the highest tested exposure duration of 32 seconds and a voltage gradient of 50 V/cm, all voltage types achieved 100 % mortality (Figure 5A). However, AC was identified as the most suitable modality due to its ability to consistently produce rapid behavioral incapacitation while minimizing morphological damage. When using these parameters, all larvae exhibited a rapid loss of equilibrium - interpreted as a proxy for loss of consciousness - within 0.89 ± 0.38 s, indicating that this method induces a very fast onset of anesthesia-like insensibility (Figure 5B).

In contrast, DC and low-frequency PDC treatments often resulted in visible morphological abnormalities, including curvature of the body axis, opaque brain tissue, and, in severe cases, skeletal deformations such as kyphosis, lordosis, or scoliosis. These effects were particularly evident at longer exposure durations (16 and especially 32s) and appeared to be exacerbated by the increased joule heating associated with these current types at 32s exposure duration. AC, by comparison, was associated with only moderate heating and produced either no immediate morphological changes or only a delayed onset of mild tissue abnormalities. Due to its combination of effectiveness and reduced physical damage, the AC 60 Hz condition was selected as the standard for all subsequent behavioral and neurophysiological experiments.

During the initial phase of electrical exposure, larvae frequently exhibited rapid, short-duration bursts of tail movement. To test whether these movements reflected voluntary escape behaviors - suggesting a period of residual consciousness - or instead represented passive, stimulus-induced muscle contractions, high-speed video analysis was conducted on agarose-embedded larvae with their tails cut free.

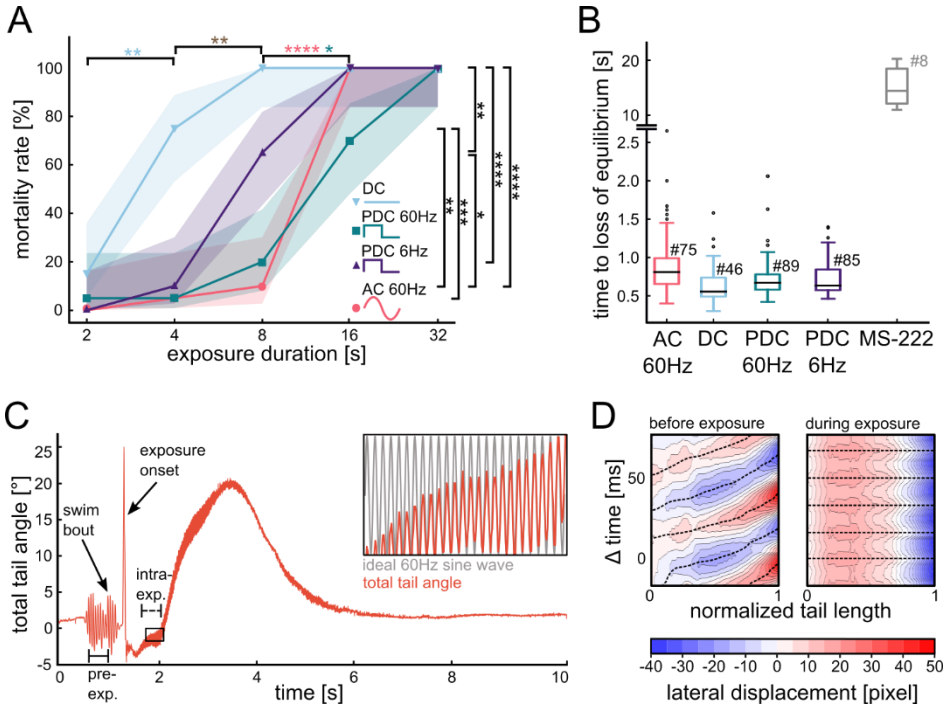

Figure 5: Behavioral results of electrical stunning. A) Mortality rates of different voltage types for different exposure durations at voltage gradient of 50V/cm. B) Time to loss of equilibrium for different voltage types. For comparison, the time to loss of equilibrium for MS-222 (336mg/l) is shown (Leyden et al., 2022). C) Total tail angle of a larva during exposure. D) Lateral displacement profile before and during electrical stunning (adapted from Burkhardt et al., 2025).

In this setup, the larva was exposed to the optimized AC field (50 V/cm, 60Hz, 32 s), and tail movements were recorded at a high temporal resolution. Kymograph analysis of tail angle over time revealed an initial large-amplitude deflection coinciding with the field onset, followed by regular oscillations that closely matched the 60 Hz frequency of the applied electric field (Figure 5C). These tail movements lacked the rostro-caudal curvature propagation typically observed in active swimming, which is necessary to generate forward motion (Müller and van Leeuwen, 2004, Figure 5D left). Instead, the entire tail underwent synchronized bilateral contractions (Figure 5D right). Further, both the tail beat amplitude and the larval body length decreased during exposure,

consistent with a tonic, symmetric muscle contraction rather than dynamic, volitional movement. Thus, these results suggest that the tail movements observed during electrical stunning do not indicate continued sensory awareness or volitional behavior but are represent passive, stimulus-induced muscle contractions.

5.1.3 Complete Loss of Visual Driven Brain Activity during Electrical Stunning

To assess the impact of electrical stunning on neural function and to confirm the effectiveness of the previously chosen parameter set (AC, SIN, 60Hz, 50V/cm, 32s), in vivo two-photon calcium imaging of zebrafish larvae during visual stimulation (full-field luminance flashes) alongside exposure to an electrical field was conducted. In non-verbal animal models, unconsciousness is operationally defined as loss of behavioral responsiveness accompanied by characteristic neural state changes (Mashour, 2024; Mashour and Hudetz, 2018). Neural readouts of unconsciousness range from global measures of brain integration, such as perturbational complexity (Casali et al., 2013) or large-scale connectivity changes during anesthesia (Boly et al., 2012), to local measures of sensory responsiveness. Because the optic tectum is the principal visual processing center in larval zebrafish and drives visually guided behaviors (Del Bene et al., 2010; Roeser and Baier, 2003), calcium imaging of tectal and pretectal neurons can provide a robust measure of sensory suppression and breakdown of visual sensorimotor processing under anesthesia (Leyden et al., 2022). Therefore, imaging focused on the optic tectum, where distinct neuronal populations are known to respond reliably to on- and off-luminance transitions (Muto et al., 2013; Thompson et al., 2016). Baseline recordings revealed stimulus-locked neural responses, characterized by distinct periodic fluctuations in calcium signals across segmented neurons. However, the application of the electric field rapidly and strongly altered neuronal activity. The onset of electrical exposure initiated a high-amplitude, fast-propagating calcium wave, accompanied by strong spatial drift and lasting morphological distortions, which made consistent neuron tracking across time points difficult (Figure 6A). Following this initial event, fluorescence intensity gradually declined, punctuated by slower secondary calcium waves that differed in temporal dynamics and propagation characteristics.

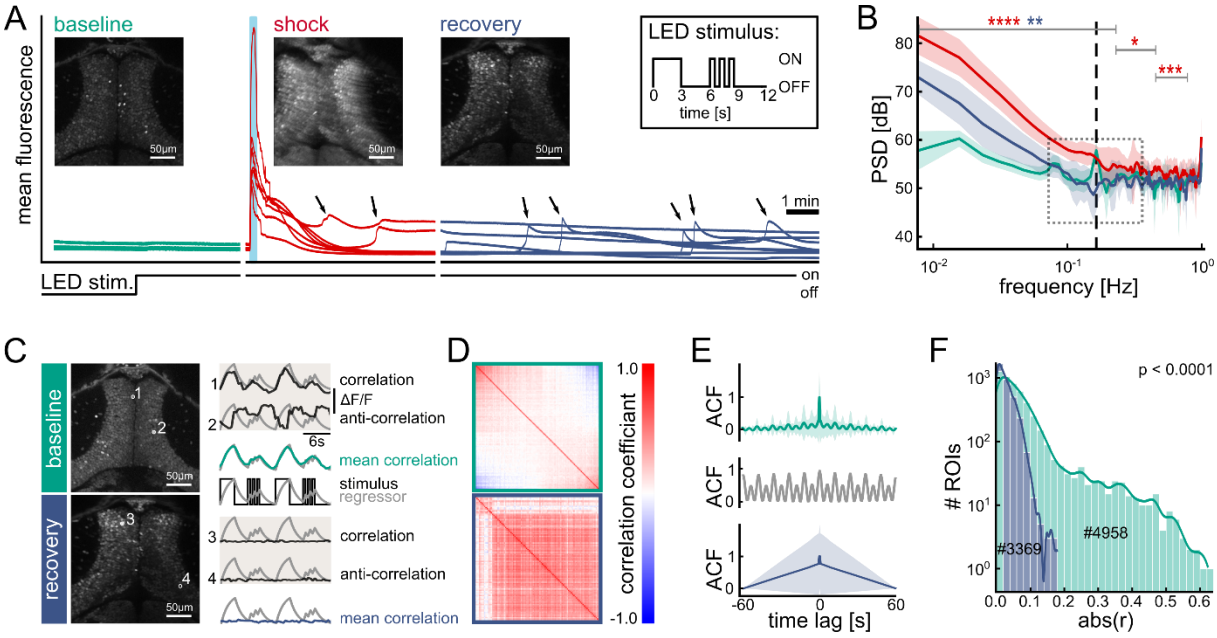

Figure 6: 2-Photon imaging results of electrical stunning. A) Mean image fluorescence before (baseline), during (shock) and after (recovery) electrical stunning. B) Power spectral density (PDS) analysis of mean fluorescence. Dashed vertical line indicates the visual stimulus frequency. C) Example and mean calcium traces of 20% best correlated ROIs before and after electrical stunning. D) ROI cross-correlation matrices for baseline and recovery. E) Mean autocorrelation function (ACF) for baseline and recovery. Gray shows ACF for visual stimulus (regressor) itself. F) Histogram of absolute ROI correlation coefficients for baseline and recovery (adapted from Burkhardt et al., 2025).

Power spectral density (PSD) calculations across all image pixels showed an absence of the stimulus frequency (0.1667 Hz) during the stunning and recovery phases, indicating that visual processing ceased entirely. Instead, signal power shifted toward low frequencies, reflecting slow, non-specific calcium fluctuations (Figure 6B). Segmented cell-based correlation analyses further supported these findings (Figure 6C). Prior to electrical stunning, 3.5% of neurons exhibited strong correlation or anti-correlation with the stimulus. After electrical exposure, no neurons met this criterion, and the correlation structure across neurons collapsed into a uniform, globally synchronous pattern (Figure 6F). Cross-correlation matrices (Figure 6D) and autocorrelation functions (Figure 6E) reflected this shift, with stimulus-locked periodicity completely abolished after electrical stunning. These results indicate that electrical stunning, when employing AC at 60Hz and 50V/cm for 32 seconds, induces an immediate and irreversible loss of stimulus-driven neuronal activity. This reflects a shutdown of sensory processing, thereby suggesting a rapid onset of unconsciousness.

5.2 Vertical and Horizontal Eye Movements

After having established and validated suitable parameters for electrical stunning as a controlled and more humane method of euthanasia, we next turn to the second major methodological gap addressed in this thesis: the investigation of vertical and combined eye movements in larval zebrafish. In contrast to the electrical stunning approach, which focused on refining experimental manipulation and animal welfare, this second line of work aimed to expand the measurable behavioral repertoire of the model organism larval zebrafish. Specifically, I sought to develop and apply experimental setups that enable quantification of vertical optokinetic (vOKR) and vestibulo-ocular (vVOR) responses - behaviors that have not been studied so far as the recording of eye movements in larval zebrafish is mostly restricted to the horizontal plane.

5.2.1 Setups for Investigating Vestibular and Visually Driven Vertical and Horizontal Eye Movements

To investigate vertical and horizontal eye movements in larval zebrafish, two custom-built experimental setups were developed. These setups allowed for precise control of both visual and vestibular stimulation, as well as accurate eye-tracking in multiple dimensions. For vertical vestibulo-ocular reflex (vVOR) experiments, a rotating setup named KEBAB (Kinematic Evaluation of Behavior during Animal Body-roll) was developed and constructed in-house. This apparatus enabled controlled rotation of individual zebrafish larvae around their rostral-caudal body axis (roll). The system was assembled using standard components from the Thorlabs 30 mm cage system, integrating an examination chamber, infrared illumination, simple visual stimulation via two LEDs, and a camera path along a single rotation axis. A Nema 17 stepper motor (ACT Motor GmbH, Germany) was used to precisely rotate the entire setup. To ensure electrical connectivity and continuous data transfer from the rotating camera system to a stationary PC, a rotating electrical slip ring was (BQLZR 0.48”, 12 Wire, 2A, 240V, Amazon) employed. Illumination was provided by 850 nm IR and white LED diodes; each paired with a 120-grid diffuser to ensure uniform lighting. Zebrafish larvae were embedded on a custom-designed triangular stage in 1.6% low melting point agarose, as described in Wang et al. (2020). Agarose surrounding the eyes were carefully removed to allow for free eye movements. The stage was then mounted on a 3D-

printed holder and secured within the setup. System operation was controlled via an Arduino Uno microcontroller with an A4988 RepRap stepper motor driver (Figure 7A). Remote control from a PC is facilitated using the Python library Telemetrix (https://mryslab.github.io/telemetrix/). The custom Python-based software vxPy (https://github.com/thladnik/vxPy) controlled rotation of the setup, presentation of visual stimuli, video recording, and real-time eye tracking.

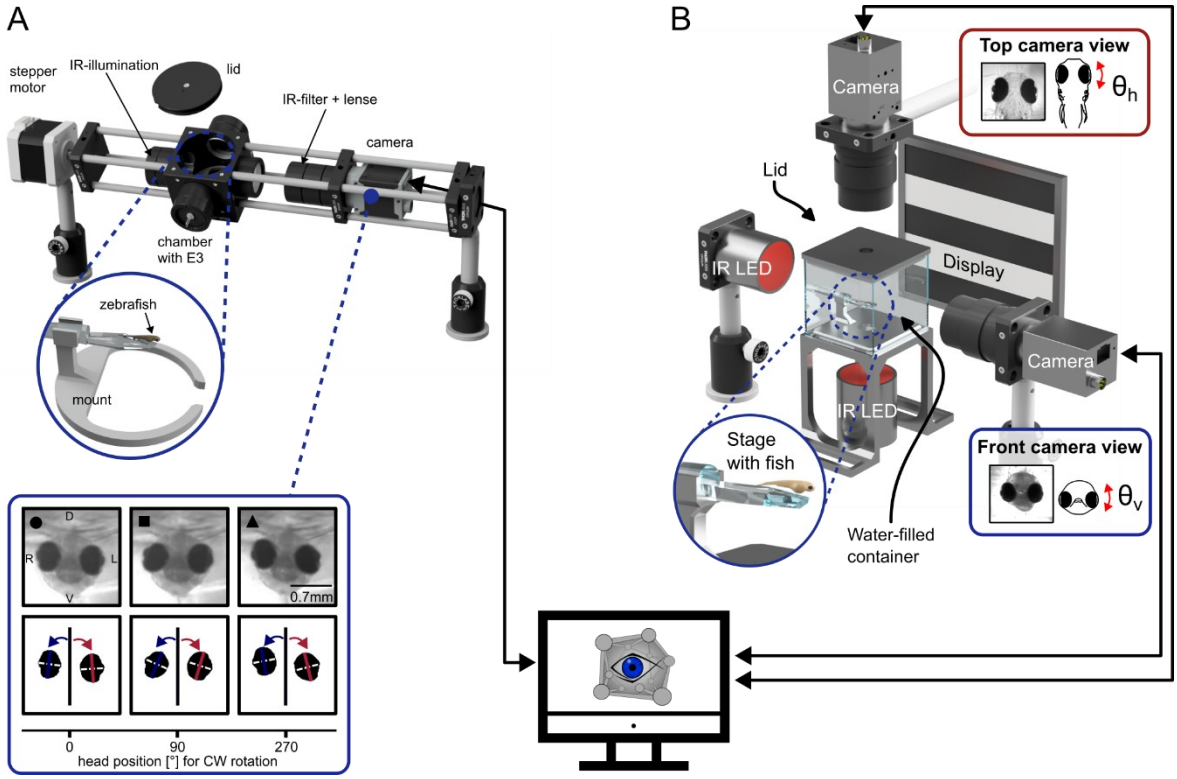

Figure 7: Setups for investigating vestibularly and visually driven vertical and horizontal eye movements. A) KEBAB, used to examine vertical eye movements during rotation of a single larva. All main parts are assembled by using standard Thorlabs components. Stepper motor, visual stimulation and eye tracking are controlled by vxPy. B) Setup with two cameras to simultaneously record vertical and horizontal eye movements. Two laterally placed displays (only one shown) are used for advanced visual stimulation. The complete setup is controlled by vxPy (adapted from Burkhardt et al., 2026).

To assess optokinetic responses (vOKR and hOKR), the visual stimulation arena described in Dehmelt et al., 2018 was modified to allow for simultaneous horizontal and vertical eye tracking. To simultaneously capture both horizontal and vertical eye movements, the displays located in front of and behind the fish were removed. Two cameras, one placed above and one in front of the fish, were used in conjunction with IR backlights positioned below and behind the fish. Larvae were positioned in the center of a translucent, water-filled container, using the same embedding technique described before. A 3D-printed black lid was placed in direct contact with the water

surface to suppress reflections at the water-air interface; a similar cover is placed at the bottom of the container. Both covers included a central opening to allow IR illumination and unobstructed camera views. The two remaining displays, one each on the left and right sides of the fish, were used to present the visual stimuli and are sufficient to elicit robust OKR behavior (Figure 7B).

5.2.2 vOKR Does Exist in Larval Zebrafish but Differs from hOKR

To characterize the repertoire of vertical eye movements in larval zebrafish, the vertical vestibulo-ocular reflex (vVOR) was first assessed. Larvae were embedded in agarose and subjected to controlled roll-axis rotations (clockwise and counter-clockwise), while vertical eye movements were recorded in complete darkness.

Across three tested rotation velocities (22.5 °/s, 45 °/s, and 90 °/s), eye position traces followed a near-sinusoidal pattern, closely aligned with head orientation (Figure 8A). Maximal eye deflection occurred at 90° and 270° head positions, and the amplitude of vertical eye movements slightly increased with stimulus velocity. No saccades (neither resetting nor spontaneous saccades) were observed during the rotational stimulus phases, while a low rate of spontaneous saccades (0.82/min) was detected during the interspersed pause periods. The vVOR gain was highest at 90 °/s rotation velocity, reaching 0.17 (Figure 8B). Phase lag measurements were minimal, with both slightly positive and negative values near zero, reflecting near-synchronous coupling of eye and head motion.

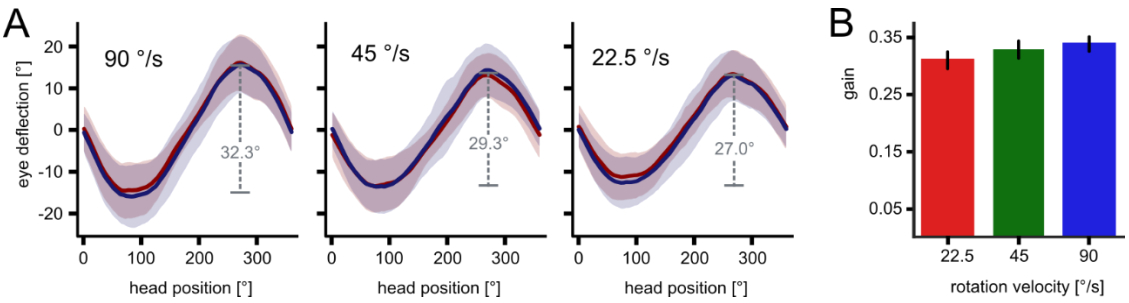

Figure 8: vVOR in zebrafish larvae. A) Stimulus triggered average (STA) of eye position during full rotation. Envelopes show standard deviation. B) Gain as ratio of sinus-fitted eye position to head position (adapted from Burkhardt et al., 2026).

To assess the vertical optokinetic response (vOKR), zebrafish larvae were exposed to vertically rotating visual stimuli composed of horizontally oriented black-and-white

stripes. Eye tracking was conducted with two cameras to monitor horizontal and vertical movements simultaneously (Figure 9A). Upon stimulus onset, larvae exhibited an initial eye movement lasting 4 - 5 seconds in the direction of the stimulus, after which eye position reached a plateau and remained largely unchanged (Figure 9B). After that start response, spontaneous saccades occurred intermittently in both directions, often involving both vertical and horizontal components (Figure 9A). Comparisons with horizontal OKR (hOKR), elicited by horizontally rotating vertical stripes, revealed that while the hOKR produced ongoing slow phases with resetting saccades, the vOKR response flattened early (Figure 9B). The average vertical deflection for vOKR peaked at 5.81° ± 0.38°, substantially lower than hOKR amplitudes (16.92° ± 0.61°). Nonetheless, the spatial frequency and angular velocity tuning of the vOKR closely resembled that of the hOKR (Figure 9C and D).

Given the transient nature of the vOKR during constant rotation, sinusoidal velocity-modulated stimuli were employed to extend the temporal window of visually driven vertical eye movements. These stimuli gradually increased and decreased velocity in alternating directions, allowing measurement of responses over full cycles. Under these conditions, larvae generated sinusoidal vertical eye movements in line with stimulus position (Figure 9E). No vertical resetting saccades were observed, although spontaneous horizontal saccades occurred. First, the repetition rate (rr) was varied while keeping angular velocity and spatial frequency constant, then the angular velocity and spatial frequency of the sinusoidal velocity function was systematically varied while repetition rate constant at 0.125Hz (Figure 9G and H). Vertical eye movements followed the stimulus closely for rr values between 0.5 Hz and 0.0078 Hz. At slower repetition rates, while gain declined, the dynamic range increased - reaching up to 10° at the lowest rates tested. Stimulus-triggered averages (STA) of eye position revealed systematic changes in phase lag with repetition rate. At high rr (0.25–0.5 Hz), eye movements lagged behind the stimulus, whereas at lower rr (<0.125 Hz), a phase advance emerged (Figure 9H). In these cases, the eyes began to reverse direction before the stimulus completed its deceleration, suggesting anticipatory movement or adaptation. The transition from lag to lead corresponded with a shift from positive to negative phase angles. This inversion indicates that eye velocity changes were aligned with decreasing stimulus acceleration, potentially implicating acceleration-sensitive or adaptive neural mechanisms.

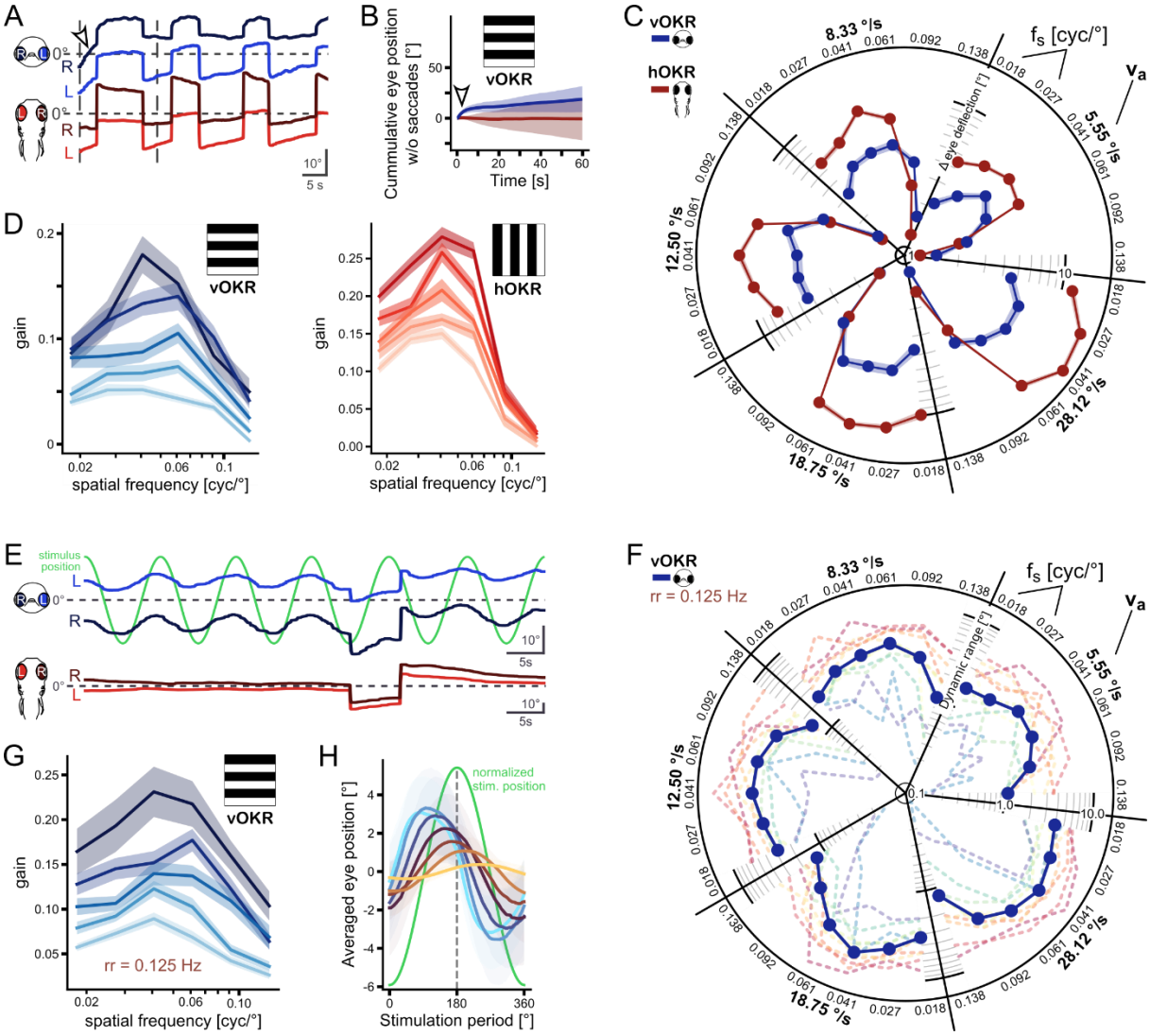

Figure 9: vOKR in response to constant and sinusoidal rotating grating. A) Example eye traces for horizontal and vertical eye movements during constant vOKR stimulation. Arrowhead indicates initial vertical start response during stimulation. B) Average cumulative eye position during constant vOKR with saccades removed. Arrowhead indicates the vertical start response and the subsequent plateau while horizontal eye position remains around zero. C) Mean amplitude within 4s after stimulation onset for vOKR and hOKR. Envelopes show SEM. D) Gain tuning to spatial frequency for vOKR and hOKR. E) Example eye traces for horizontal and vertical eye movements during sinusoidal vOKR stimulation. F) Dynamic range of vertical eye movements during sinusoidal vOKR. Dashed lines show mean dynamic range of individual fish. G) Gain tuning to spatial frequency for sinusoidal vOKR. H). Average response to one stimulus period for different repetition rates (rr) during sinusoidal vOKR. The phase lag/advance is visible and indicated by dashed vertical line (turning point of stimulus) (adapted from Burkhardt et al., 2026).

5.2.3 Zebrafish Larvae Exhibit Distinct Pure Vertical and Pure Horizontal Spontaneous Saccades During vOKR

During the experiments, zebrafish larvae exhibited spontaneous saccadic eye movements in both vertical and horizontal planes during optokinetic stimulation (Figure 10A), while no saccades were observed during vestibulo-ocular reflex testing. Significantly, the frequency of saccades during vOKR stimulation was similar to that observed in the absence of visual stimulation, suggesting these saccades were spontaneously generated rather than stimulus-driven. Moreover, neither the direction of the visual stimulus nor its temporal profile (constant versus sinusoidal) significantly altered saccade rates during vOKR. vOKR-evoked saccades were systematically analyzed to differentiate their directional components, classifying 4696 detected saccades into four distinct categories based on their plane of motion. Clusters 1 and 2 comprised saccades with exclusively vertical (10.5%) or horizontal (14.0%) components, respectively.

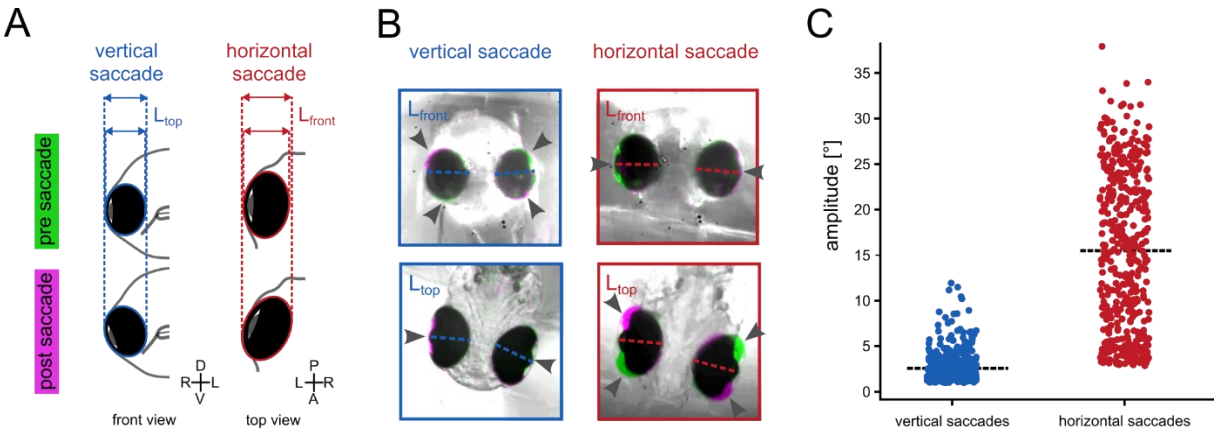

Figure 10: Vertical and horizontal saccades during vOKR and hOKR. A) Schematic of minor axis length change (ellipse fitting) during vertical and horizontal saccades. During vertical saccades, the minor axis length in the top camera is expected to change, whereas the minor axis length in the front camera should remain constant. For horizontal saccades the expectation is vice versa. These length changes together with the angle between the major axis and the body axis were used to detect pure vertical and horizontal eye movements. (B) Difference image of the eyes' pre-saccadic (green) and post-saccadic (magenta) positions for pure vertical and pure horizontal example saccades. Arrows indicate the area where position changed. For pure vertical saccades, the top camera showed changes only at the lateral parts of the eyes, whereas the front camera exhibited changes at the dorsal and ventral parts of the eyes. Conversely, during pure horizontal saccades, the image changes were reversed (change at lateral parts of eyes in front camera and at anterior/posterior parts of eyes in the top view camera). (C) Saccade amplitude scatter plot of pure vertical and pure horizontal saccades (adapted from Burkhardt et al., 2026).

The remaining 75.5% of saccades involved deflections in both planes. However, combined eye movements in these clusters could not be reliably separated due to a method-dependent projection artifact: large horizontal displacements occasionally

distorted the apparent shape of the eye in the frontal view, thereby confounding vertical axis estimation and leading to misclassifications of purely large horizontal saccades. Pure vertical and pure horizontal saccades were further illustrated by visual confirmation through false-color imaging of pre- and post-saccadic frames (Figure 10B). Pure vertical saccades rarely surpassed 10° and sometimes included minor horizontal deviations. In contrast, pure horizontal saccades demonstrated greater amplitudes, with some exceeding 30°, underscoring a functional asymmetry between vertical and horizontal saccadic capabilities in larval zebrafish (Figure 10C).

6. Discussion

A central goal of this thesis was to help zebrafish neuroscience to mature methodologically by improving available behavioral readouts, which are wide established for mammalian model organisms but are still in the early stages for zebrafish research, and improving animal welfare by investigating a more reliable and humane euthanasia method, which is currently missing - especially for zebrafish larvae. I therefore developed and validated two complementary methodological platforms: one for controlled behavioral and physiological manipulation using electrical fields, alongside behavioral recording and 2-photon calcium imaging; and another for expanding oculomotor readouts beyond the horizontal axis through either simultaneous measurement of vertical and horizontal eye movements or pure vertical eye movements recording during visual and vestibular stimulation.

In the electrical stunning project, the resulting setups provide a reliable, modular, and experimentally well-controlled way to apply defined electrical fields to larval zebrafish while monitoring behavior and neural responsiveness in vivo. These setups not only enabled the identification of robust parameters for rapid euthanasia with minimal morphological damage but also provided novel neurophysiological validation for euthanasia protocols. Moreover, working with this platform revealed some engineering constraints essential for routine adoption and scalability. These insights structure the first part of the discussion: I first interpret the biological and neurophysiological findings from electrical stunning and then use them to outline the challenges that a next-generation stunning technology must address to become a widely adoptable standard.

In the vOKR project, the experimental approach was deliberately versatile: by extending existing visual stimulation arenas and implementing single- and dual-camera tracking, we quantified vertical optokinetic behavior (vOKR) in zebrafish larvae. This provided the first systematic descriptions of larval zebrafish vOKR dynamics in the literature, alongside comparisons to the vestibulo-ocular reflex (vVOR). However, also these experiments revealed some limitation of the methodological advance: when horizontal and vertical components co-occur, the mapping from 3D eye rotations to 2D camera projections becomes ambiguous, making vertical estimates unreliable - particularly during large horizontal deflections. Accordingly, the second part of the

discussion turns from what the dual-camera system enabled to what it still cannot unambiguously resolve and how this could be remedied in future applications.
The discussion will conclude by weighing these options against this thesis's guiding principle - methods that meaningfully expand behavioral access while remaining practical, modular, and adoptable - and identifying the most promising direction for future work.

6.1. Electrical Stunning

6.1.1. Electrical Stunning is a reliable and humane Euthanasia Alternative

One of the objectives of this study was not only to evaluate the behavioral and neurophysiological effects of electrical stunning on zebrafish larvae but also to develop a robust and transferable euthanasia protocol which can reliably be used by labs worldwide. Therefore, parameters that are both effective and feasible to implement across international laboratory settings were prioritized (e.g. using AC at a frequency near 50/60 HZ, which is available worldwide). 50 V/cm alternating current (AC) at 60 Hz for 32 seconds was identified to be the most reliable configuration, achieving 100% mortality with minimal variability and morphological damage. While both 16 s and 32 s exposures yielded full mortality at this field strength, only the longer duration was used to confirm reliable suppression of stimulus-associated neural activity using calcium imaging, ensuring greater consistency under variable conditions. Notably, this parameter set remains effective even when power density is reduced, indicating a safety margin for experimental variations. Due to its compatibility with common lab infrastructure and alignment with regulatory guidelines (e.g., EU Directive 2010/63/EU), this protocol offers a readily adoptable refinement for zebrafish euthanasia.
A key advantage of electrical stunning over established methods is its rapid onset of unconsciousness, which is an important factor when working towards minimization of potential distress and suffer ("AVMA Guidelines for the Euthanasia of Animals," 2020). In our experiments, loss of equilibrium - used as a proxy for loss of consciousness (Meyer, 2015) - occurred within about one second (0.89 ± 0.38 s) after exposure to 50 V/cm AC. This is significantly faster than anesthesia using MS-222, which typically takes 15-34 seconds depending on concentration and developmental stage (Collymore

et al., 2016; Ferreira et al., 2022; Leyden et al., 2022; Wilson et al., 2009). While rapid cooling induces unconsciousness within 15s, it requires up to 12 hours of exposure to ensure lethality in larvae, which raises concerns about prolonged distress (Chen et al., 2014; Wallace et al., 2018). By contrast, electrical stunning delivers both rapid stunning and definitive euthanasia, with no recovery observed in any larvae even after overnight monitoring. The absence of aversive behaviors, as observed during anesthesia with MS-222 (Mocho et al., 2022), further underscores the method's potential to reduce potential stress.

Among the waveform types tested - direct current (DC), pulsed direct current (PDC), and alternating current (AC) - sinusoidal AC was most suitable for euthanizing larval zebrafish. While all waveforms induced rapid behavioral incapacitation, DC and low-frequency PDC caused severe morphological damage, such as body axis deformities and tissue ruptures, likely due to strong muscle contractions (Lines et al., 2003; Nordgreen et al., 2008; Robb et al., 2002) and higher Joule heating during exposure. These effects are not only welfare-relevant but could also compromise subsequent applications, such as tissue analysis. In contrast, AC treatments produced minimal structural abnormalities, with temperature increases remaining within biologically tolerable limits (<38 °C) (Ádám et al., 2000; Halloran et al., 2000; Hardy et al., 2007; Murtha and Keller, 2003). This also minimizes emotional discomfort for observers and operators - an often-overlooked but still important aspect of humane euthanasia ("AVMA Guidelines for the Euthanasia of Animals," 2020). Given its efficacy, low risk of tissue damage, and compatibility with standard laboratory settings, AC at 50 V/cm and 60 Hz is recommended for electrical euthanasia of zebrafish larvae.

These findings show that electrical stunning with optimized parameters (50 V/cm AC, 60 Hz, 32 s) provides a highly effective and humane euthanasia method for zebrafish larvae. Although tested specifically at 4 dpf, the method should be equally effective for older larvae, as sensitivity to electric fields is thought to increase with body size (Bohl et al., 2010). The immediate loss of equilibrium and complete cessation of coordinated stimulus-driven brain activity indicate rapid unconsciousness. As electrical stunning is already a permitted euthanasia method for fish in the European Union, its adoption in laboratory protocols would offer a meaningful refinement aligned with the 3Rs principle.

6.1.2. Slow Propagating Calcium Waves

During the investigation of neuronal activity alongside simultaneous electrical stunning, a rapid and synchronous rise in intracellular calcium levels - a fast-propagating calcium wave - that coincided with the onset of the electric field could be observed. This initial calcium influx is likely driven by electroporation-induced transmembrane ion flow, particularly from the extracellular space (Cho et al., 1999), and may contribute to mitochondrial dysfunction, ATP depletion, and subsequent disruption of ionic homeostasis, ultimately leading to cell death (Duchen, 1999; Garcia-Dorado et al., 2012; Hajnóczky et al., 2003; Smaili et al., 2009). Although the precise mechanisms of organismal death via this AC-based electrical stunning remain to be fully elucidated, the involvement of multiple, potentially interacting, cell death pathways is probable (Batista Napotnik et al., 2021). In addition to this initial wave, a series of slow propagating calcium waves emerged in the larval zebrafish brain approximately 10-15 minutes after treatment. Preliminary and unpublished epifluorescence recordings of individual 4 dpf transgenic zebrafish larvae showed that these waves tend to propagate from caudal to rostral brain regions with variable velocities and intensities – displaying an increase in speed over time (Figure 11B). Their onset occurred several minutes after electrical exposure and persisted as discrete events, often recurring multiple times per individual fish with an inter-wave interval of approximately 10 min (Figure 11A).

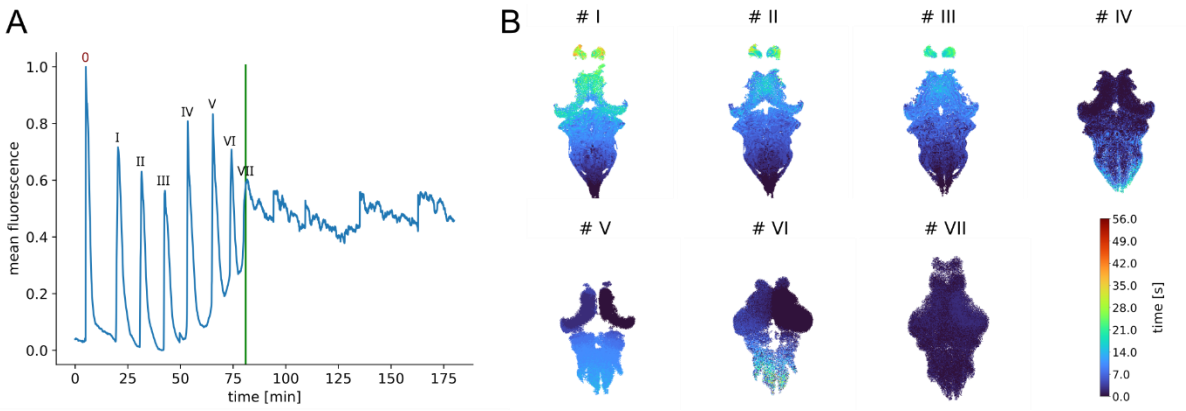

Figure 11: Preliminary results for slow propagating calcium waves following electrical stunning. A) Normalized mean fluorescence intensity of video frames. Peak 0 marks the initial wave during electrical stunning. Peak I and following mark the slow propagating waves following electrical stunning. B) Individual lag maps for each slow propagating wave in A (Burkhardt and Fischer et al., unpublished).

Interestingly, similar waves could be observed in fish euthanized by sodium azide (data not shown), a chemical that induces cell death via mitochondrial dysfunction without directly disturbing membrane integrity or ionic gradients. Although the spatial and temporal characteristics of the sodium azide-induced calcium waves and also their origins differed from those observed post-electrical stunning, this finding might suggest that the phenomenon is not specific to electrical stunning or electroporation-related damage. Instead, it could imply a broader physiological response, potentially linked to the cellular processes of organismal death or coordinated ionic dysregulation during terminal neuronal collapse. These calcium waves could not be observed in surviving fish. Thus, the presence of these waves correlated strongly with irreversible organismal death, rather than reversible neuronal silencing or immobilization.

Brust-Mascher and Webb (1998) first reported calcium waves in fish keratocytes after application of electrical pulses with a voltage gradients ranging from 55 to 120 V/cm (Brust-Mascher and Webb, 1998). These waves exhibited a rapid rise phase and a slow decay, propagating within the cell at an average speed of 66 ± 40 µm/s. These characteristics closely resemble those of the initial calcium wave observed in the zebrafish brain during electrical stunning in the present study, which also propagated across the brain within a few seconds. According to Brust-Mascher and Webb, the electric field stimulated calcium influx through plasma membrane calcium channels. Once intracellular calcium reached a certain threshold, additional calcium was thought to be released from internal stores, leading to a propagating wave. Notably, they excluded electroporation as the underlying mechanism for the initial calcium rise, as no structural damage to cells was observed. Observations of slow propagating calcium waves following an initial event also comes from Xu et al. (2017), who described a calcium wave in the zebrafish brain that started in the hindbrain approximately 1801 ± 291.2 seconds after cardiac arrest and propagated in a caudal-to-rostral direction (Xu et al., 2017). This wave was associated with neuronal death and brain damage. The delay between cardiac arrest and the onset of this wave is comparable to the timing of the first slow propagating calcium wave observed in this study post electrical stunning, and the slow propagation speed described by Xu et al. also closely matches our observations (approximately 48 seconds across the brain). Similar waves have also been reported in rats following decapitation, where massive ion channel activation results in a loss of membrane potential and synchronized neuronal depolarization. Rijn et al. (2011) recorded a slow (5-15s), large-amplitude EEG wave approximately 50

seconds after decapitation of a rat (Rijn et al., 2011). This wave was hypothesized to result from a massive opening of ion channels leading to a depolarizing event. Due to the lack of energy following decapitation, neurons could no longer maintain their transmembrane potential, resulting in oscillations and ultimately the observed wave, which has been interpreted as a marker of neuronal death (Zandt et al., 2011).

The multiple slow-propagating waves observed in the present study post electrical stunning also share some features with a phenomenon known as spreading depolarization (SD), which was previously described in both mammalian and insect brains. SD refers to a slow-moving wave of depolarization that propagates across brain tissue at a velocity of 2-6 mm/min (Takano et al., 2007). This leads to a complete loss of membrane potential due to ionic gradient collapse, resulting in transient silencing of neural activity. In mammals, SD has been associated with neuronal damage in the context of stroke and traumatic brain injury (Dreier and Reiffurth, 2015; Shuttleworth et al., 2020), and it has also been observed in neurocritical care settings in humans, where it transiently suppresses cortical activity. SD is further associated with structural cellular alterations such as swelling, fragmentation of the endoplasmic reticulum, dendritic spine disruption, and other morphological distortions (Shuttleworth et al., 2020).

Slow propagating calcium waves observed in zebrafish larvae following electrical stunning and subsequent death might likely reflect a process of progressive bioenergetic collapse that triggers recurrent spreading depolarization-like events rather than left over physiological neuronal activity. During electrical stunning neural tissue is exposed to strong electric fields capable of inducing membrane depolarization and electroporation, resulting in uncontrolled ion flux and acute calcium entry into neurons (Cho et al., 1999; Morotomi-Yano et al., 2014). Although most cells may survive the immediate exposure, electroporation-associated membrane injury and calcium overload will most likely impair mitochondrial function, leading to delayed ATP depletion and gradual failure of ATP-dependent ion pumps such as the Na^+/K^+-ATPase (Duchen, 1999; Garcia-Dorado et al., 2012; Nicholls, 2008). As metabolic reserves decline, extracellular potassium accumulates and glutamate might be released from depolarized neurons, conditions known to trigger SD (Andrew et al., 2017; Astrup et al., 1980; Leis et al., 2005). During SD, neurons undergo massive sodium and calcium influx accompanied by potassium efflux, producing large intracellular calcium transients (Ayata and Lauritzen, 2015; Dreier, 2011). In metabolically compromised

brain tissue, SD events can recur repeatedly and eventually culminate in terminal spreading depolarization, marking the irreversible collapse of neuronal ion homeostasis (Dreier et al., 2018). Experimental inhibition of mitochondrial respiration using sodium azide induces neuronal calcium influx, demonstrating that metabolic failure alone can generate large calcium elevations resembling those seen after electrical stunning (Marino et al., 2007). Furthermore, SD events impose substantial energetic demands because restoration of ion gradients requires ATP, and repeated waves are commonly observed in metabolically stressed tissue as partial recovery alternates with renewed depolarization (Bosche et al., 2010; Dreier et al., 2017). Calcium in this context likely acts primarily as a downstream reporter of global ionic collapse rather than the principal propagating signal, as extracellular potassium accumulation and glutamate-mediated depolarization are considered the main drivers of SD propagation (Andrew et al., 2017). Together, these findings support a model in which electrical stunning initiates membrane injury and mitochondrial dysfunction, leading to energy failure after a latent period that triggers spreading depolarization-like waves due to increased extracellular potassium levels whose associated calcium influx appears as the slow propagating waves observed in zebrafish brain tissue.

6.1.3. Open Questions regarding Electrical Stunning as a Euthanasia Method

Besides the still not fully answered question about the mechanism and the meaning of the slowly propagating calcium waves, two further questions with regard to electrical stunning of zebrafish larvae remain unanswered. First, although electrical stunning has an immediate onset, causing fish to lose equilibrium, behavior, and coordinated neuronal activity within a second, the extent of stress larvae experience during exposure is unclear. Second, it is unknown how much the method damages the larvae's tissue, which could potentially complicate or even prevent subsequent post-mortem experiments such as toxicology, morphological studies, or transcriptomics.

In the past, stress as a result of exposure to different noxious stimuli was measured using the stress protein (hsp70) response in zebrafish larvae (Bai et al., 2022; Scheil et al., 2010; Xiong et al., 2017). To investigate potential stress during electrical stunning and hopefully further confirm the method as a more humane alternative than overdoses with MS-222 or hypothermia, hsp70-measurements could be conducted within all three groups, allowing direct comparison of stress responses to the

euthanasia methods. Another way of quantifying stress during and after electrical exposure could be the measurements of cortisol which is as major stress hormone regulating multiple organismal responses to stressful stimuli (Mommsen et al., 1999). Whole-body or tissue cortisol assays exist which could be used for that purpose, allowing a final confirmation of electrical stunning as a humane and less stressful euthanasia method (Steenbergen et al., 2012; Yeh et al., 2013).

To examine possible morphological effects of electrical stunning on different zebrafish tissues, zebrafish tissue could be analyzed post electrical stunning using hematoxylin and eosin staining of both treated and control larvae (Sabaliauskas et al., 2006). Such stainings would allow for a precise description of zebrafish morphology after exposure and investigation of possible alterations like neuronal swelling or shrinking, abnormal intercellular spaces, signs of hypertrophy, atrophy, karyolitic processes and many more and have already been used in the past to characterize morphological changes after euthanasia via MS-222 and eugenol (Ayala-Soldado et al., 2023).

6.1.4. Electrical Stunning: Limitations and further Directions

The electrical stunning setups introduced in this thesis were developed solely for larval zebrafish. However, for daily use in routine laboratory procedures, where both larval and adult zebrafish must be euthanized for various reasons, this represents a current limitation. To enable regular use beyond larvae, a more robust and user-friendly electrical stunning chamber must be developed. Ideally, it should be 3D-printable, allowing laboratories worldwide to easily fabricate it themselves. Additionally, the chamber's capacity should be increased for convenience, and the setups adapted for adult fish. Finally, the electric circuits generating the field must be simplified, eliminating the need for the programmable power source used in this study. One approach is to design a modular stunning system compatible with standard zebrafish housing or breeding tanks. A preliminary layout demonstrated its feasibility (Figure 12). By adjusting the distance between the two electrodes, the setup can accommodate both larval and adult zebrafish using the same electrical circuit.

Beyond further development of the setup itself, applying an electrical field to zebrafish larvae may offer further opportunities to refine experimental procedures and help establish standards for behavioral assays in larval zebrafish. One promising avenue is the adaptation of electrical stunning as a reversible anesthesia method for larval and

adult zebrafish. The aim would be to achieve a rapid, consistent, and fully reversible anesthetic state through the applications of electrical fields without triggering aversive behaviors, physiological stress, or longer lasting effects (Francis and Dingley, 2015). The experimental platform developed in this study already allows precise exposure of larval zebrafish to different electrical fields while monitoring behavioral and neurophysiological responses in real time using IR-camera recording and 2-photon calcium imaging. By systematically varying parameters such as voltage type, amplitude, frequency, and exposure duration, conditions that reliably suppress sensory processing and motor output while enabling full recovery within a defined timeframe could potentially be found. This approach would provide a non-pharmacological alternative to chemical anesthetics like MS-222, which often elicit aversive reactions and exhibit variable efficacy in larvae (Mocho et al., 2022). It could also streamline workflows by eliminating preparation and washout times. Preliminary work which investigated so called electro immobilization does exist (Nguyen et al., 2019; Reid et al., 2019) and underpins the feasibility of electroanesthesia. Since the induction of unconsciousness is rapid and predictable at defined voltage gradients, I hypothesize that adjusting amplitude or exposure time could enable temporary neural suppression below the threshold for irreversible damage.

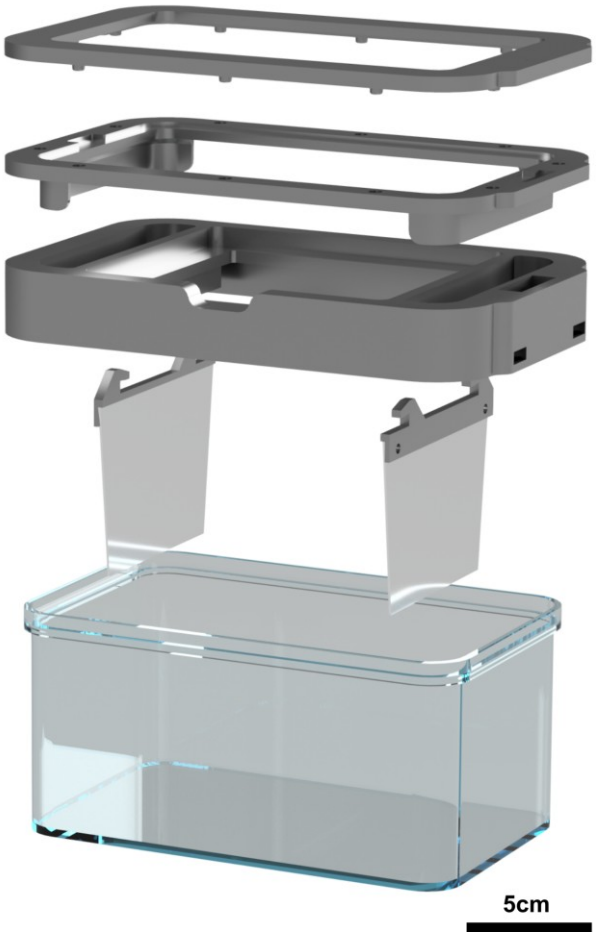

Figure 12: Concept drawing of a 3D-printable setup. Concept drawing of a modular and 3D-printable setup for electrical stunning, suitable for both larval and adult zebrafish and compatible with standard zebrafish breeding tanks (Burkhardt et al., unpublished).

Electrical stunning offers a promising methodological advancement for zebrafish research. The developed setups enable controlled application of electrical fields while remaining compatible with common experimental approaches such as behavioral tracking and two-photon calcium imaging. Our results demonstrate that AC-based

electrical stimulation induces rapid loss of behavioral responsiveness and suppression of visually evoked neural activity, supporting its potential as a reliable and humane alternative to current euthanasia protocols. Although further work is required to refine parameters and adapt the system for broader laboratory use, the presented approach provides a practical and accessible solution for implementing electrical stunning in zebrafish experiments.

Having addressed this methodological challenge and thereby bringing zebrafish animal welfare closer to standards used in mammals, the discussion now turns to the second major topic of this thesis: the investigation of vertical eye movements in larval zebrafish. Like the field of electrical stunning, this area has historically received comparatively little methodological attention. As discussed in the following sections, the newly developed camera-based eye-tracking approaches enabled robust investigation of vertical eye movements alongside visual and vestibular stimulation while revealing important limitations of current camera-based experimental setups that point toward future technical improvements.

6.2. Vertical Optokinetic Eye Movements

6.2.1. vOKR vs. vVOR Performance

In contrast to the robust horizontal optokinetic response (hOKR), the vertical optokinetic response (vOKR) in larval zebrafish exhibits much reduced performance. During constant rotation stimuli, the vOKR consists of a brief initial eye movement toward the stimulus, followed by a plateau phase at ~10° deflection without further tracking or resetting saccades - unlike the hOKR's well-defined alternating slow and quick phases. This absence of vertical resetting saccades is in contrast with reports in adult goldfish, which display occasional but distinct vertical quick phases despite minimal slow-phase responses (Tadokoro et al., 2025). The reason of the difference so far is unclear but may reflect developmental or species-specific adaptations (Easter and Nicola, 1996; Leary et al., 2025).

During vOKR stimulation, larval zebrafish frequently generate saccades that most of the time include both a horizontal and vertical component. These saccades are not stimulus-locked, indicating they are rather spontaneous than visually driven. Notably, this activity occurs under visual stimulation but is entirely suppressed during vestibular

stimulation, suggesting that vestibular inputs exert stronger inhibition on spontaneous saccade generation than visual inputs in the vertical domain. From an ethological perspective, a strong vOKR may offer limited functional utility for larval zebrafish. Vertical rotations most likely occur infrequently or are rapidly compensated by vestibular and postural reflexes, thereby reducing the need for prolonged vertical gaze stabilization through the OKR. (Masseck and Hoffmann, 2009; Robinson, 1981; Sugioka et al., 2023). Furthermore, while spontaneous vertical saccades are uncommon, their presence indicate that the oculomotor apparatus and extraocular muscles can accommodate vertical movements – which rules out mechanical constraints as the basis for the diminished vOKR amplitude and gain.

Interestingly, the tuning properties of the transient vOKR - such as spatial frequency and angular velocity preferences - closely match those of the hOKR, indicating that early visual processing is not the bottleneck. This observation, together with the larger dynamic range observed in vVOR, indicates limitations within the visuomotor transformation pathway. In particular, motoneurons exhibiting high vertical eye position thresholds could be selectively engaged by vestibular rather than visual inputs (Aksay et al., 2000; Brysch et al., 2019), or there may be distinct motoneuron populations specialized for different saccadic types (Brysch et al., 2019; Dowell et al., 2025; Leyden et al., 2021).

6.2.2. Phase Advance at lower Repetition Rates

In this study, a striking phase advance was found in the vertical optokinetic response of larval zebrafish during low-frequency sinusoidal stimulation. Specifically, the eyes began to reverse their direction prior to the stimulus during the deceleration phase of unidirectional motion. This finding seems counterintuitive, as optokinetic responses typically exhibit a phase lag, reflecting inherent sensorimotor delays. The consistency and immediacy of this behavior across stimulus repetitions strongly argue against learned or predictive mechanisms, which would require longer periods of exposure or explicit training (Marsh and Baker, 1997; Miki et al., 2018). Interestingly, this phase advance shares some similarities with the motion aftereffect (MAE) - a phenomenon where prolonged motion exposure leads to illusory motion in the opposite direction (Anstis et al., 1998). However, several key differences suggest a different underlying mechanism. Unlike the classic MAE, the observed eye reversal occurred while the

visual stimulus was still in motion and was reliably elicited after only a few seconds of stimulation - much shorter than the durations typically required to induce MAE in zebrafish (Pérez-Schuster et al., 2016; Wu et al., 2020). One possible account for the phase advance involves reciprocal inhibition between two populations of direction-selective neurons tuned to opposing velocities. Over time, the population selective for the stimulus direction might adapt, narrowing the activity gap between the two groups until stimulus deceleration disinhibits the non-preferred population, eliciting a reverse-direction vOKR. Yet, this adaptation occurs far more rapidly than prior reports of motion aftereffect in zebrafish (Pérez-Schuster et al., 2016; Wu et al., 2020). Alternatively, phase advances might arise because DS neurons - beyond velocity tuning - are also sensitive to acceleration (Cao et al., 2004; Thiel et al., 2007), interpretable as swift adaptation; hence, they could drop activity even as the stimulus persists in the same direction without acceleration. Here, opposing eye movements need not be visually guided but could stem from passive elastic recoil within the oculomotor plant (Miri et al., 2022). Consistent with this idea, centripetal movements emerged only after stimulus velocity reversal, such that vOKR toward eccentric positions invariably matched stimulus direction. One way to disentangle these possibilities would be to use a visual vOKR stimulus that, after a short period of acceleration followed by constant stimulus velocity, ends in one of three ways: a sudden stop of motion, prolonged stimulus movement without changing velocity, or a defined deceleration trajectory approaching 0 °/s. Depending on the eye's response, this would provide further evidence on whether the observed phase advance reflects MAE-like behavior or acceleration tuning and passive back drift.

6.2.3. Dual Camera Eye Tracking: Limitations and further Directions

In this study a dual-camera system was used for concurrent tracking of vertical and horizontal eye movements in larval zebrafish. Compared to single-plane tracking methods, this is a substantial improvement, as different eye movements in multiple planes can be recorded simultaneously (Figure 13A). However, this method which also involves fitting ellipses to binarized eye images from two orthogonally aligned cameras imposes a fundamental constraint on accuracy and robustness for multi-axis eye movements, arising from optical distortions and geometric uncertainties in projecting the 3D eye onto 2D planes. Specifically, rotations involving both horizontal and vertical

movements cause apparent geometry changes in camera views that do not linearly correspond to actual angular displacements. This highlights a general problem: the eyes of larval zebrafish are not ideal for camera-based tracking solutions. From a dorsal view, the laterally placed eyes have an elliptical shape, making visual tracking of horizontal eye movements - based on background subtraction and subsequent ellipse fitting, using the angle of the major axis as a readout of eye position - straightforward. From a frontal view, the eyes also have a slightly elliptical shape, allowing an easy initial ellipse fit, which however changes once the fish start moving its eyes horizontally (Katz et al., 2021).

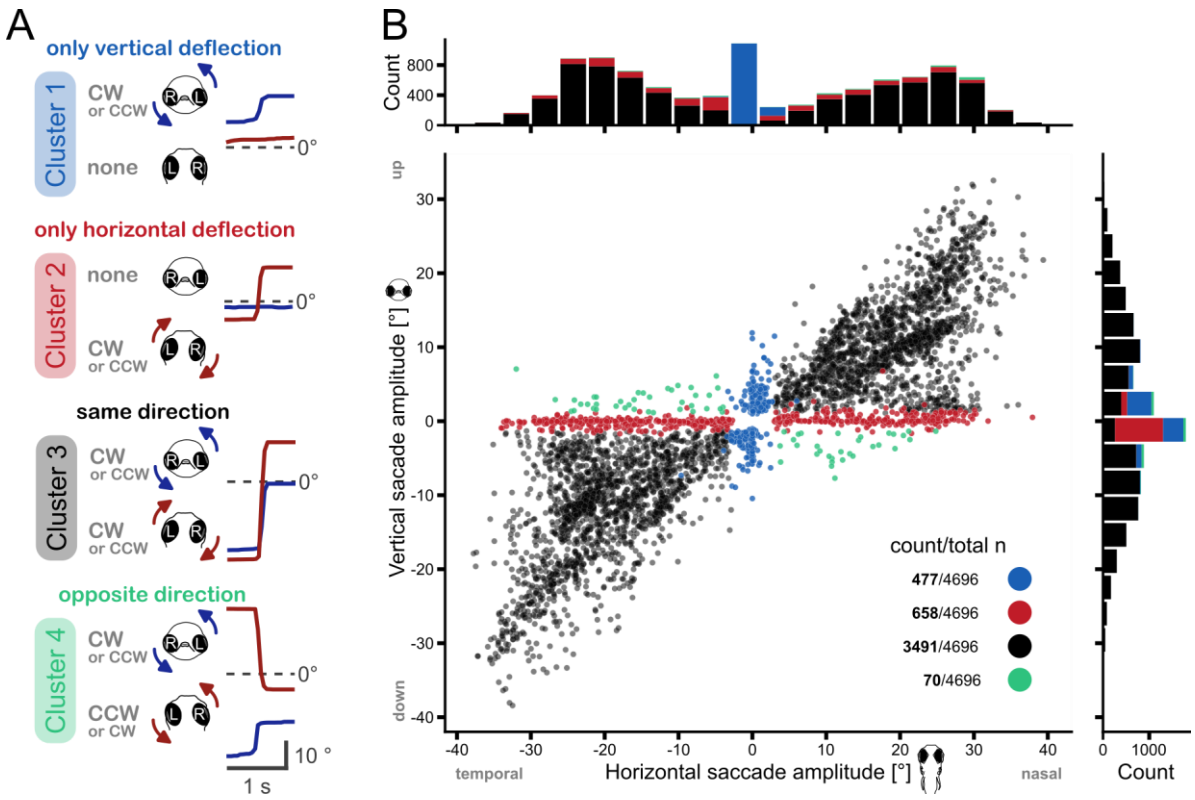

Figure 13: Saccade Clusters during vertical OKR (vOKR) stimulation. (A) Four different saccade types have been observed and can be distinguished by their appearance in the vertical and horizontal eye trace. Example vertical (blue) and horizontal (red) eye traces show characteristics of each cluster type. Scale on the right corresponds to all eye traces. Note, that cluster 3 and 4 contain both mixed (vertical-horizontal) and pure horizontal saccades. Cluster 3 and 4 were therefore not further analyzed. (B) Scatterplot of apparent horizontal and vertical amplitudes of all observed saccades, clustered by the saccade type during vOKR stimulus (adapted from Burkhardt et al., 2026).

Therefore, two problems arise when tracking vertical eye movements. First, during large horizontal eye movements, the frontal projection shifts from elliptical towards spherical, which can alter the major axis angle and thus yield false vertical eye

positions. This projection artifact becomes even more pronounced when the fish's eyes are slightly rotated around the torsional axis - for example, if it is not perfectly horizontally embedded. Second, from the front, the laterally placed eyes are partially obscured by the fish's body - which, although transparent - may interfere with background subtraction and subsequent ellipse fitting. These problems are unlikely to affect horizontal eye tracking, as vertical movements are too small to significantly alter the major axis, and the fish's body is much thinner from dorsal to ventral than from caudal to rostral, making transillumination and background subtraction much easier. These compound motions thus generate a “crosstalk”, appearing as eye movements in both horizontal and vertical planes despite potentially dominant uniaxial component (Figure 13B, cluster 3 and 4). A prominent challenge therefore is the misinterpretation of mixed saccades - those with both vertical and horizontal components - due to the described projection artifacts. Especially when large horizontal deflections lead to more circular projections in the frontal view, this increases uncertainty in vertical orientation estimates, leading to over- or underestimation of small vertical components. This issue was evident in the data, where slow-quick phase dynamics characteristic of the horizontal optokinetic response (hOKR) appeared - albeit at reduced amplitudes - in the vertical traces. Although these might suggest true vertical components during hOKR, projection distortions confound such interpretations. While metrics like changes in minor axis length effectively validated pure vertical or horizontal saccades, they fail to decompose multidimensional movements under dynamic stimuli. Given the zebrafish eye's anatomy and oculomotor range, many saccades and optokinetic responses might likely involve multi-axis motion.

Future refinements of the experimental setup could allow disentangling vertical, horizontal, and torsional components of eye motion. In mammals, precise tracking of 3D-eye-positions is often reached by using search coils that precisely measure the eye’s position as the animal moves them within a magnetic field (Bartl et al., 1996; Hess et al., 1992; Kenyon, 1985; Tweed et al., 1990). Due to the tiny eyes of larval zebrafish and the fact that they move underwater, search coils unfortunately are no real option, leaving video recording as the only viable option for tracking eye motion. Another approach for video recording of eye movements could be the use of retroreflective markers glued to the fish’s eye, enabling precise 3D tracking. This approach has been successfully applied in adult goldfish (Tadokoro et al., 2025),

however, the small size of the larval zebrafish eye again makes this approach nearly impossible. One straightforward extension would therefore be the addition of a third camera, for example positioned at an oblique angle or along the rostral-caudal axis. This configuration would provide a third projection plane, enabling full 3D triangulation of eye surface markers via stereophotogrammetric methods. Such approaches are well established in biomechanics (Chhimpa et al., 2025) and could, in principle, be adapted to larval zebrafish through the use of high-resolution optics and synchronized imaging. As an alternative to multi-camera hardware, inverse kinematic models based on the known anatomical geometry of the eye could be employed to infer 3D orientations from 2D projections. These models could incorporate symmetry assumptions, biomechanical rotation constraints, and the geometry of extraocular muscle attachments. Optimization algorithms could then be used to estimate eye orientations that best reproduce the observed elliptical projections across one or multiple views.

6.3. Conclusion

A central motivation of this thesis was to address a growing imbalance in zebrafish neuroscience: while neural recording technologies have advanced rapidly, behavioral and animal welfare methodologies have lagged behind. The guiding principle of this work was therefore to develop methodological solutions that expand behavioral access while remaining practical, modular, and readily adoptable within existing experimental infrastructures.

The electrical stunning platform is one such innovation. It enables controlled exposure of zebrafish larvae to defined electrical fields while remaining compatible with behavioral tracking and two-photon imaging. This technically accessible system facilitates investigations and implementation of electrical stunning as a euthanasia method. The rapid loss of behavioral responsiveness and suppression of visually evoked neural activity under AC stimulation suggest it as a fast, reproducible alternative to common methods like anesthetic overdose or hypothermic shock. Crucially, it aligns with the refinement principle of the 3Rs by minimizing potential stress and suffering.

This thesis's second contribution tackles another but equally important key limitation in larval zebrafish behavioral assays: the restricted dimensionality of traditional eye-

tracking methods. While the horizontal optokinetic response has long been a standard for visuomotor studies, vertical eye movements have received little attention despite their ecological and neurobiological importance. The dual-camera tracking system developed here simultaneously measures vertical and horizontal movements, revealing a distinct vertical optokinetic response with dynamic properties differing from the horizontal one.

When evaluated against the guiding principle of this thesis - methods that meaningfully expand behavioral access while remaining technically accessible - the two methodological approaches offer complementary strategies. Electrical stunning refines experimental conditions and enhances animal welfare, while multidimensional eye tracking enriches measurable behavioral outputs, forging stronger links between neural activity and behavior. The results presented and discussed in this thesis demonstrate that both methodologies enabled the discovery of novel findings: namely, the first parameter set for humane and rapid euthanasia of zebrafish larvae, supported by comprehensive behavioral and neurophysiological data, and the first characterization of vertical eye movements in larval zebrafish, encompassing both visually and vestibularly driven movements. Both technical approaches prioritize modular design, compatibility with existing imaging pipelines, and use of widely available components, lowering adoption barriers for labs without specialized engineering expertise.

Among the outlined future directions, expanding multidimensional behavioral measurements holds particular promise. As brain-wide neural recordings become widely used, capturing comparably rich behavioral data will be essential for signal interpretation. Extending behavioral assays beyond single-dimensional readouts - such as purely horizontal eye movements - towards more comprehensive descriptions of sensorimotor behavior therefore represents a critical step towards bridging neural dynamics and behavior. In this sense, the methodological developments presented in this thesis should be viewed less as finalized experimental tools and more as conceptual frameworks for expanding the zebrafish behavioral toolkit. By demonstrating that practical, modular, and accessible solutions can substantially increase behavioral resolution in zebrafish experiments, this work contributes to the broader effort of aligning behavioral methodologies with the rapidly advancing technologies used to observe the vertebrate brain.

Bibliography

Ádám, A., Bártfai, R., Lele, Z., Krone, P.H., Orbán, L., 2000. Heat-Inducible Expression of a Reporter Gene Detected by Transient Assay in Zebrafish. Exp. Cell Res. 256, 282–290. https://doi.org/10.1006/excr.2000.4805

Ahrens, M.B., Orger, M.B., Robson, D.N., Li, J.M., Keller, P.J., 2013. Whole-brain functional imaging at cellular resolution using light-sheet microscopy. Nat. Methods 10, 413–420. https://doi.org/10.1038/nmeth.2434

Aksay, E., Baker, R., Seung, H.S., Tank, D.W., 2000. Anatomy and Discharge Properties of Pre-Motor Neurons in the Goldfish Medulla That Have Eye-Position Signals During Fixations. J. Neurophysiol. 84, 1035–1049. https://doi.org/10.1152/jn.2000.84.2.1035

Amores, A., Catchen, J., Ferrara, A., Fontenot, Q., Postlethwait, J.H., 2011. Genome Evolution and Meiotic Maps by Massively Parallel DNA Sequencing: Spotted Gar, an Outgroup for the Teleost Genome Duplication. Genetics 188, 799–808. https://doi.org/10.1534/genetics.111.127324

Andrew, R.D., Hsieh, Y.-T., Brisson, C.D., 2017. Spreading depolarization triggered by elevated potassium is weak or absent in the rodent lower brain. J. Cereb. Blood Flow Metab. 37, 1735–1747. https://doi.org/10.1177/0271678X16657344

Anisman, H., McIntyre, D.C., 2002. Conceptual, Spatial, and Cue Learning in the Morris Water Maze in Fast or Slow Kindling Rats: Attention Deficit Comorbidity. J. Neurosci. 22, 7809–7817. https://doi.org/10.1523/JNEUROSCI.22-17-07809.2002

Anstis, S., Verstraten, F.A.J., Mather, G., 1998. The motion aftereffect. Trends Cogn. Sci. 2, 111–117. https://doi.org/10.1016/S1364-6613(98)01142-5

Arqué, G., Fotaki, V., Fernández, D., Lagrán, M.M. de, Arbonés, M.L., Dierssen, M., 2008. Impaired Spatial Learning Strategies and Novel Object Recognition in Mice Haploinsufficient for the Dual Specificity Tyrosine-Regulated Kinase-1A (Dyrk1A). PLOS ONE 3, e2575. https://doi.org/10.1371/journal.pone.0002575

Arvin, S., Rasmussen, R.N., Yonehara, K., 2021. EyeLoop: An Open-Source System for High-Speed, Closed-Loop Eye-Tracking. Front. Cell. Neurosci. 15. https://doi.org/10.3389/fncel.2021.779628

Ashley, P.J., Sneddon, L.U., McCrohan, C.R., 2007. Nociception in fish: stimulus–response properties of receptors on the head of trout *Oncorhynchus mykiss*. Brain Res. 1166, 47–54. https://doi.org/10.1016/j.brainres.2007.07.011

Ashley, P.J., Sneddon, L.U., McCrohan, C.R., 2006. Properties of corneal receptors in a teleost fish. Neurosci. Lett. 410, 165–168. https://doi.org/10.1016/j.neulet.2006.08.047

Astrup, J., Rehncrona, S., Siesjö, B.K., 1980. The increase in extracellular potassium concentration in the ischemic brain in relation to the preischemic functional activity and cerebral metabolic rate. Brain Res. 199, 161–174. https://doi.org/10.1016/0006-8993(80)90238-3

AVMA Guidelines for the Euthanasia of Animals [WWW Document], 2020. URL https://olaw.nih.gov/policies-laws/avma-guidelines-2020.htm (accessed 1.14.22).

Ayala-Soldado, N., Mora-Medina, R., Lora-Benítez, A.J., Gonçalves Reis, L. de P., Molina-López, A.M., Moyano-Salvago, M. del R., 2023. Comparative study of

tricaine methanesulfonate (MS-222) and eugenol as euthanasia agents in zebrafish (Danio rerio) as an experimental model. Lab. Anim. 57, 236–246. https://doi.org/10.1177/00236772221143939
Ayata, C., Lauritzen, M., 2015. Spreading Depression, Spreading Depolarizations, and the Cerebral Vasculature. Physiol. Rev. 95, 953–993. https://doi.org/10.1152/physrev.00027.2014
Bagnall, M.W., Schoppik, D., 2018. Development of vestibular behaviors in zebrafish. Curr. Opin. Neurobiol., Developmental Neuroscience 53, 83–89. https://doi.org/10.1016/j.conb.2018.06.004
Bai, L., Shi, P., Jia, K., Yin, H., Xu, J., Yan, X., Liao, K., 2022. Triflumizole Induces Developmental Toxicity, Liver Damage, Oxidative Stress, Heat Shock Response, Inflammation, and Lipid Synthesis in Zebrafish. Toxics 10, 698. https://doi.org/10.3390/toxics10110698
Baier, H., Wullimann, M.F., 2021. Anatomy and function of retinorecipient arborization fields in zebrafish. J. Comp. Neurol. 529, 3454–3476. https://doi.org/10.1002/cne.25204
Bartl, K., Siebold, C., Glasauer, S., Helmchen, C., Büttner, U., 1996. A simplified calibration method for three-dimensional eye movement recordings using search-coils. Vision Res. 36, 997–1006. https://doi.org/10.1016/0042-6989(95)00201-4
Batista Napotnik, T., Polajžer, T., Miklavčič, D., 2021. Cell death due to electroporation – A review. Bioelectrochemistry 141, 107871. https://doi.org/10.1016/j.bioelechem.2021.107871
Beck, J.C., Gilland, E., Tank, D.W., Baker, R., 2004. Quantifying the Ontogeny of Optokinetic and Vestibuloocular Behaviors in Zebrafish, Medaka, and Goldfish. J. Neurophysiol. 92, 3546–3561. https://doi.org/10.1152/jn.00311.2004
Behavioral Research [WWW Document], 2026. URL https://www.harvardapparatus.com/behavioral-research.html (accessed 2.10.26).
Bellegarda, C., Auer, F., Schoppik, D., 2025. Zebrafish as a model to understand extraocular motor neuron diversity. Curr. Opin. Neurobiol. 90, 102964. https://doi.org/10.1016/j.conb.2024.102964
Bianco, I.H., Kampff, A.R., Engert, F., 2011. Prey Capture Behavior Evoked by Simple Visual Stimuli in Larval Zebrafish. Front. Syst. Neurosci. 5. https://doi.org/10.3389/fnsys.2011.00101
Bianco, I.H., Ma, L.-H., Schoppik, D., Robson, D.N., Orger, M.B., Beck, J.C., Li, J.M., Schier, A.F., Engert, F., Baker, R., 2012. The Tangential Nucleus Controls a Gravito-inertial Vestibulo-ocular Reflex. Curr. Biol. 22, 1285–1295. https://doi.org/10.1016/j.cub.2012.05.026
Bilotta, J., Saszik, S., 2001. The zebrafish as a model visual system. Int. J. Dev. Neurosci. 19, 621–629. https://doi.org/10.1016/S0736-5748(01)00050-8
Bohl, R.J., Henry, T.B., Strange, R.J., 2010. Electroshock-induced mortality in freshwater fish embryos increases with embryo diameter: a model based on results from 10 species. J. Fish Biol. 76, 975–986. https://doi.org/10.1111/j.1095-8649.2010.02552.x
Bohl, R.J., Henry, T.B., Strange, R.J., Rakes, P.L., 2009. Effects of Electroshock on Cyprinid Embryos: Implications for Threatened and Endangered Fishes. Trans. Am. Fish. Soc. 138, 768–776. https://doi.org/10.1577/T08-149.1

Boly, M., Moran, R., Murphy, M., Boveroux, P., Bruno, M.-A., Noirhomme, Q., Ledoux, D., Bonhomme, V., Brichant, J.-F., Tononi, G., Laureys, S., Friston, K., 2012. Connectivity Changes Underlying Spectral EEG Changes during Propofol-Induced Loss of Consciousness. J. Neurosci. 32, 7082–7090. https://doi.org/10.1523/JNEUROSCI.3769-11.2012

Bosche, B., Graf, R., Ernestus, R.-I., Dohmen, C., Reithmeier, T., Brinker, G., Strong, A.J., Dreier, J.P., Woitzik, J., 2010. Recurrent spreading depolarizations after subarachnoid hemorrhage decreases oxygen availability in human cerebral cortex. Ann. Neurol. 67, 607–617. https://doi.org/10.1002/ana.21943

Britten, K.H., 2008. Mechanisms of Self-Motion Perception. Annu. Rev. Neurosci. 31, 389–410. https://doi.org/10.1146/annurev.neuro.29.051605.112953

Brockerhoff, S.E., 2006. Measuring the optokinetic response of zebrafish larvae. Nat. Protoc. 1, 2448–2451. https://doi.org/10.1038/nprot.2006.255

Brockerhoff, S.E., Hurley, J.B., Niemi, G.A., Dowling, J.E., 1997. A New Form of Inherited Red-Blindness Identified in Zebrafish. J. Neurosci. 17, 4236–4242. https://doi.org/10.1523/JNEUROSCI.17-11-04236.1997

Brust-Mascher, I., Webb, W.W., 1998. Calcium Waves Induced by Large Voltage Pulses in Fish Keratocytes. Biophys. J. 75, 1669–1678. https://doi.org/10.1016/S0006-3495(98)77609-X

Brysch, C., Leyden, C., Arrenberg, A.B., 2019. Functional architecture underlying binocular coordination of eye position and velocity in the larval zebrafish hindbrain. BMC Biol. 17, 110. https://doi.org/10.1186/s12915-019-0720-y

Budick, S.A., O'Malley, D.M., 2000. Locomotor repertoire of the larval zebrafish: swimming, turning and prey capture. J. Exp. Biol. 203, 2565–2579. https://doi.org/10.1242/jeb.203.17.2565

Burkhardt, D.-S., Arrenberg, A., 2024. Software synchASRcontrol. G-Node. https://doi.org/10.21203/rs.3.rs-4021167/v1

Burkhardt, D.-S., Leyden, C., Thomas, C., Brysch, C., Dehmelt, F.A., Arrenberg, A.B., 2025. Behavioral and neurophysiological effects of electrical stunning on zebrafish larvae. Lab Anim. 1–9. https://doi.org/10.1038/s41684-024-01505-0

Burkhardt, D.-S., Moeller, G., Deligand, L., Fichtner, C., Hladnik, T.C., Arrenberg, A.B., 2026. Vertical Optokinetic Eye Movements in the Larval Zebrafish. J. Exp. Biol. jeb.251770. https://doi.org/10.1242/jeb.251770

Cao, P., Gu, Y., Wang, S.-R., 2004. Visual Neurons in the Pigeon Brain Encode the Acceleration of Stimulus Motion. J. Neurosci. 24, 7690–7698. https://doi.org/10.1523/JNEUROSCI.2384-04.2004

Casali, A.G., Gosseries, O., Rosanova, M., Boly, M., Sarasso, S., Casali, K.R., Casarotto, S., Bruno, M.-A., Laureys, S., Tononi, G., Massimini, M., 2013. A Theoretically Based Index of Consciousness Independent of Sensory Processing and Behavior. Sci. Transl. Med. 5, 198ra105-198ra105. https://doi.org/10.1126/scitranslmed.3006294

Chandroo, K.P., Yue, S., Moccia, R.D., 2004. An evaluation of current perspectives on consciousness and pain in fishes. Fish Fish. 5, 281–295. https://doi.org/10.1111/j.1467-2679.2004.00163.x

Chen, K., Wang, C.-Q., Fan, Y.-Q., Xie, Y.-S., Yin, Z.-F., Xu, Z.-J., Zhang, H.-L., Cao, J.-T., Han, Z.-H., Wang, Y., Song, D.-Q., 2014. The Evaluation of Rapid Cooling As an Anesthetic Method for the Zebrafish. Zebrafish 11, 71–75. https://doi.org/10.1089/zeb.2012.0858

Chhimpa, G.R., Kumar, A., Garhwal, S., Kumar, D., Wani, N.A., Wani, M.A., Shakil, K.A., Chhimpa, G.R., Kumar, A., Garhwal, S., Kumar, D., Wani, N.A., Wani,

M.A., Shakil, K.A., 2025. A Comprehensive Framework for Eye Tracking: Methods, Tools, Applications, and Cross-Platform Evaluation. J. Eye Mov. Res. 18. https://doi.org/10.3390/jemr18050047
Chico, T.J.A., Ingham, P.W., Crossman, D.C., 2008. Modeling Cardiovascular Disease in the Zebrafish. Trends Cardiovasc. Med. 18, 150–155. https://doi.org/10.1016/j.tcm.2008.04.002
CHO, H.J., KIM, J.G., LEE, J.Y., LEE, S., JAHNG, J.W., 2006. Repetitive Dextromethorphan at Adolescence Affects Water Maze Learning in Female Rats. Int. J. Neurosci. 116, 91–101. https://doi.org/10.1080/00207450500341415
Cho, M.R., Thatte, H.S., Silvia, M.T., Golan, D.E., 1999. Transmembrane calcium influx induced by ac electric fields. FASEB J. 13, 677–683. https://doi.org/10.1096/fasebj.13.6.677
Clemence, M., Leaman, J., 2016. Public attitudes to animal research in 2016.
Collewijn, H., 1980. Sensory control of optokinetic nystagmus in the rabbit. Trends Neurosci. 3, 277–280. https://doi.org/10.1016/0166-2236(80)90101-0
Collymore, C., Banks, E.K., Turner, P.V., 2016. Lidocaine Hydrochloride Compared with MS222 for the Euthanasia of Zebrafish (Danio rerio). J. Am. Assoc. Lab. Anim. Sci. 55, 816–820.
Commission Delegated Directive (EU) 2024/1262 of 13 March 2024 amending Directive 2010/63/EU, 2024.
dal Maschio, M., Donovan, J.C., Helmbrecht, T.O., Baier, H., 2017. Linking Neurons to Network Function and Behavior by Two-Photon Holographic Optogenetics and Volumetric Imaging. Neuron 94, 774-789.e5. https://doi.org/10.1016/j.neuron.2017.04.034
Davis, S.N., Zhu, Y., Schoppik, D., 2025. Larval zebrafish maintain elevation with multisensory control of posture and locomotion. J. Exp. Biol. 228, jeb250087. https://doi.org/10.1242/jeb.250087
Deeti, S., O'Farrell, S., Kennedy, B.N., 2014. Early safety assessment of human oculotoxic drugs using the zebrafish visualmotor response. J. Pharmacol. Toxicol. Methods 69, 1–8. https://doi.org/10.1016/j.vascn.2013.09.002
Dehmelt, F.A., Meier, R., Hinz, J., Yoshimatsu, T., Simacek, C.A., Huang, R., Wang, K., Baden, T., Arrenberg, A.B., 2021. Spherical arena reveals optokinetic response tuning to stimulus location, size, and frequency across entire visual field of larval zebrafish. eLife 10, e63355. https://doi.org/10.7554/eLife.63355
Dehmelt, F.A., von Daranyi, A., Leyden, C., Arrenberg, A.B., 2018. Evoking and tracking zebrafish eye movement in multiple larvae with ZebEyeTrack. Nat. Protoc. 13, 1539–1568. https://doi.org/10.1038/s41596-018-0002-0
Del Bene, F., Wyart, C., Robles, E., Tran, A., Looger, L., Scott, E.K., Isacoff, E.Y., Baier, H., 2010. Filtering of Visual Information in the Tectum by an Identified Neural Circuit. Science 330, 669–673. https://doi.org/10.1126/science.1192949
Directive 2010/63/EU, 2010.
Dolan, C.R., Miranda, L.E., 2004. Injury and Mortality of Warmwater Fishes Immobilized by Electrofishing. North Am. J. Fish. Manag. 24, 118–127. https://doi.org/10.1577/M02-115
Dowell, C.K., Hawkins, T., Bianco, I.H., 2025. Subsets of extraocular motoneurons produce kinematically distinct saccades during hunting and exploration. Curr. Biol. 35, 554-573.e6. https://doi.org/10.1016/j.cub.2024.12.010

Dowell, C.K., Lau, J.Y.N., Antinucci, P., Bianco, I.H., 2024. Kinematically distinct saccades are used in a context-dependent manner by larval zebrafish. Curr. Biol. 34, 4382-4396.e5. https://doi.org/10.1016/j.cub.2024.08.008

Dreier, J.P., 2011. The role of spreading depression, spreading depolarization and spreading ischemia in neurological disease. Nat. Med. 17, 439–447. https://doi.org/10.1038/nm.2333

Dreier, J.P., Fabricius, M., Ayata, C., Sakowitz, O.W., William Shuttleworth, C., Dohmen, C., Graf, R., Vajkoczy, P., Helbok, R., Suzuki, M., Schiefecker, A.J., Major, S., Winkler, M.K., Kang, E.-J., Milakara, D., Oliveira-Ferreira, A.I., Reiffurth, C., Revankar, G.S., Sugimoto, K., Dengler, N.F., Hecht, N., Foreman, B., Feyen, B., Kondziella, D., Friberg, C.K., Piilgaard, H., Rosenthal, E.S., Westover, M.B., Maslarova, A., Santos, E., Hertle, D., Sánchez-Porras, R., Jewell, S.L., Balança, B., Platz, J., Hinzman, J.M., Lückl, J., Schoknecht, K., Schöll, M., Drenckhahn, C., Feuerstein, D., Eriksen, N., Horst, V., Bretz, J.S., Jahnke, P., Scheel, M., Bohner, G., Rostrup, E., Pakkenberg, B., Heinemann, U., Claassen, J., Carlson, A.P., Kowoll, C.M., Lublinsky, S., Chassidim, Y., Shelef, I., Friedman, A., Brinker, G., Reiner, M., Kirov, S.A., Andrew, R.D., Farkas, E., Güresir, E., Vatter, H., Chung, L.S., Brennan, K., Lieutaud, T., Marinesco, S., Maas, A.I., Sahuquillo, J., Dahlem, M.A., Richter, F., Herreras, O., Boutelle, M.G., Okonkwo, D.O., Bullock, M.R., Witte, O.W., Martus, P., van den Maagdenberg, A.M., Ferrari, M.D., Dijkhuizen, R.M., Shutter, L.A., Andaluz, N., Schulte, A.P., MacVicar, B., Watanabe, T., Woitzik, J., Lauritzen, M., Strong, A.J., Hartings, J.A., 2017. Recording, analysis, and interpretation of spreading depolarizations in neurointensive care: Review and recommendations of the COSBID research group. J. Cereb. Blood Flow Metab. 37, 1595–1625. https://doi.org/10.1177/0271678X16654496

Dreier, J.P., Major, S., Foreman, B., Winkler, M.K.L., Kang, E.-J., Milakara, D., Lemale, C.L., DiNapoli, V., Hinzman, J.M., Woitzik, J., Andaluz, N., Carlson, A., Hartings, J.A., 2018. Terminal spreading depolarization and electrical silence in death of human cerebral cortex. Ann. Neurol. 83, 295–310. https://doi.org/10.1002/ana.25147

Dreier, J.P., Reiffurth, C., 2015. The Stroke-Migraine Depolarization Continuum. Neuron 86, 902–922. https://doi.org/10.1016/j.neuron.2015.04.004

Driever, W., Solnica-Krezel, L., Schier, A.F., Neuhauss, S.C.F., Malicki, J., Stemple, D.L., Stainier, D.Y.R., Zwartkruis, F., Abdelilah, S., Rangini, Z., Belak, J., Boggs, C., 1996. A genetic screen for mutations affecting embryogenesis in zebrafish. Development 123, 37–46. https://doi.org/10.1242/dev.123.1.37

Duchen, M.R., 1999. Contributions of mitochondria to animal physiology: from homeostatic sensor to calcium signalling and cell death. J. Physiol. 516, 1–17. https://doi.org/10.1111/j.1469-7793.1999.001aa.x

Dunlop, R., Laming, P., 2005. Mechanoreceptive and Nociceptive Responses in the Central Nervous System of Goldfish (Carassius auratus) and Trout (Oncorhynchus mykiss). J. Pain 6, 561–568. https://doi.org/10.1016/j.jpain.2005.02.010

Dunlop, R., Millsopp, S., Laming, P., 2006. Avoidance learning in goldfish (*Carassius auratus*) and trout (*Oncorhynchus mykiss*) and implications for pain perception. Appl. Anim. Behav. Sci. 97, 255–271. https://doi.org/10.1016/j.applanim.2005.06.018

Dwyer, W.P., Erdahl, D.A., 1995. Effects of Electroshock Voltage, Wave Form, and Pulse Rate on Survival of Cutthroat Trout Eggs. North Am. J. Fish. Manag. 15,

647–650. https://doi.org/10.1577/1548-8675(1995)015%253C0647:EOEVWF%253E2.3.CO;2
Easter Jr., S.S., Nicola, G.N., 1997. The development of eye movements in the zebrafish (Danio rerio). Dev. Psychobiol. 31, 267–276. https://doi.org/10.1002/(SICI)1098-2302(199712)31:4%253C267::AID-DEV4%253E3.0.CO;2-P
Easter, Jr., Stephen S., Nicola, G.N., 1996. The Development of Vision in the Zebrafish (Danio rerio). Dev. Biol. 180, 646–663. https://doi.org/10.1006/dbio.1996.0335
Ehrlich, D.E., Schoppik, D., 2017a. Control of Movement Initiation Underlies the Development of Balance. Curr. Biol. 27, 334–344. https://doi.org/10.1016/j.cub.2016.12.003
Ehrlich, D.E., Schoppik, D., 2017b. Control of Movement Initiation Underlies the Development of Balance. Curr. Biol. 27, 334–344. https://doi.org/10.1016/j.cub.2016.12.003
Erickson, R.G., Barmack, N.H., 1980. A comparison of the horizontal and vertical optokinetic reflexes of the rabbit. Exp. Brain Res. 40, 448–456. https://doi.org/10.1007/BF00236153
Favre-Guilmard, C., Auguet, M., Chabrier, P.-E., 2009. Different antinociceptive effects of botulinum toxin type A in inflammatory and peripheral polyneuropathic rat models. Eur. J. Pharmacol. 617, 48–53. https://doi.org/10.1016/j.ejphar.2009.06.047
Feierstein, C.E., Portugues, R., Orger, M.B., 2015. Seeing the whole picture: A comprehensive imaging approach to functional mapping of circuits in behaving zebrafish. Neuroscience, Contributions from different model organisms to brain research 296, 26–38. https://doi.org/10.1016/j.neuroscience.2014.11.046
Feitsma, H., Cuppen, E., 2008. Zebrafish as a Cancer Model. Mol. Cancer Res. 6, 685–694. https://doi.org/10.1158/1541-7786.MCR-07-2167
Ferreira, J.M., Félix, L., Jorge, S., Monteiro, S.M., Olsson, I.A.S., Valentim, A.M., 2022. Anesthesia Overdose Versus Rapid Cooling for Euthanasia of Adult Zebrafish. Zebrafish 19, 148–159. https://doi.org/10.1089/zeb.2022.0001
Fetcho, J.R., Liu, K.S., 1998. Zebrafish as a Model System for Studying Neuronal Circuits and Behavior. Ann. N. Y. Acad. Sci. 860, 333–345. https://doi.org/10.1111/j.1749-6632.1998.tb09060.x
Francis, J., Dingley, J., 2015. Electroanaesthesia – from torpedo fish to TENS. Anaesthesia 70, 93–103. https://doi.org/10.1111/anae.12887
Gabriel, J.P., Trivedi, C.A., Maurer, C.M., Ryu, S., Bollmann, J.H., 2012. Layer-Specific Targeting of Direction-Selective Neurons in the Zebrafish Optic Tectum. Neuron 76, 1147–1160. https://doi.org/10.1016/j.neuron.2012.12.003
Garcia-Dorado, D., Ruiz-Meana, M., Inserte, J., Rodriguez-Sinovas, A., Piper, H.M., 2012. Calcium-mediated cell death during myocardial reperfusion. Cardiovasc. Res. 94, 168–180. https://doi.org/10.1093/cvr/cvs116
Gaylor, D.C., Prakah-Asante, K., Lee, R.C., 1988. Significance of cell size and tissue structure in electrical trauma. J. Theor. Biol. 133, 223–237. https://doi.org/10.1016/S0022-5193(88)80007-9
Gross, J., Farokhkish, B., Cornacione, M., Shaw, S., Nguyen, P.L., Henry, T.B., 2015. Potential Use of Direct Current Electric Fields to Eradicate Rainbow Trout Embryos from Freshwater Ecosystems. North Am. J. Fish. Manag. 35, 871–879. https://doi.org/10.1080/02755947.2015.1059910

Grunwald, D.J., Eisen, J.S., 2002. Headwaters of the zebrafish — emergence of a new model vertebrate. Nat. Rev. Genet. 3, 717–724. https://doi.org/10.1038/nrg892
Haddon, C., Lewis, J., 1996. Early ear development in the embryo of the Zebrafish, Danio rerio. J. Comp. Neurol. 365, 113–128. https://doi.org/10.1002/(SICI)1096-9861(19960129)365:1%253C113::AID-CNE9%253E3.0.CO;2-6
Haffter, P., Granato, M., Brand, M., Mullins, M.C., Hammerschmidt, M., Kane, D.A., Odenthal, J., J. M. van Eeden, F., Jiang, Y.-J., Heisenberg, C.-P., Kelsh, R.N., Furutani-Seiki, M., Vogelsang, E., Beuchle, D., Schach, U., Fabian, C., Nüsslein-Volhard, C., 1996. The identification of genes with unique and essential functions in the development of the zebrafish, Danio rerio. Development 123, 1–36. https://doi.org/10.1242/dev.123.1.1
Hajnóczky, G., Davies, E., Madesh, M., 2003. Calcium signaling and apoptosis. Biochem. Biophys. Res. Commun. 304, 445–454. https://doi.org/10.1016/S0006-291X(03)00616-8
Halloran, M.C., Sato-Maeda, M., Warren, J.T., Jr, Su, F., Lele, Z., Krone, P.H., Kuwada, J.Y., Shoji, W., 2000. Laser-induced gene expression in specific cells of transgenic zebrafish. Development 127, 1953–1960. https://doi.org/10.1242/dev.127.9.1953
Hardy, M.E., Ross, L.V., Chien, C.-B., 2007. Focal gene misexpression in zebrafish embryos induced by local heat shock using a modified soldering iron. Dev. Dyn. 236, 3071–3076. https://doi.org/10.1002/dvdy.21318
He, J.-H., Gao, J.-M., Huang, C.-J., Li, C.-Q., 2014. Zebrafish models for assessing developmental and reproductive toxicity. Neurotoxicol. Teratol. 42, 35–42. https://doi.org/10.1016/j.ntt.2014.01.006
Hendricks, M., Jesuthasan, S., 2007. Electroporation-based methods for in vivo, whole mount and primary culture analysis of zebrafish brain development. Neural Develop. 2, 6. https://doi.org/10.1186/1749-8104-2-6
Henry, T.B., Grizzle, J.M., 2004. Survival of largemouth bass, bluegill and channel catfish embryos after electroshocking. J. Fish Biol. 64, 1206–1216. https://doi.org/10.1111/j.0022-1112.2004.00384.x
Hess, B.J.M., Van Opstal, A.J., Straumann, D., Hepp, K., 1992. Calibration of three-dimensional eye position using search coil signals in the rhesus monkey. Vision Res. 32, 1647–1654. https://doi.org/10.1016/0042-6989(92)90157-E
Howe, K., Clark, M.D., Torroja, C.F., Torrance, J., Berthelot, C., Muffato, M., Collins, J.E., Humphray, S., McLaren, K., Matthews, L., McLaren, S., Sealy, I., Caccamo, M., Churcher, C., Scott, C., Barrett, J.C., Koch, R., Rauch, G.-J., White, S., Chow, W., Kilian, B., Quintais, L.T., Guerra-Assunção, J.A., Zhou, Y., Gu, Y., Yen, J., Vogel, J.-H., Eyre, T., Redmond, S., Banerjee, R., Chi, J., Fu, B., Langley, E., Maguire, S.F., Laird, G.K., Lloyd, D., Kenyon, E., Donaldson, S., Sehra, H., Almeida-King, J., Loveland, J., Trevanion, S., Jones, M., Quail, M., Willey, D., Hunt, A., Burton, J., Sims, S., McLay, K., Plumb, B., Davis, J., Clee, C., Oliver, K., Clark, R., Riddle, C., Elliott, D., Threadgold, G., Harden, G., Ware, D., Begum, S., Mortimore, B., Kerry, G., Heath, P., Phillimore, B., Tracey, A., Corby, N., Dunn, M., Johnson, C., Wood, J., Clark, S., Pelan, S., Griffiths, G., Smith, M., Glithero, R., Howden, P., Barker, N., Lloyd, C., Stevens, C., Harley, J., Holt, K., Panagiotidis, G., Lovell, J., Beasley, H., Henderson, C., Gordon, D., Auger, K., Wright, D., Collins, J., Raisen, C., Dyer, L., Leung, K., Robertson, L., Ambridge, K., Leongamornlert,

D., McGuire, S., Gilderthorp, R., Griffiths, C., Manthravadi, D., Nichol, S., Barker, G., Whitehead, S., Kay, M., Brown, J., Murnane, C., Gray, E., Humphries, M., Sycamore, N., Barker, D., Saunders, D., Wallis, J., Babbage, A., Hammond, S., Mashreghi-Mohammadi, M., Barr, L., Martin, S., Wray, P., Ellington, A., Matthews, N., Ellwood, M., Woodmansey, R., Clark, G., Cooper, J.D., Tromans, A., Grafham, D., Skuce, C., Pandian, R., Andrews, R., Harrison, E., Kimberley, A., Garnett, J., Fosker, N., Hall, R., Garner, P., Kelly, D., Bird, C., Palmer, S., Gehring, I., Berger, A., Dooley, C.M., Ersan-Ürün, Z., Eser, C., Geiger, H., Geisler, M., Karotki, L., Kirn, A., Konantz, J., Konantz, M., Oberländer, M., Rudolph-Geiger, S., Teucke, M., Lanz, C., Raddatz, G., Osoegawa, K., Zhu, B., Rapp, A., Widaa, S., Langford, C., Yang, F., Schuster, S.C., Carter, N.P., Harrow, J., Ning, Z., Herrero, J., Searle, S.M.J., Enright, A., Geisler, R., Plasterk, R.H.A., Lee, C., Westerfield, M., de Jong, P.J., Zon, L.I., Postlethwait, J.H., Nüsslein-Volhard, C., Hubbard, T.J.P., Crollius, H.R., Rogers, J., Stemple, D.L., 2013. The zebrafish reference genome sequence and its relationship to the human genome. Nature 496, 498–503. https://doi.org/10.1038/nature12111

Huang, Y.-Y., 2008. The optokinetic response in zebrafish and its applications. Front. Biosci. 13, 1899. https://doi.org/10.2741/2810

Hunter, P.R., Lowe, A.S., Thompson, I.D., Meyer, M.P., 2013. Emergent Properties of the Optic Tectum Revealed by Population Analysis of Direction and Orientation Selectivity. J. Neurosci. 33, 13940–13945. https://doi.org/10.1523/JNEUROSCI.1493-13.2013

Kasprick, D.S., Kish, P.E., Junttila, T.L., Ward, L.A., Bohnsack, B.L., Kahana, A., 2011. Microanatomy of Adult Zebrafish Extraocular Muscles. PLOS ONE 6, e27095. https://doi.org/10.1371/journal.pone.0027095

Katz, S.R., Yakovlev, M.A., Vanselow, D.J., Ding, Y., Lin, A.Y., Parkinson, D.Y., Wang, Y., Canfield, V.A., Ang, K.C., Cheng, K.C., 2021. Whole-organism 3D quantitative characterization of zebrafish melanin by silver deposition micro-CT. eLife 10, e68920. https://doi.org/10.7554/eLife.68920

Kels, B.D., Grzybowski, A., Grant-Kels, J.M., 2015. Human ocular anatomy. Clin. Dermatol., Eye and Skin Disorders: Part 1 33, 140–146. https://doi.org/10.1016/j.clindermatol.2014.10.006

Kenyon, R.V., 1985. A soft contact lens search coil for measuring eye movements. Vision Res. 25, 1629–1633. https://doi.org/10.1016/0042-6989(85)90133-6

Key, B., 2016. Why fish do not feel pain. Anim. Sentience 1. https://doi.org/10.51291/2377-7478.1011

Key, B., 2015. Fish do not feel pain and its implications for understanding phenomenal consciousness. Biol. Philos. 30, 149–165. https://doi.org/10.1007/s10539-014-9469-4

Kimmel, C.B., Ballard, W.W., Kimmel, S.R., Ullmann, B., Schilling, T.F., 1995. Stages of embryonic development of the zebrafish. Dev. Dyn. 203, 253–310. https://doi.org/10.1002/aja.1002030302

Kist, A.M., Portugues, R., 2019. Optomotor Swimming in Larval Zebrafish Is Driven by Global Whole-Field Visual Motion and Local Light-Dark Transitions. Cell Rep. 29, 659-670.e3. https://doi.org/10.1016/j.celrep.2019.09.024

Kitama, T., Ishida, M., Luan, H., Kawasaki, T., Sato, Y., 2001. Difference between Horizontal and Vertical Optokinetic Nystagmus in Cats at Upright Position. Jpn. J. Physiol. 51, 463–474. https://doi.org/10.2170/jjphysiol.51.463

Koenderink, J.J., van Doorn, A.J., 1987. Facts on optic flow. Biol. Cybern. 56, 247–254. https://doi.org/10.1007/BF00365219
Köhler, A., Collymore, C., Finger-Baier, K., Geisler, R., Kaufmann, L., Pounder, K.C., Schulte-Merker, S., Valentim, A., Varga, Z.M., Weiss, J., Strähle, U., 2017. Report of Workshop on Euthanasia for Zebrafish—A Matter of Welfare and Science. Zebrafish 14, 547–551. https://doi.org/10.1089/zeb.2017.1508
Kolz, A.L., 2006. Electrical Conductivity as Applied to Electrofishing. Trans. Am. Fish. Soc. 135, 509–518. https://doi.org/10.1577/T05-148.1
Korhonen, L., Hansson, I., Maugras, C., Wehrle, R., Kairisalo, M., Borgkvist, A., Jokitalo, E., Sotelo, C., Fisone, G., Dusart, I., Lindholm, D., 2008. Expression of X-chromosome linked inhibitor of apoptosis protein in mature purkinje cells and in retinal bipolar cells in transgenic mice induces neurodegeneration. Neuroscience 156, 515–526. https://doi.org/10.1016/j.neuroscience.2008.08.005
Kotnik, T., Rems, L., Tarek, M., Miklavčič, D., 2019. Membrane Electroporation and Electropermeabilization: Mechanisms and Models. Annu. Rev. Biophys. 48, 63–91. https://doi.org/10.1146/annurev-biophys-052118-115451
Kubo, F., Hablitzel, B., Dal Maschio, M., Driever, W., Baier, H., Arrenberg, A.B., 2014. Functional Architecture of an Optic Flow-Responsive Area that Drives Horizontal Eye Movements in Zebrafish. Neuron 81, 1344–1359. https://doi.org/10.1016/j.neuron.2014.02.043
Lambert, F.M., Beck, J.C., Baker, R., Straka, H., 2008. Semicircular Canal Size Determines the Developmental Onset of Angular Vestibuloocular Reflexes in Larval Xenopus. J. Neurosci. 28, 8086–8095. https://doi.org/10.1523/JNEUROSCI.1288-08.2008
Land, M.F., 2015. Eye movements of vertebrates and their relation to eye form and function. J. Comp. Physiol. A 201, 195–214. https://doi.org/10.1007/s00359-014-0964-5
Lawrence, C., 2016. New frontiers for zebrafish management, in: Methods in Cell Biology. Elsevier, pp. 483–508. https://doi.org/10.1016/bs.mcb.2016.04.015
Leary, P., Bellegarda, C., Quainoo, C., Goldblatt, D., Rosti, B., Schoppik, D., 2025. Sensation is dispensable for the maturation of the vestibulo-ocular reflex. Science 387, 85–90. https://doi.org/10.1126/science.adr9982
Lee, R.C., 2005. Cell Injury by Electric Forces. Ann. N. Y. Acad. Sci. 1066, 85–91. https://doi.org/10.1196/annals.1363.007
Leis, J.A., Bekar, L.K., Walz, W., 2005. Potassium homeostasis in the ischemic brain. Glia 50, 407–416. https://doi.org/10.1002/glia.20145
Leyden, C., Brüggemann, T., Debinski, F., Simacek, C.A., Dehmelt, F.A., Arrenberg, A.B., 2022. Efficacy of Tricaine (MS-222) and Hypothermia as Anesthetic Agents for Blocking Sensorimotor Responses in Larval Zebrafish. Front. Vet. Sci. 9, 864573. https://doi.org/10.3389/fvets.2022.864573
Leyden, C., Brysch, C., Arrenberg, A.B., 2021. A distributed saccade-associated network encodes high velocity conjugate and monocular eye movements in the zebrafish hindbrain. Sci. Rep. 11, 12644. https://doi.org/10.1038/s41598-021-90315-2
Lidster, K., Readman, G.D., Prescott, M.J., Owen, S.F., 2017. International survey on the use and welfare of zebrafish Danio rerio in research. J. Fish Biol. 90, 1891–1905. https://doi.org/10.1111/jfb.13278
Lim, K.H., Kim, H.K., Park, S., Han, E., Song, I., Yoon, H.S., Kim, J., Lee, Y., Jang, Y.H., Rah, Y.C., Lee, S.H., Choi, J., 2024. Measuring Optokinetic Reflex and

Vestibulo-Ocular Reflex in Unilateral Vestibular Organ Damage Model of Zebrafish. J. Assoc. Res. Otolaryngol. 25, 167–177. https://doi.org/10.1007/s10162-024-00936-3
Lin, T.-F., Huang, M.Y.-Y., 2023. A quantitative approach to study the adaptation of rhythmic eye movements and the resulting tonic eye deviation in larval zebrafish. J. Neurosci. Res. 101, 1504–1518. https://doi.org/10.1002/jnr.25220
Lines, J.A., Robb, D.H., Kestin, S.C., Crook, S.C., Benson, T., 2003. Electric stunning: a humane slaughter method for trout. Aquac. Eng. 28, 141–154. https://doi.org/10.1016/S0144-8609(03)00021-9
Lopez-Luna, J., Al-Jubouri, Q., Al-Nuaimy, W., Sneddon, L.U., 2017. Impact of analgesic drugs on the behavioural responses of larval zebrafish to potentially noxious temperatures. Appl. Anim. Behav. Sci. 188, 97–105. https://doi.org/10.1016/j.applanim.2017.01.002
Marino, P., Norreel, J.-C., Schachner, M., Rougon, G., Amoureux, M.-C., 2009. A polysialic acid mimetic peptide promotes functional recovery in a mouse model of spinal cord injury. Exp. Neurol., Brain Stimulation in Psychiatry 219, 163–174. https://doi.org/10.1016/j.expneurol.2009.05.009
Marino, S., Marani, L., Nazzaro, C., Beani, L., Siniscalchi, A., 2007. Mechanisms of sodium azide-induced changes in intracellular calcium concentration in rat primary cortical neurons. NeuroToxicology 28, 622–629. https://doi.org/10.1016/j.neuro.2007.01.005
Marques, J.C., Lackner, S., Félix, R., Orger, M.B., 2018. Structure of the Zebrafish Locomotor Repertoire Revealed with Unsupervised Behavioral Clustering. Curr. Biol. 28, 181-195.e5. https://doi.org/10.1016/j.cub.2017.12.002
Marsh, E., Baker, R., 1997. Normal and Adapted Visuooculomotor Reflexes in Goldfish. J. Neurophysiol. 77, 1099–1118. https://doi.org/10.1152/jn.1997.77.3.1099
Mashour, G.A., 2024. Anesthesia and the neurobiology of consciousness. Neuron 112, 1553–1567. https://doi.org/10.1016/j.neuron.2024.03.002
Mashour, G.A., Hudetz, A.G., 2018. Neural Correlates of Unconsciousness in Large-Scale Brain Networks. Trends Neurosci. 41, 150–160. https://doi.org/10.1016/j.tins.2018.01.003
Masseck, O.A., Hoffmann, K.-P., 2009. Comparative Neurobiology of the Optokinetic Reflex. Ann. N. Y. Acad. Sci. 1164, 430–439. https://doi.org/10.1111/j.1749-6632.2009.03854.x
Matsuda, K., Kubo, F., 2021. Circuit Organization Underlying Optic Flow Processing in Zebrafish. Front. Neural Circuits 15. https://doi.org/10.3389/fncir.2021.709048
Maximino, C., 2011. Modulation of nociceptive-like behavior in zebrafish (Danio rerio) by environmental stressors. Psychol. Neurosci. 4, 149–155. https://doi.org/10.3922/j.psns.2011.1.017
Merker, B., 2016. The line drawn on pain still holds. Anim. Sentience 1. https://doi.org/10.51291/2377-7478.1104
Meyer, R.E., 2015. Euthanasia and Humane Killing, in: Veterinary Anesthesia and Analgesia. John Wiley & Sons, Ltd, pp. 130–143. https://doi.org/10.1002/9781119421375.ch6
Migault, G., Beiza-Canelo, N., Chatterjee, S., Debrégeas, G., Bormuth, V., 2024. Distinct and Asymmetric Neuronal Responses to Pitch- and Roll-Axis Vestibular Stimulation in larval zebrafish. https://doi.org/10.1101/2024.03.22.586054

Miki, S., Baker, R., Hirata, Y., 2018. Cerebellar Role in Predictive Control of Eye Velocity Initiation and Termination. J. Neurosci. 38, 10371–10383. https://doi.org/10.1523/JNEUROSCI.1375-18.2018
Mione, M.C., Trede, N.S., 2010. The zebrafish as a model for cancer. Dis. Model. Mech. 3, 517–523. https://doi.org/10.1242/dmm.004747
Miri, A., Bhasin, B.J., Aksay, E.R.F., Tank, D.W., Goldman, M.S., 2022. Oculomotor plant and neural dynamics suggest gaze control requires integration on distributed timescales. https://doi.org/10.1101/2021.06.30.450653
Mo, W., Chen, F., Nechiporuk, A., Nicolson, T., 2010. Quantification of vestibular-induced eye movements in zebrafish larvae. BMC Neurosci. 11, 110. https://doi.org/10.1186/1471-2202-11-110
Mocho, J.-P., Lang, F., Valentin, G., Bedu, S., McKimm, R., Ramos, J., Saavedra Torres, Y., Wheatley, S.E., Higgins, J., Millington, M.E., Lundegaard, P.R., Chamorro Valverde, R., Jenčič, V., von Krogh, K., 2022. A Multi-Site Assessment of Anesthetic Overdose, Hypothermic Shock, and Electrical Stunning as Methods of Euthanasia for Zebrafish (Danio rerio) Embryos and Larvae. Biology 11, 546. https://doi.org/10.3390/biology11040546
Mommsen, T.P., Vijayan, M.M., Moon, T.W., 1999. Cortisol in teleosts: dynamics, mechanisms of action, and metabolic regulation. Rev. Fish Biol. Fish. 9, 211–268. https://doi.org/10.1023/A:1008924418720
Morotomi-Yano, K., Akiyama, H., Yano, K., 2014. Different involvement of extracellular calcium in two modes of cell death induced by nanosecond pulsed electric fields. Arch. Biochem. Biophys. 555–556, 47–54. https://doi.org/10.1016/j.abb.2014.05.020
Mueller, K.P., Neuhauss, S.C.F., 2010. Quantitative measurements of the optokinetic response in adult fish. J. Neurosci. Methods 186, 29–34. https://doi.org/10.1016/j.jneumeth.2009.10.020
Müller, U.K., van Leeuwen, J.L., 2004. Swimming of larval zebrafish: ontogeny of body waves and implications for locomotory development. J. Exp. Biol. 207, 853–868. https://doi.org/10.1242/jeb.00821
Murtha, J.M., Keller, E.T., 2003. Characterization of the heat shock response in mature zebrafish (*Danio rerio*). Exp. Gerontol. 38, 683–691. https://doi.org/10.1016/S0531-5565(03)00067-6
Muto, A., Ohkura, M., Abe, G., Nakai, J., Kawakami, K., 2013. Real-Time Visualization of Neuronal Activity during Perception. Curr. Biol. 23, 307–311. https://doi.org/10.1016/j.cub.2012.12.040
Naumann, E.A., Fitzgerald, J.E., Dunn, T.W., Rihel, J., Sompolinsky, H., Engert, F., 2016. From Whole-Brain Data to Functional Circuit Models: The Zebrafish Optomotor Response. Cell 167, 947-960.e20. https://doi.org/10.1016/j.cell.2016.10.019
Neuhauss, S.C.F., 2003. Behavioral genetic approaches to visual system development and function in zebrafish. J. Neurobiol. 54, 148–160. https://doi.org/10.1002/neu.10165
Neuhauss, S.C.F., Biehlmaier, O., Seeliger, M.W., Das, T., Kohler, K., Harris, W.A., Baier, H., 1999. Genetic Disorders of Vision Revealed by a Behavioral Screen of 400 Essential Loci in Zebrafish. J. Neurosci. 19, 8603–8615. https://doi.org/10.1523/JNEUROSCI.19-19-08603.1999
Nguyen, P.L., Yefimov, B.A., Coffin, A., Cooper, C., 2019. Electroimmobilization as an Alternative Method to Chemical Immobilization of Larval Fish. Trans. Am. Fish. Soc. 148, 725–738. https://doi.org/10.1002/tafs.10167

Nicholls, D.G., 2008. Oxidative Stress and Energy Crises in Neuronal Dysfunction. Ann. N. Y. Acad. Sci. 1147, 53–60. https://doi.org/10.1196/annals.1427.002
Nordgreen, A.H., Slinde, E., Møller, D., Roth, B., 2008. Effect of Various Electric Field Strengths and Current Durations on Stunning and Spinal Injuries of Atlantic Herring. J. Aquat. Anim. Health 20, 110–115. https://doi.org/10.1577/H07-010.1
Nordgreen, J., Garner, J.P., Janczak, A.M., Ranheim, B., Muir, W.M., Horsberg, T.E., 2009. Thermonociception in fish: Effects of two different doses of morphine on thermal threshold and post-test behaviour in goldfish (*Carassius auratus*). Appl. Anim. Behav. Sci. 119, 101–107. https://doi.org/10.1016/j.applanim.2009.03.015
Nordgreen, J., Horsberg, T.E., Ranheim, B., Chen, A.C.N., 2007. Somatosensory evoked potentials in the telencephalon of Atlantic salmon (Salmo salar) following galvanic stimulation of the tail. J. Comp. Physiol. A 193, 1235–1242. https://doi.org/10.1007/s00359-007-0283-1
Orger, M.B., 2016. The Cellular Organization of Zebrafish Visuomotor Circuits. Curr. Biol. 26, R377–R385. https://doi.org/10.1016/j.cub.2016.03.054
Pérez-Schuster, V., Kulkarni, A., Nouvian, M., Romano, S.A., Lygdas, K., Jouary, A., Dipoppa, M., Pietri, T., Haudrechy, M., Candat, V., Boulanger-Weill, J., Hakim, V., Sumbre, G., 2016. Sustained Rhythmic Brain Activity Underlies Visual Motion Perception in Zebrafish. Cell Rep. 17, 1098–1112. https://doi.org/10.1016/j.celrep.2016.09.065
Poon, K.L., Brand, T., 2013. The zebrafish model system in cardiovascular research: A tiny fish with mighty prospects. Glob. Cardiol. Sci. Pract. 2013, 4. https://doi.org/10.5339/gcsp.2013.4
Portugues, R., Feierstein, C.E., Engert, F., Orger, M.B., 2014. Whole-Brain Activity Maps Reveal Stereotyped, Distributed Networks for Visuomotor Behavior. Neuron 81, 1328–1343. https://doi.org/10.1016/j.neuron.2014.01.019
Qian, H., Zhu, Y., Ramsey, D.J., Chappell, R.L., Dowling, J.E., Ripps, H., 2005. Directional Asymmetries in the Optokinetic Response of Larval Zebrafish (Danio rerio). Zebrafish 2, 189–196. https://doi.org/10.1089/zeb.2005.2.189
Raja, S.N., Carr, D.B., Cohen, M., Finnerup, N.B., Flor, H., Gibson, S., Keefe, F.J., Mogil, J.S., Ringkamp, M., Sluka, K.A., Song, X.-J., Stevens, B., Sullivan, M.D., Tutelman, P.R., Ushida, T., Vader, K., 2020. The revised International Association for the Study of Pain definition of pain: concepts, challenges, and compromises. PAIN 161, 1976. https://doi.org/10.1097/j.pain.0000000000001939
Ravan, A., Chemla, Y.R., Gruebele, M., 2025. Larval zebrafish swim bouts in three dimensions reveal both new and redundant behaviours. J. R. Soc. Interface 22, 20250065. https://doi.org/10.1098/rsif.2025.0065
Readman, G.D., Owen, S.F., Murrell, J.C., Knowles, T.G., 2013. Do Fish Perceive Anaesthetics as Aversive? PLOS ONE 8, e73773. https://doi.org/10.1371/journal.pone.0073773
Reid, C.H., Vandergoot, C.S., Midwood, J.D., Stevens, E.D., Bowker, J., Cooke, S.J., 2019. On the Electroimmobilization of Fishes for Research and Practice: Opportunities, Challenges, and Research Needs. Fisheries 44, 576–585. https://doi.org/10.1002/fsh.10307
Reilly, S.C., Quinn, J.P., Cossins, A.R., Sneddon, L.U., 2008. Novel candidate genes identified in the brain during nociception in common carp (*Cyprinus carpio*)

and rainbow trout (*Oncorhynchus mykiss*). Neurosci. Lett. 437, 135–138. https://doi.org/10.1016/j.neulet.2008.03.075
Renninger, S.L., Orger, M.B., 2013. Two-photon imaging of neural population activity in zebrafish. Methods, Zebrafish Methods 62, 255–267. https://doi.org/10.1016/j.ymeth.2013.05.016
Reynolds, J.B., 1996. Electrofishing.
Rijn, C.M. van., Krijnen, H., Menting-Hermeling, S., Coenen, A.M.L., 2011. Decapitation in Rats: Latency to Unconsciousness and the 'Wave of Death.' PLoS ONE 6, e16514. https://doi.org/10.1371/journal.pone.0016514
Rinkwitz, S., Mourrain, P., Becker, T.S., 2011. Zebrafish: An integrative system for neurogenomics and neurosciences. Prog. Neurobiol. 93, 231–243. https://doi.org/10.1016/j.pneurobio.2010.11.003
Rinner, O., Rick, J.M., Neuhauss, S.C.F., 2005. Contrast Sensitivity, Spatial and Temporal Tuning of the Larval Zebrafish Optokinetic Response. Invest. Ophthalmol. Vis. Sci. 46, 137–142. https://doi.org/10.1167/iovs.04-0682
Robb, D.H.F., O' Callaghan, M., Lines, J.A., Kestin, S.C., 2002. Electrical stunning of rainbow trout (Oncorhynchus mykiss): factors that affect stun duration. Aquaculture 205, 359–371. https://doi.org/10.1016/S0044-8486(01)00677-9
Robinson, D.A., 1981. Control of Eye Movements, in: Comprehensive Physiology. John Wiley & Sons, Ltd, pp. 1275–1320. https://doi.org/10.1002/cphy.cp010228
Roeser, T., Baier, H., 2003. Visuomotor Behaviors in Larval Zebrafish after GFP-Guided Laser Ablation of the Optic Tectum. J. Neurosci. 23, 3726–3734. https://doi.org/10.1523/JNEUROSCI.23-09-03726.2003
Rombough, P., 2002. Gills are needed for ionoregulation before they are needed for O2 uptake in developing zebrafish, Danio rerio. J. Exp. Biol. 205, 1787–1794. https://doi.org/10.1242/jeb.205.12.1787
Rombough, P.J., 2007. Ontogenetic changes in the toxicity and efficacy of the anaesthetic MS222 (tricaine methanesulfonate) in zebrafish (Danio rerio) larvae. Comp. Biochem. Physiol. A. Mol. Integr. Physiol. 148, 463–469. https://doi.org/10.1016/j.cbpa.2007.06.415
Rose, J.D., 2002. The Neurobehavioral Nature of Fishes and the Question of Awareness and Pain. Rev. Fish. Sci. 10, 1–38. https://doi.org/10.1080/20026491051668
Ruiz-Medina, J., Morgado-Bernal, I., Redolar-Ripoll, D., Aldavert-Vera, L., Segura-Torres, P., 2008. Intracranial self-stimulation facilitates a spatial learning and memory task in the Morris water maze. Neuroscience 154, 424–430. https://doi.org/10.1016/j.neuroscience.2008.03.059
Russel, W. M. S., Burch, R. L., 1959. The Principles of Humane Experimental Technique. Methuen.
Sabaliauskas, N.A., Foutz, C.A., Mest, J.R., Budgeon, L.R., Sidor, A.T., Gershenson, J.A., Joshi, S.B., Cheng, K.C., 2006. High-throughput zebrafish histology. Methods, Zebrafish as a Model for Development 39, 246–254. https://doi.org/10.1016/j.ymeth.2006.03.001
Scheil, V., Zürn, A., Köhler, H.-R., Triebskorn, R., 2010. Embryo development, stress protein (Hsp70) responses, and histopathology in zebrafish (Danio rerio) following exposure to nickel chloride, chlorpyrifos, and binary mixtures of them. Environ. Toxicol. 25, 83–93. https://doi.org/10.1002/tox.20477
Sharber, N.G., Carothers, S.W., Sharber, J.P., De Vos, J.C., House, D.A., 1994. Reducing Electrofishing-Induced Injury of Rainbow Trout. North Am. J. Fish.

Manag. 14, 340–346. https://doi.org/10.1577/1548-8675(1994)014%253C0340:REIIOR%253E2.3.CO;2
Shuttleworth, C.W., Andrew, R.D., Akbari, Y., Ayata, C., Balu, R., Brennan, K.C., Boutelle, M., Carlson, A.P., Dreier, J.P., Fabricius, M., Farkas, E., Foreman, B., Helbok, R., Henninger, N., Jewell, S.L., Jones, S.C., Kirov, S.A., Lindquist, B.E., Maciel, C.B., Okonkwo, D., Reinhart, K.M., Robertson, R.M., Rosenthal, E.S., Watanabe, T., Hartings, J.A., 2020. Which Spreading Depolarizations Are Deleterious To Brain Tissue? Neurocrit. Care 32, 317–322. https://doi.org/10.1007/s12028-019-00776-7
Sloman, K.A., Bouyoucos, I.A., Brooks, E.J., Sneddon, L.U., 2019. Ethical considerations in fish research. J. Fish Biol. 94, 556–577. https://doi.org/10.1111/jfb.13946
Smaili, S., Hirata, H., Ureshino, R., Monteforte, P.T., Morales, A.P., Muler, M.L., Terashima, J., Oseki, K., Rosenstock, T.R., Lopes, G.S., Bincoletto, C., 2009. Calcium and cell death signaling in neurodegeneration and aging. An. Acad. Bras. Ciênc. 81, 467–475. https://doi.org/10.1590/S0001-37652009000300011
Sneddon, L.U., 2018. Comparative Physiology of Nociception and Pain. Physiology 33, 63–73. https://doi.org/10.1152/physiol.00022.2017
Sneddon, L.U., 2012. Clinical Anesthesia and Analgesia in Fish. J. Exot. Pet Med., Clinical Anesthesia and Analgesia 21, 32–43. https://doi.org/10.1053/j.jepm.2011.11.009
Sneddon, L.U., 2003. The evidence for pain in fish: the use of morphine as an analgesic. Appl. Anim. Behav. Sci. 83, 153–162. https://doi.org/10.1016/S0168-1591(03)00113-8
Sneddon, L.U., Elwood, R.W., Adamo, S.A., Leach, M.C., 2014. Defining and assessing animal pain. Anim. Behav. 97, 201–212. https://doi.org/10.1016/j.anbehav.2014.09.007
Snyder, D. E., 2003. Electrofishing and Its Harmful Effects on Fish (Information and Technology Report No. USGS/BRD/ITR--2003-0002). U.S. Department of the Interior and U.S. Geological Survey.
Soivio, A., Nyholm, K., Huhti, M., 1977. Effects of anaesthesia with MS 222, neutralized MS 222 and benzocaine on the blood constituents of rainbow trout, Salmo gairdneri. J. Fish Biol. 10, 91–101. https://doi.org/10.1111/j.1095-8649.1977.tb04045.x
Spencer, R.F., Porter, J.D., 2006. Biological organization of the extraocular muscles, in: Büttner-Ennever, J.A. (Ed.), Progress in Brain Research, Neuroanatomy of the Oculomotor System. Elsevier, pp. 43–80. https://doi.org/10.1016/S0079-6123(05)51002-1
Steenbergen, P.J., Metz, J.R., Flik, G., Richardson, M.K., Champagne, D.L., 2012. Methods to Quantify Basal and Stress-Induced Cortisol Response in Larval Zebrafish, in: Kalueff, A.V., Stewart, A.M. (Eds.), Zebrafish Protocols for Neurobehavioral Research. Humana Press, Totowa, NJ, pp. 121–141. https://doi.org/10.1007/978-1-61779-597-8_9
Stewart, A.M., Braubach, O., Spitsbergen, J., Gerlai, R., Kalueff, A.V., 2014. Zebrafish models for translational neuroscience research: from tank to bedside. Trends Neurosci. 37, 264–278. https://doi.org/10.1016/j.tins.2014.02.011
Strykowski, J.L., Schech, J.M., 2015. Effectiveness of recommended euthanasia methods in larval zebrafish (Danio rerio). J. Am. Assoc. Lab. Anim. Sci. JAALAS 54, 81–84.

Sugioka, T., Tanimoto, M., Higashijima, S., 2023. Biomechanics and neural circuits for vestibular-induced fine postural control in larval zebrafish. Nat. Commun. 14, 1217. https://doi.org/10.1038/s41467-023-36682-y
Sun, P., Zhang, Y., Zhao, F., Wu, J.-P., Pun, S.H., Peng, C., Du, M., Vai, M.I., Liu, D., Chen, F., 2018. An Assay for Systematically Quantifying the Vestibulo-Ocular Reflex to Assess Vestibular Function in Zebrafish Larvae. Front. Cell. Neurosci. 12.
Tadokoro, S., Miki, S., Yamanaka, T., Hirata, Y., 2025. Horizontal, vertical, and torsional optokinetic responses and their adaptations in fish. J. Neurophysiol. 133, 965–986. https://doi.org/10.1152/jn.00565.2024
Takabayashi, A., Ohmura-Iwasaki, T., Mori, S., 2003. Changes of vertical eye movements of goldfish for different otolith stimulation by linear acceleration. Adv. Space Res., Space Life Sciences: Gravitational Biology: 2002 32, 1527–1532. https://doi.org/10.1016/S0273-1177(03)90391-7
Takano, T., Tian, G.-F., Peng, W., Lou, N., Lovatt, D., Hansen, A.J., Kasischke, K.A., Nedergaard, M., 2007. Cortical spreading depression causes and coincides with tissue hypoxia. Nat. Neurosci. 10, 754–762. https://doi.org/10.1038/nn1902
Tavares, B., Lopes, S.S., 2013. The Importance of Zebrafish in Biomedical Research. Acta Médica Port. 26, 583–592. https://doi.org/10.20344/amp.4628
Teulier, L., Guillard, L., Leon, C., Romestaing, C., Voituron, Y., 2018. Consequences of electroshock-induced narcosis in fish muscle: from mitochondria to swim performance. J. Fish Biol. 92, 1805–1818. https://doi.org/10.1111/jfb.13621
Thiel, A., Greschner, M., Eurich, C.W., Ammermüller, J., Kretzberg, J., 2007. Contribution of Individual Retinal Ganglion Cell Responses to Velocity and Acceleration Encoding. J. Neurophysiol. 98, 2285–2296. https://doi.org/10.1152/jn.01342.2006
Thompson, A.W., Vanwalleghem, G.C., Heap, L.A., Scott, E.K., 2016. Functional Profiles of Visual-, Auditory-, and Water Flow-Responsive Neurons in the Zebrafish Tectum. Curr. Biol. 26, 743–754. https://doi.org/10.1016/j.cub.2016.01.041
Tracey, W.D., 2017. Nociception. Curr. Biol. 27, R129–R133. https://doi.org/10.1016/j.cub.2017.01.037
Tulenko, F.J., Currie, P., 2020. Chapter 12 - Zebrafish Myology, in: Cartner, S.C., Eisen, J.S., Farmer, S.C., Guillemin, K.J., Kent, M.L., Sanders, G.E. (Eds.), The Zebrafish in Biomedical Research, American College of Laboratory Animal Medicine. Academic Press, pp. 115–121. https://doi.org/10.1016/B978-0-12-812431-4.00012-9
Tweed, D., Cadera, W., Vilis, T., 1990. Computing three-dimensional eye position quaternions and eye velocity from search coil signals. Vision Res. 30, 97–110. https://doi.org/10.1016/0042-6989(90)90130-D
Valentim, A.M., van Eeden, F.J., Strähle, U., Olsson, I.A.S., 2016. Euthanizing zebrafish legally in Europe. EMBO Rep. 17, 1688–1689. https://doi.org/10.15252/embr.201643153
van den Berg, A.V., Collewijn, H., 1988. Directional asymmetries of human optokinetic nystagmus. Exp. Brain Res. 70, 597–604. https://doi.org/10.1007/BF00247608
Wallace, C.K., Bright, L.A., Marx, J.O., Andersen, R.P., Mullins, M.C., Carty, A.J., 2018. Effectiveness of Rapid Cooling as a Method of Euthanasia for Young Zebrafish (Danio rerio). J. Am. Assoc. Lab. Anim. Sci. 57, 58–63.

Wang, K., Hinz, J., Haikala, V., Reiff, D.F., Arrenberg, A.B., 2019. Selective processing of all rotational and translational optic flow directions in the zebrafish pretectum and tectum. BMC Biol. 17, 29. https://doi.org/10.1186/s12915-019-0648-2

Wang, K., Hinz, J., Zhang, Y., Thiele, T.R., Arrenberg, A.B., 2020. Parallel Channels for Motion Feature Extraction in the Pretectum and Tectum of Larval Zebrafish. Cell Rep. 30, 442-453.e6. https://doi.org/10.1016/j.celrep.2019.12.031

Warren, W.H., Hannon, D.J., 1988. Direction of self-motion is perceived from optical flow. Nature 336, 162–163. https://doi.org/10.1038/336162a0

White, L.J., Thomson, J.S., Pounder, K.C., Coleman, R.C., Sneddon, L.U., 2017. The impact of social context on behaviour and the recovery from welfare challenges in zebrafish, *Danio rerio*. Anim. Behav. 132, 189–199. https://doi.org/10.1016/j.anbehav.2017.08.017

Wilson, J.M., Bunte, R.M., Carty, A.J., 2009. Evaluation of Rapid Cooling and Tricaine Methanesulfonate (MS222) as Methods of Euthanasia in Zebrafish (Danio rerio). J. Am. Assoc. Lab. Anim. Sci. 48, 785–789.

Wong, D., Keyserlingk, M.A.G. von, Richards, J.G., Weary, D.M., 2014. Conditioned Place Avoidance of Zebrafish (Danio rerio) to Three Chemicals Used for Euthanasia and Anaesthesia. PLOS ONE 9, e88030. https://doi.org/10.1371/journal.pone.0088030

Wu, Y., dal Maschio, M., Kubo, F., Baier, H., 2020. An Optical Illusion Pinpoints an Essential Circuit Node for Global Motion Processing. Neuron 108, 722-734.e5. https://doi.org/10.1016/j.neuron.2020.08.027

Xiong, X., Luo, S., Wu, B., Wang, J., 2017. Comparative Developmental Toxicity and Stress Protein Responses of Dimethyl Sulfoxide to Rare Minnow and Zebrafish Embryos/Larvae. Zebrafish 14, 60–68. https://doi.org/10.1089/zeb.2016.1287

Xu, D., Wang, B., Zhao, X., Zheng, Y., Du, J., Wang, Y., 2017. General anesthetics protects against cardiac arrest-induced brain injury by inhibiting calcium wave propagation in zebrafish. Mol. Brain 10, 44. https://doi.org/10.1186/s13041-017-0323-x

Yeh, C.-M., Glöck, M., Ryu, S., 2013. An Optimized Whole-Body Cortisol Quantification Method for Assessing Stress Levels in Larval Zebrafish. PLOS ONE 8, e79406. https://doi.org/10.1371/journal.pone.0079406

Zandt, B.-J., Haken, B. ten, Dijk, J.G. van, Putten, M.J.A.M. van, 2011. Neural Dynamics during Anoxia and the “Wave of Death.” PLOS ONE 6, e22127. https://doi.org/10.1371/journal.pone.0022127

Zhang, Y., Huang, R., Nörenberg, W., Arrenberg, A.B., 2022. A robust receptive field code for optic flow detection and decomposition during self-motion. Curr. Biol. 32, 2505-2516.e8. https://doi.org/10.1016/j.cub.2022.04.048

Zhao, S., Huang, J., Ye, J., 2015. A fresh look at zebrafish from the perspective of cancer research. J. Exp. Clin. Cancer Res. 34, 80. https://doi.org/10.1186/s13046-015-0196-8

7. Appendix

7.1 Publication 1

Behavioral and Neurophysiological Effects of Electrical Stunning on Zebrafish Larvae

Burkhardt, D.-S., Leyden, C., Thomas, C, Brysch, C, Dehmelt, F. A., Arrenberg, A. B. (2025). *Lab Animal* 54, 50-58. DOI: https://doi.org/10.1038/s41684-024-01505-0

lab animal

Article

https://doi.org/10.1038/s41684-024-01505-0

Behavioral and neurophysiological effects of electrical stunning on zebrafish larvae

Check for updates

David-Samuel Burkhardt, Claire Leyden, Carina Thomas, Christian Brysch, Florian Alexander Dehmelt & Aristides B. Arrenberg

Two methods dominate the way that zebrafish larvae are euthanized after experimental procedures: anesthetic overdose and rapid cooling. Although MS-222 is easy to apply, this anesthetic takes about a minute to act and fish show aversive reactions and interindividual differences, limiting its reliability. Rapid cooling kills larvae after several hours and is not listed as an approved method in the relevant European Union directive. Electrical stunning is a promising alternative euthanasia method for zebrafish but has not yet been fully established. Here we characterize both behavioral and neurophysiological effects of electrical stunning in 4-day-old zebrafish larvae. We identified the electric field characteristics and stimulus duration (50 V/cm alternating current for 32 s) that reliably euthanizes free-swimming larvae and agarose-embedded larvae with an easy-to-implement protocol. Behavioral analysis and calcium neurophysiology show that larvae lose consciousness and stop responding to touch and visual stimuli very quickly (<1 s). Electrically stunned larvae no longer show coordinated brain activity. Their brains instead undergo a series of concerted whole-brain calcium waves over the course of many minutes before the cessation of all brain signals. Consistent with the need to implement the 3R at all stages of animal experimentation, the rapid and reliable euthanasia achieved by electrical stunning has potential for refinement of the welfare of more than 5 million zebrafish used annually in biomedical research worldwide.

The zebrafish (*Danio rerio*) is one of the most common model organisms in neuroscience and biomedical research, with more than 5 million individuals used in animal experiments annually[1,2]. Because this figure excludes many animals used just for breeding instead of experiments, or animals used below the legal age limit (5 days post fertilization, or dpf), the total number is even higher. Also, it is expected that the overall number will further increase owing to the promising characteristics of this model organism and its continued spread into many areas of research[3]. Good scientific practice alone already requires well-designed and planned animal experiments[4], but this is further reinforced by an increasing awareness of the use of animals for scientific research in society[5] and the still unanswered question of to what extent fish perceive and suffer from pain[6–8]. Within the European Union (EU), directive 2010/63/EU states the legal euthanasia methods for fish: percussive blow to head, anesthetic overdose and electrical stunning. However, uncertainties persist concerning the application of these methods to zebrafish larvae (Fig. 1a).

First, percussive blows to the head are not practical or safe to perform because larvae are only 4 mm in size[9]. Second, overdose of the anesthetic MS-222, which in adult fish leads to death through asphyxiation and hypoxemia due to blocked gill ventilation[10], does not reliably work on zebrafish larvae, as they rely on cutaneous gas exchange during early gill development[11,12]. At 12–14 dpf, cutaneous gas exchange is no longer sufficient to meet the minimal respiratory requirements[13]. Thus, despite the onset of a cardiac arrest when using a high concentration of MS-222 (900 mg/l), zebrafish larvae regain consciousness when transferred back to regular tank water[11]. Moreover, MS-222 triggers aversive reactions in zebrafish[14,15]. Behaviors such as piping, twitching and erratic swimming have been observed in fish when exposed to both unbuffered and buffered MS-222 solutions[16]. Fish even seem to prefer to spend more time in

Werner Reichardt Centre for Integrative Neuroscience and Institute for Neurobiology, University of Tuebingen, Tuebingen, Germany.
e-mail: aristides.arrenberg@uni-tuebingen.de

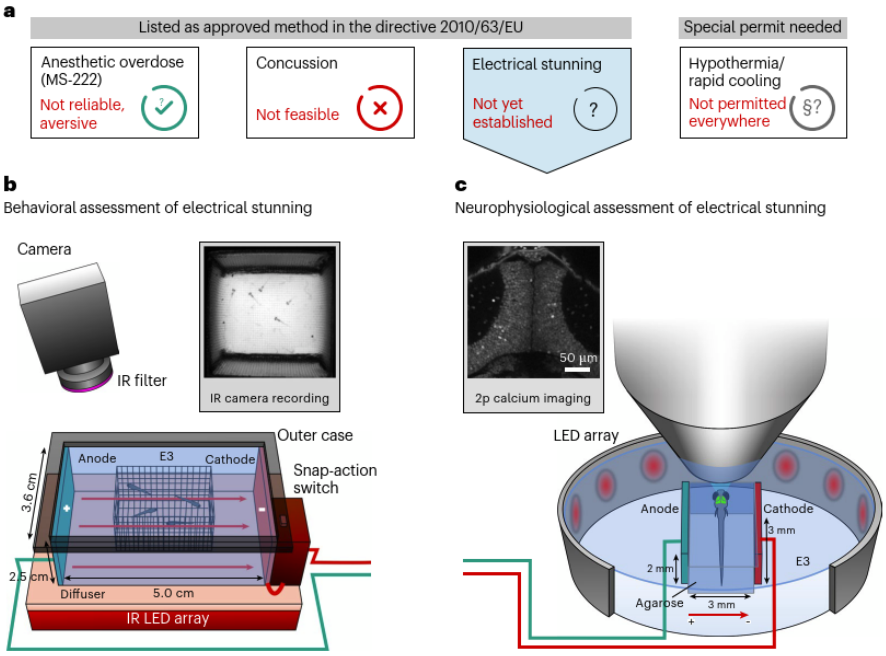

Fig. 1 | Developing a protocol for humane euthanasia via electrical stunning. **a**, An illustration of different euthanasia methods for zebrafish. **b**, The electrical stunning chamber with cuboid net container allows imaging of behavior. **c**, The brain activity of immobilized animals can be measured via 2-photon (2p) calcium imaging during visual stimulation and electrical stunning.

a dark environment than in an illuminated environment containing the anesthetic MS-222, which may indicate that fish would rather undergo discomfort than be exposed to MS-222 (ref. 17). Furthermore, the efficacy of MS-222 is variable across animals[13].

Another euthanasia method that is not universally permitted by law for zebrafish but is often used after special approval by the local authorities is rapid cooling, in which the animals are placed in cold water (2–4 °C). The resulting hypothermic shock is thought to cause death by slowing the rate of cellular activities and neural impulses, finally leading to cardiac arrest[11]. It is mostly considered a humane alternative to an anesthetic overdose, because fish exhibit signs of distress over a much shorter period compared with MS-222-treated animals[16,18]. While the onset of unconsciousness is probably fast[19], zebrafish larvae survive long periods in cold water[20]. In fact, rapid cooling in larvae younger than 14 dpf requires an exposure of at least 12 h for reliable euthanasia[21]. These results highlight how little is known about the exact timing of death resulting from this method at early stages of development, prolonging the time window in which suffering is possible[22].

Legislation including the relevant EU directive alternatively permits the application of electricity for euthanasia and refers to this as electrical stunning, even if death, not stunning, is the intended outcome. Electrical stunning protocols have successfully been established for larger fish[23]. However, its suitability has scarcely been investigated for laboratory zebrafish[20] and electrical stunning has never been successfully established as a humane euthanasia method for zebrafish. Knowledge about reliable parameters including voltage gradient, exposure duration, voltage type, the needed water conductivity and the resulting power density in the fish body are missing[1]. There is also no known adequate and approved equipment available on the market that could be used for this purpose[18] (see Mocho et al.[20] for a previous report on electrical stunning[20]). Euthanasia by electrical stunning is most likely to be achieved by asphyxiation of the stunned fish[24]. In small fish larvae with sufficient cutaneous oxygen supply, the mechanism of euthanasia is probably cell death due to unrecoverable damage to the cell membrane integrity or energy depletion of the fish[25]. Larger cells seem particularly susceptible to electric-field-induced membrane damage[26], which is why the effectiveness of electrical stunning is expected to increase with fish size. Also, different voltage types (such as direct current (DC), pulsed direct current (PDC) or alternating current (AC) and the associated frequencies) are thought to directly influence mortality rate and tissue damage[27–31]. Different aspects of electrical stunning have been investigated for various fish species at different stages of development, but the parameters were often not systematically varied and the effects of electrical stunning on zebrafish behavior and brain activity were not systematically recorded[20,27,32]. To the best of our knowledge, there is not a single study in which potential suffering and stress associated with electrical stunning was quantified in zebrafish, nor in which neural correlates of such experiences were quantified, such as changes to sensory processing induced by the euthanasia method.

Here, we investigated electrical stunning as an alternative humane euthanasia method for zebrafish larvae on both the behavioral and the neurophysiological level using calcium imaging (Fig. 1b,c). We examined and compared different voltage types (DC, PDC and AC) and exposure durations (2 s to 32 s) and their influence on mortality rate and tissue damage. We identified a set of parameters that reliably work at a voltage frequency close to the main frequency of 50 or 60 Hz and for a standard embryo medium conductivity of 670 µS/cm (ref. 33), resulting in a 100% mortality rate. Besides behavioral examination we also investigated neuronal activity patterns using calcium imaging, confirming the total loss of coordinated and stimulus-associated neuronal activity and behavior during and after electrical stunning.

Results

Mortality rates and behavioral effects of electrical stunning

To identify the optimal parameter set encompassing voltage gradient, voltage type and exposure duration for electrical stunning, we exposed larvae to DC, AC (60 Hz) or PDC (60 Hz or 6 Hz, duty cycle 50%)

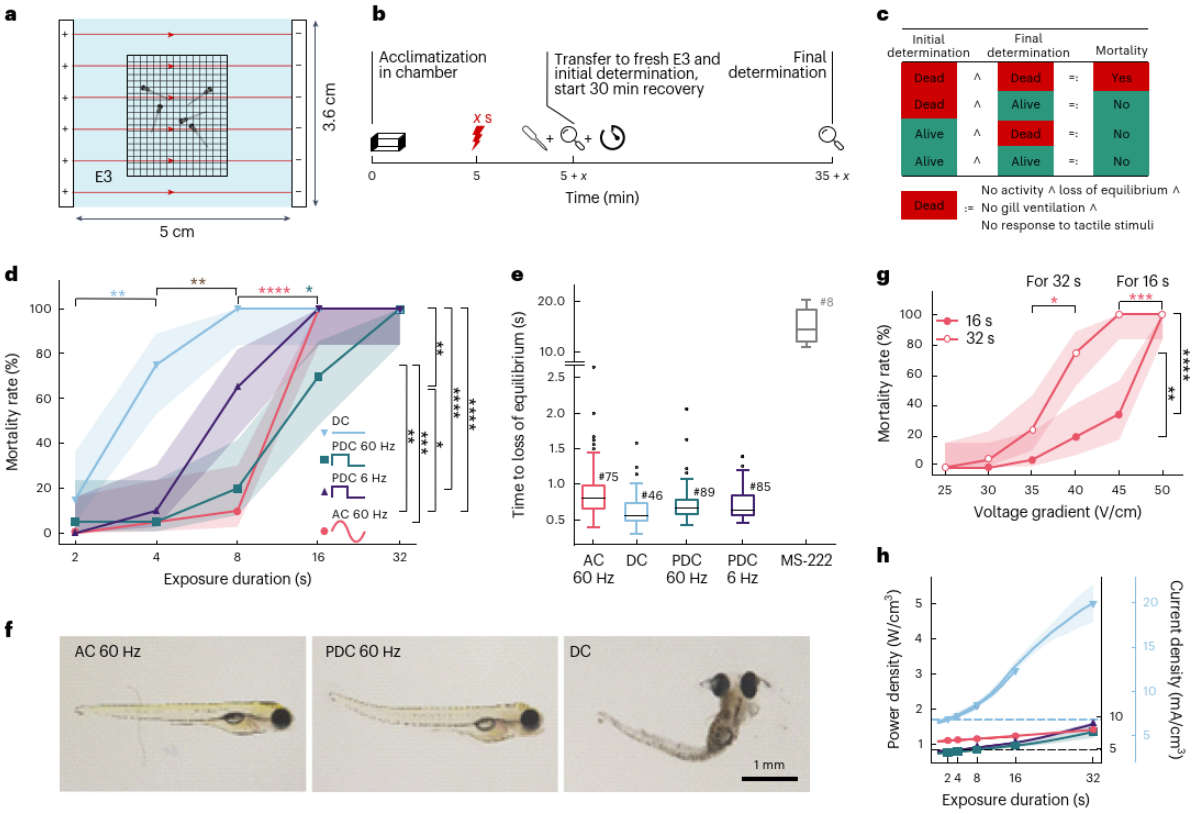

Fig. 2 | Electric AC fields are well suited for euthanasia of larvae. a, A schematic of the experimental setup. **b**, The protocol for assessing mortality. *x* is the exposure duration that was systematically varied over trials. **c**, The logical matrix defining under which condition within the experimental procedure a larva was considered dead. **d**, Mortality rates of different voltage types for different exposure durations at a voltage gradient of 50 V/cm. The asterisks indicate significances by *z*-test for proportions followed by Bonferroni correction between exposure durations for the same voltage type (colored asterisks) and between voltage types for the same exposure duration (black asterisks); $^{*}P < 0.05$, $^{**}P < 0.01$, $^{***}P < 0.001$, $^{****}P < 0.0001$. The envelopes show 95% Wilson confidence intervals. $n = 400$ larvae, $n = 4$ shock exposure trials with 5 larvae each. **e**, The time to loss of equilibrium for different voltage types (animal numbers are provided next to the hash symbols) For comparison, the time to loss of equilibrium for MS-222 (336 mg/l)[22] is shown in gray. **f**, Morphological effects of electrical stunning at 50 V/cm, 32 s, directly after exposure. **g**, Mortality rates of 16 s and 32 s exposure duration for different voltage gradients at AC voltage. The asterisks indicate significance by *z*-test for proportions followed by Bonferroni correction between voltage gradients and exposure durations; $^{*}P < 0.05$, $^{**}P < 0.01$, $^{***}P < 0.001$, $^{****}P < 0.0001$. The envelopes show 95% Wilson confidence intervals. $n = 240$, $n = 4$ shock exposures with 5 larvae each. **h**, The mean power density and current density of different voltage types for different exposure durations at 50 V/cm. Power and current densities were calculated on the basis of measured currents during the experiment. The dashed lines indicate the expected power density without joule heating (light blue, DC; black, AC and PDC). Light blue *y* axis on the right is for DC and the black *y* axis on the right for AC and PDC experiments. The envelopes show s.d.

electric fields (50 V/cm) in the water bath (Fig. 2a, $n = 20$ larvae per condition; 4 trials with 5 animals per trial). Mortality was assessed as loss of equilibrium, lack of locomotor activity, lack of gill ventilation and lack of responses to tactile stimuli (Fig. 2b,c and Methods). For five different exposure durations (from 32 s to 2 s in logarithmic steps), we conducted four independent trials involving five larvae each. Different mortality rates occurred at different exposure times depending on the type of voltage used. At 32 s of exposure, all voltage types resulted in 100% mortality. For 16 s of exposure, only 60 Hz PDC was not able to reach a 100% mortality rate. At 8 s of exposure, significant divergence in mortality rates among voltage types emerged for the first time (*z*-test for proportions, $P < 0.01$), with rates dropping below 20% for all types at 2 s (Fig. 2d). Behavioral loss of equilibrium was immediate across all voltage types, occurring within 900 ms (AC, 0.89 s ± 0.38 s; DC, 0.64 s ± 0.25 s; PDC 60 Hz, 0.73 s ± 0.28 s; PDC 6 Hz, 0.72 s ± 0.22 s (average ± s.d.)), suggesting an instant onset of loss of sensation (that is, anesthesia) (Fig. 2e)[34].

Depending on the voltage type used, several morphological changes, including body curvature, opaque brain tissue and sometimes fractures, could be observed for longer exposure durations (32 s and 16 s) for all voltage types. Morphological abnormalities were recorded directly, 15 and 30 min after exposure. These included visible destruction of tissue, skin and eyes as well as severe deformation of the body axis (lordosis, kyphosis and scoliosis) for DC and 6 Hz PDC and only up to medium-grade body axis deformation for AC and 60 Hz PDC (Fig. 2f and Supplementary Fig. 1). Many AC-treated larvae showed no morphological phenotype directly after stunning and only developed a phenotype over the course of 30 min. None of the larvae exhibiting abnormalities survived.

Because AC voltage and exposure durations of 16 and 32 s achieved 100% mortality with a fast onset and only minimal morphological abnormalities, we next refined these parameters with regard to the voltage gradient. We tested five different voltage gradients (from 45 V/cm to 20 V/cm) for 16 s and 32 s exposure duration. Already for 45 V/cm, mortality rates differed significantly, and only the 32 s trial still reached 100% mortality

rate (*z*-test for proportions, $P < 0.0001$) (Fig. 2g). We therefore concluded that AC (60 Hz), 50 V/cm and 32 s is a reliable and effective parameter set to achieve 100% mortality rate, and it was used for all subsequent calcium imaging experiments to assess the effects of electrical stunning on the neurophysiological level. To extend our observation period and confirm that no larvae recover, we conducted another, independent experiment using our optimal parameter set (AC, 60 Hz, 50 V/cm, 32 s) and we included one additional observation time point in the morning of the day following the electrical stunning. Again, all larvae were dead after the 30 min recovery period. None of the larvae came back to life overnight and none of them showed a heartbeat the next morning ($n = 20$ larvae, 4 trials with 5 fish each).

Electrolysis and joule heating

During experiments using the exposure chamber, electrolysis could be observed as small bubbles formed at the electrode surfaces. Because the pH of the E3 medium remained stable at 7 after electrical stunning, this was not investigated further. However, electrolysis effects should be explored more comprehensively for a final implementation of electrical stunning.

Furthermore, an increase in temperature and, thus, in electrical current was observed during exposure to AC, DC and PDC for all exposure durations. Temperature increases ranged from 1.26 ± 0.33 °C for PDC (60 Hz) and 2 s exposure duration to 24.25 ± 0.22 °C (average ± s.d.) for DC and 32 s exposure duration (Supplementary Fig. 2). The temperature rise was 13.3 ± 0.53 °C for AC (60 Hz), 50 V/cm, 32 s, with 36.1 °C being the maximum temperature reached. The observed change in temperature is due to joule heating, where an electric current heats a medium. In turn, the conductivity changes, which again influences the current magnitude. These effects lead to a rise in power density in the exposure chamber, which in principle could have influenced the mortality rates (Fig. 2h). No rise in temperature was observed during calcium imaging experiments (see below), where a single larva was agarose-embedded between two small electrodes. This is most likely due to the substantially smaller electrode surfaces and the proportionally larger E3 volume in the Petri dish, which serves as a heat sink. To rule out that the temperature rise and increased power density affect mortality rates for AC at 50 V/cm and 32 s exposure duration, and to ensure comparability between the mortality rate experiments using the exposure chamber and the calcium imaging experiments not using it, a transfer experiment was carried out where single agarose-embedded larvae were exposed to an AC field with 50 V/cm for 32 s using the small electrodes (Methods). After exposure, larvae were freed from agarose and mortality was determined using the same behavioral criteria as used for free-swimming experiments. No difference in mortality rate was observed ($n = 6$ larvae with 100% mortality rate). Thus, even in the absence of a rise in power density associated with the exposure chamber, 100% mortality can be achieved with AC at 50 V/cm and a 32 s exposure duration.

Swim bursts during electrical stunning

Within the first seconds of exposure to any tested electrical field, we observed short bursts of tail movements, either during or after loss of equilibrium (Supplementary Video 1). If this corresponded to a planned locomotion behavior, this might have implications regarding the state of the animal and associated potential of suffering. To rule out any such kind of active locomotion, we recorded a high-speed video of a single embedded larva with its tail cut free and exposed to an AC field at 50 V/cm for 32 s (Fig. 3a). A kymograph of the total angle of the tail revealed a strong initial tail deflection at exposure onset followed by a tail beat frequency perfectly matching the 60 Hz sinusoidal frequency of the electric field applied, strongly suggesting that the observed muscle movements were passively driven by the electric field (Fig. 3b,e, top and Supplementary Video 2). Furthermore, both tail beat amplitude and standard length[35] decreased during exposure (preexposure 3.9 mm, intraexposure 3.1 mm; Fig. 3c), presumably as a result of bilateral tail muscle contraction driven by the electric field. Also, the spatiotemporal curvature pattern of the tail differed drastically for tail undulations during exposure as compared with a spontaneous swim bout (Fig. 3d). During the spontaneous swim bout, the point of maximal curvature traveled along the tail in rostrocaudal direction for each tail undulation at a frequency of 20 Hz (Fig. 3e, bottom), which is conducive to forward swimming[36]. However, during electric field exposure, the stereotypic spatiotemporal pattern could not be observed, that is, the complete tail contracted at once in an abnormal, bilaterally synchronized fashion.

The observed phenomenon might be related to the pseudo-forced swimming described previously[37], although the voltage type used in that study was DC.

Loss of visually driven neural activity during electrical stunning

To quantify and compare neuronal activity before, during and after electrical stunning, two-photon calcium imaging was performed while applying a simple and strong visual on–off stimulus (full-field flash) and simultaneously exposing larvae to an electric field (AC, SIN, 60 Hz, 50 V/cm, 32 s; Fig. 4a). Recordings were done in the optic tectum, which is known to be a hub in visual processing and contains different populations of neurons well responding to on and off flashes[38,39]. Because the visual system of zebrafish larvae develops rapidly, strong optokinetic responses and associated sensory-driven neural activity are already established by 4 dpf (refs. 40,41). The absence of such sensory-driven activity can thus serve as a reliable indicator of defective neural processing.

Mean fluorescence time courses across all pixels obtained from the calcium recordings before (baseline), during (shock) and after (recovery) electrical stunning revealed drastic changes in activity patterns and overall intensities (Fig. 4b). Exposure to the electrical field also gave rise to a fast-propagating calcium wave (<2 s) with high mean fluorescence intensities along with strong spatial drifts (>20 µm), resulting in permanent morphological changes that impeded consistent segmentation of individual neurons across recording time (Supplementary Video 3). After exposure, mean fluorescence intensity across each image frame decreased until the occurrence of further, slowly (>2 s) propagating calcium waves, with different characteristics than the initial wave (Fig. 4b). Due to these strong changes in fluorescence intensity, adjustment of laser power and photomultiplier tube (PMT) gain between individual recordings was necessary to avoid overexposure and damage to the PMTs. Thus, absolute fluorescence intensities cannot and should not be compared across recordings.

To investigate whether visual processing still occurred during and after electrical stunning, the mean power spectral density (PSD) of all pixels within a recording was analyzed across all fish, where for intact vision-related processing the stimulus main frequency (0.1667 Hz) should not be affected much by spatial drifts of the larva in the recording window (Supplementary Fig. 3). As expected, PSD analysis revealed a total loss of the visual stimulus main frequency (0.1667 Hz) during shock and recovery ($P < 0.01$ between 0 Hz and 0.22 Hz for shock and recovery recording, two-way repeated-measures analysis of variance (ANOVA) followed by Tukey's honest significant difference (HSD) test; Fig. 4c,d). A further PSD analysis covering only the period during exposure to the electric field (32 s) confirmed this observation (Fig. 4d, middle, inset). Furthermore, the mean power density strongly increased toward lower frequencies during shock and recovery recordings, representing the observation of brain-wide, slowly changing calcium intensity.

Next, we segmented neurons in each the baseline and recovery recording to ask how the population tuning to the visual stimuli changed. The optic tectum contains diverse sets of neurons, some correlated and others anti-correlated or not correlated with our luminance stimulus. Also, on average, fluorescence time courses of neurons should inherit some form of periodicity as the stimulus itself consisted of various periodic parts. By contrast, during and after exposure, all these characteristics should have vanished to confirm loss of intact neural processing and the effectiveness of electrical stunning as a euthanasia method. In

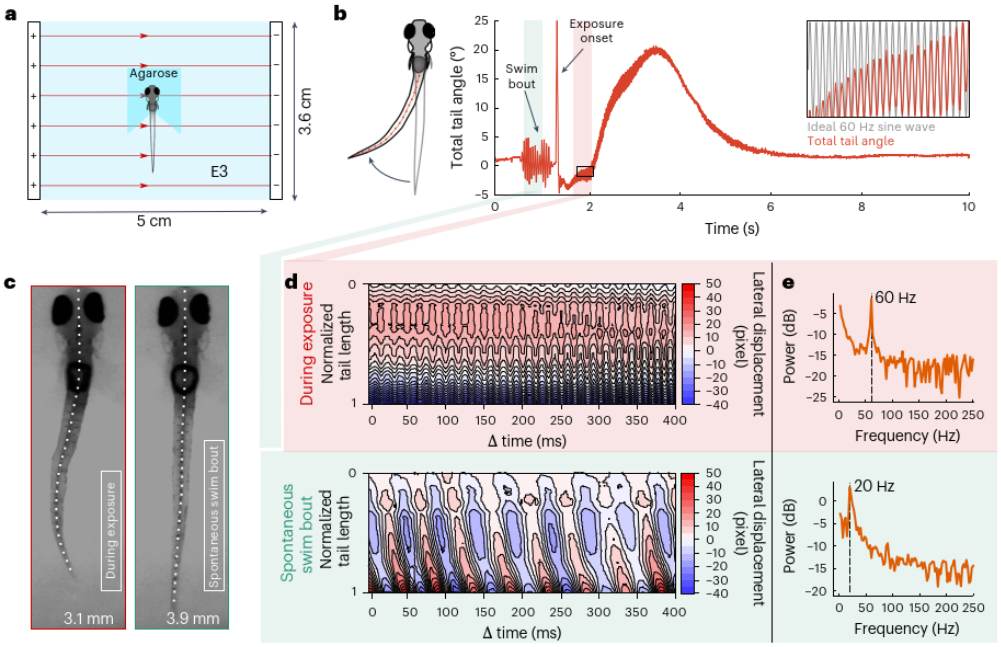

Fig. 3 | The AC field drives direct muscle contractions. a, A schematic of the experimental setup. Agarose surrounding the larva's tail has been removed. **b**, Left, a schematic of larva illustrating tail displacement during electrical stunning. The orange arrows indicate the skeleton used for computing the total tail angle. Right, the total tail angle during exposure. The arrows indicate a spontaneous swim bout and the exposure onset. The inset shows the tail angle during exposure, which perfectly matched a 60 Hz sinusoidal wave. **c**, The length of the larva during (left) and before (right) electrical stunning. **d**, Top, the lateral tail displacement profile during electrical stunning. Bottom: the lateral tail displacement profile during the spontaneous swim bout. **e**, Top, the power spectrum during electrical stunning. Bottom, the power spectrum during the spontaneous swim bout. $n = 2$.

total, 4,958 segmented regions of interest (ROIs) were analyzed during baseline recording and 3,369 ROIs during recovery ($n = 7$ fish). The difference in number of detected ROIs is due to the technical difficulty of detecting ROIs during recovery. Neurons in the optic tectum showed diverse activity patterns during baseline recording with regard to visual stimulation, where 3.5% of the overall number of neurons were correlated or anti-correlated to the visual regressor with a correlation coefficient above 0.3 (Fig. 4e,h). During recovery recordings, not a single neuron had a correlation coefficient higher than 0.3. Also, a Levene test revealed a significant difference in the variance of correlation with the visual regressor between both recordings ($P < 0.0001$). To characterize the stimulus-related activity, we quantified the pairwise cross-correlation between the 20% best correlated neurons within each fish for both baseline and recovery recording (Fig. 4f). Neurons within each matrix were sorted by their correlation coefficient from positive to negative, resulting in a structure with two visible anti-correlated populations (red and blue) during baseline recording. These populations correspond to neurons responding to either the on or off phase of the visual stimulus. No similar structure could be found during the recovery recording, where almost all neurons correlated with each other, which could be explained by an overall synchronous decrease in fluorescence due to the fading out of the initial calcium wave. Finally, an autocorrelation function (ACF) of both recordings yielded a perfect periodic pattern for the baseline recording representing the periodic stimulus-related activity pattern, and nothing but linear decrease during the recovery recording (Fig. 4g).

All these results strongly indicate that, during electrical stunning and afterward, no neural processing with respect to visual perception was possible, as the dominance of monotonous calcium signals indicates nonintact brain activity and presumable loss of sensation.

Discussion

In this study, we investigated electrical stunning as an alternative euthanasia method for zebrafish larvae. We systematically evaluated different voltage types, voltage gradients and exposure durations, resulting in a robust parameter set that can be implemented under real-world conditions (32 s, 50 V/cm, AC, 100% mortality). We further demonstrated that observed tail movements during exposure are unrelated to any kind of voluntary locomotion and that electrical stunning provokes an immediate loss of coordinated neuronal activity—and, therefore, probably suppresses any sensation that could arouse suffering. Importantly, larvae never recovered from this terminal state, and their rapid loss of equilibrium confirms that electrical stunning minimizes the remaining time window before complete incapacitation, especially compared with previously established euthanasia methods.

Reliable parameters are straightforward to implement

One of our major aims was not only to comprehensively examine the effects of electrical stunning on behavioral and neurophysiological levels but also to devise a reliable parameter set that can be implemented in practice across international and disciplinary boundaries. Therefore, an important consideration was to also examine a sinusoidal AC voltage with a frequency near 50 or 60 Hz, as is common in many countries. While both 32 s and 16 s exposures lead to 100% mortality at 50 V/cm (Fig. 2d), we recommend 32 s to account for possible variations in specific future implementations. We confirmed the loss of stimulus-associated neural activity only for a 32 s exposure and not for a 16 s exposure, posing a limitation to the 16 s. Despite joule heating raising the resulting power density to 1.4 W/cm^3 after 32 s during behavioral assays (Fig. 2h), the calcium imaging experiments showed that 0.85 W/cm^3 is in fact sufficient to reliably euthanize zebrafish larvae. This is in accordance with published findings

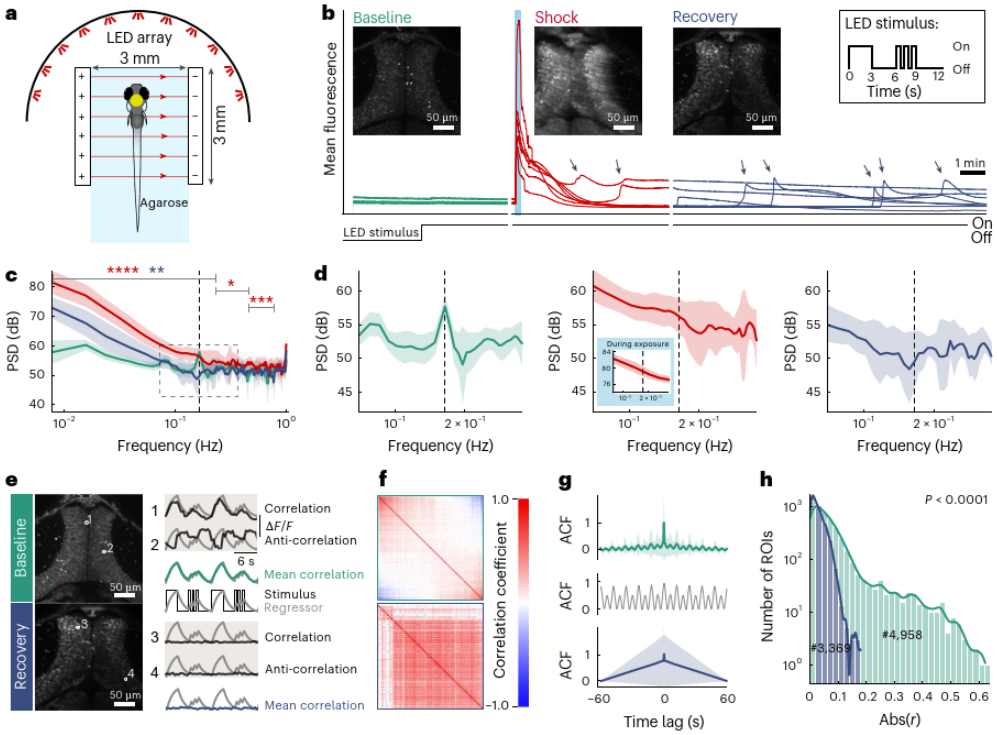

Fig. 4 | Absence of sensory-evoked neural activity during and after electrical stunning. a, A schematic of the experimental setup positioned under the two-photon microscope. The yellow dot indicates the imaged brain area (optic tectum). **b**, Mean calcium signals for baseline, shock and recovery recording for all fish (one trace per fish). The light-blue bar indicates exposure duration. The LED stimulus trace indicates when a visual stimulus was used or not. The arrows highlight the occurrence of slowly propagating calcium waves occurring after electrical stunning. **c**, The mean PSD for baseline, shock and recovery recording (green, red and dark blue as used in **b**). The envelopes show s.d. The dashed line indicates the visual stimulus main frequency of 0.1667 Hz. The asterisks indicate periods with significant differences to baseline recording (two-way repeated-measures ANOVA followed by Tukey's HSD test; $^{*}P<0.05$, $^{**}P<0.01$, $^{***}P<0.001$, $^{****}P<0.0001$). **d**, The inset of **c** for baseline, shock and recovery recordings. **e**, Example calcium traces of neurons (black) (anti-)correlated with the stimulus (gray), and mean correlation traces (green and dark blue) of 20% best correlated ROIs for baseline and recovery recording. **f**, ROI cross-correlation matrices for baseline and recovery recording (top and bottom). **g**, The mean ACF for baseline and recovery recording (top and bottom). The envelopes show s.d. Gray shows the ACF for the stimulus (regressor) itself. **h**, A histogram of absolute ROI cross-correlation coefficients (Abs(r)) for baseline and recovery recordings. Hash symbols indicate the overall number of neurons (ROIs) used. P value derived from Levene test. $n=7$.

that a calculated power density of 0.7 W/cm^3 with PDC at 50 Hz, 25 V/cm and 1120-1130 µS/cm (ref. 20) is sufficient to euthanize zebrafish larvae, whereas a power density of 0.00086 W/cm^3 using AC at 12.5 V/cm and 2000 µS/cm (ref. 42) has no influence on the survival rate. Although the conductivity of small fish species is thought to be less than 30 µS/cm (ref. 43) and, therefore, the conductivity of a zebrafish larva is most likely even smaller, our medium for electrical stunning with a conductivity of 680 µS/cm was chosen specifically to be consistent with a standard E3 embryo medium (5 mM NaCl, 0.17 mM KCl, 0.33 mM $CaCl_2$, 0.33 mM $MgSO_4$ and 10^{-5}% methylene blue) as it is commonly used for zebrafish larvae[33].

The suggested parameters should be easy to implement in an electrical stunning setup owing to their characteristics, and the principle layout of the exposure chamber introduced in our experimental setup (Fig. 1b and Supplementary Fig. 4) might provide a possibility to build and establish safe and adequate devices as required by the EU directive 2010/63/EU[18].

Electrical stunning reduces time window to onset of euthanasia

We have demonstrated that loss of equilibrium can be reliably induced within a single second using electrical stunning, which is an important aspect when evaluating an euthanasia method[44]. On a behavioral level, an animal is likely to be unconscious from the time point on its losing its righting reflex (which in our study is equivalent to the loss of equilibrium)[34]. Tricaine (MS-222) is known to work relatively slowly in this respect, as it takes between 25 s and 34 s for adult zebrafish to lose equilibrium at a concentration of 250 mg/l (refs. 15,16,45). Even at 336 mg/l it takes about 15 s for larvae until the loss of the righting reflex[22]. Although for rapid cooling the time window to onset decreases to less than 15 s for larval zebrafish, a constant exposure to cold is still required for 12 h to ensure reliable euthanasia[19,21]. The much faster onset time (0.89 s ± 0.38 s, average ± s.d. for AC, 50 V/cm) for electrical stunning therefore has an immediate effect on the reduction of any possible stress and suffering. Aversive reactions shown by larvae as reported for tricaine use[20] were not observed.

AC is the best-suited voltage type for electrical stunning

Depending on voltage type and voltage gradient, different injuries such as tissue disruption, vertebral dislocations and even fractures are known to occur in fish. These injuries most likely arise from strong muscle contractions caused by direct electrical stimulation of either muscles or the neuromuscular pathway and are influenced by the voltage type used as well as the voltage gradient and frequency[23,46,47]. There are different findings regarding how different types of voltage affect mortality and injuries in fish. According to ref. 31, using DC or reducing the frequency

at PDC results in less injury to fish whereas AC is most likely to cause tetany, potentially resulting in injury and mortality. Also, ref. 48 reported that spinal injuries have mostly been associated with AC, and there are numerous reports about non-DC waveform that together with different frequencies negatively affected injury and survival rates[23,47–50]. However, this does not seem to be the case for embryos and zebrafish larvae, which are found to be more vulnerable to DC[27,28,42,51]. This concurs with our findings, where DC (50 V/cm, 32 s) led to severe tissue destruction and ruptures (Fig. 2f). DC treatment was also associated with the highest reached temperatures due to joule heating (up to 46.9 ± 0.4 °C), which probably contributed to the morphological defects of larvae via thermal denaturation of proteins. During treatments with AC, however, the temperature increased only mildly and stayed below 38 °C (50 V/cm, 32 s, AC 35.03 ± 0.77 °C), a temperature that is frequently used for live zebrafish in genetic experiments[52–55], while only up to medium body axis deformations could be observed. However, further studies are needed to ascertain whether cells and tissue of AC-euthanized larvae remain intact and useable for any postmortem analyses. Although the DC-associated injuries and body deformations are unlikely to impact larval welfare relative to AC, given DC's loss of equilibrium also occurring in within 1 s (0.64 s ± 0.25 s), the observable injuries might misconstrue electrical stunning as an unsuitable euthanasia method. To avoid this issue and taking into account that a good euthanasia method should also consider the emotional effect on observers and operators[44], we endorse AC as the most compelling voltage type for electrical stunning applications on zebrafish larvae.

Electrical stunning with AC is followed by widespread propagating calcium waves

Over the course of investigating neuronal activity during and after electrical stunning, we observed a strong synchronous rise of intracellular calcium (also referred to as a fast-propagating calcium wave) alongside the onset of the electrical field as well as concomitant morphological changes. Most likely, this first wave was caused by the influx of calcium from extracellular space driven by the electric field[56]. This influx might in turn have led to ATP depletion and mitochondrial failure due to the loss of membrane potential, further causing imbalance of calcium and potassium and, finally, cell death[57–60]. The exact mechanism underlying cell and organismal death in zebrafish larvae via AC-based electrical stunning remains unclear. Several (interacting) cell death pathways have been discussed in a recent review on the effects of electroporation[25]. Although we did not characterize the differences between the initial fast-propagating and following slow-propagating calcium waves in detail, they seemed to differ in propagating speed, maximum calcium intensity and place of origin. The slow-propagating calcium waves (as seen by eye) might be similar to earlier observations in zebrafish larvae, where a slow wave occurred after cardiac arrest, traveling in a caudal–rostral direction and thought to be associated with neuronal death and brain damage[61]. Other brain-wide calcium waves in zebrafish larvae, akin to what is called a spreading depolarization[62,63], could be observed in the context of heat-induced neural dysfunctions[64]. In rats, the presence of a large-amplitude electroencephalography wave after decapitation has been described. It was assumed that the wave reflects a massive opening of ion channels (depolarizing wave) that occurred owing to neurons lacking energy, which might have led to a breakdown of transmembrane potential, leading to oscillations and the observed wave[65,66]. Although a comprehensive elucidation of the mechanism and relevance of these slow-propagating calcium waves necessitates further investigation, our findings, alongside perception of visual stimuli and behavior of larvae during and after electrical stunning, argue against their association with suffering or stress.

Electrical stunning is an effective alternative euthanasia method

In summary, our results suggest that electrical stunning, when using the proposed parameters, is an effective euthanasia method for zebrafish larvae. Although only examined for 4 dpf in this study, the suggested parameter set is most likely to also reliably work for older zebrafish larvae, as vulnerability of fish to electrical current is thought to increase with body size[26]. Besides immediate loss of equilibrium, the irrevocable loss of coordinated and sensory-driven neuronal activity strongly indicate rapid onset of unconsciousness during treatment[34]. As far as we know, the only other studies examining neuronal activity alongside exposure of electrical fields to fish were performed applying electroencephalography on African catfish and cichlids. In these studies, a general epileptiform insult could be observed, which was followed by fibrillation after electrical stunning[67,68]. The slowly propagating calcium waves after electrical stunning observed in this study encourage further investigation, but they most likely do not influence the efficacy of the euthanasia method itself or the animal's welfare. Given the fact that electrical stunning is already a permitted euthanasia method for fish in the EU, its implementation in laboratory routines could plausibly contribute to a refinement in the sense of 3R (replacement, reduction and refinement)[4,69] across many disparate research labs.

Online content

Any methods, additional references, Nature Portfolio reporting summaries, source data, extended data, supplementary information, acknowledgements, peer review information; details of author contributions and competing interests; and statements of data and code availability are available at https://doi.org/10.1038/s41684-024-01505-0.

Received: 6 March 2024; Accepted: 16 December 2024
Published online: 27 January 2025

References

1. Lidster, K., Readman, G. D., Prescott, M. J. & Owen, S. F. International survey on the use and welfare of zebrafish *Danio rerio* in research. *J. Fish Biol.* **90**, 1891–1905 (2017).
2. Tavares, B. & Lopes, S. S. The importance of zebrafish in biomedical research. *Acta Médica Port* **26**, 583–592 (2013).
3. Lawrence, C. in *Methods in Cell Biology* Vol. 135, 483–508 (Elsevier, 2016).
4. Russel, W. M. S. & Burch, R. L. *The Principles of Humane Experimental Technique* (Methuen, 1959).
5. Clemence, M. & Leaman, J. *Public Attitudes to Animal Research in 2016* (Ipsos MORI, 2016).
6. Diggles, B. K. et al. Reasons to be skeptical about sentience and pain in fishes and aquatic invertebrates. *Rev. Fish. Sci. Aquac.* **32**, 127–150 (2024).
7. Rose, J. D. et al. Can fish really feel pain? *Fish Fish.* **15**, 97–133 (2014).
8. Sneddon, L. U. Pain in aquatic animals. *J. Exp. Biol.* **218**, 967–976 (2015).
9. Valentim, A. M., van Eeden, F. J., Strähle, U. & Olsson, I. A. S. Euthanizing zebrafish legally in Europe. *EMBO Rep.* **17**, 1688–1689 (2016).
10. Soivio, A., Nyholm, K. & Huhti, M. Effects of anaesthesia with MS 222, neutralized MS 222 and benzocaine on the blood constituents of rainbow trout, *Salmo gairdneri*. *J. Fish Biol.* **10**, 91–101 (1977).
11. Strykowski, J. L. & Schech, J. M. Effectiveness of recommended euthanasia methods in larval zebrafish (*Danio rerio*). *J. Am. Assoc. Lab. Anim. Sci.* **54**, 81–84 (2015).
12. Rombough, P. Gills are needed for ionoregulation before they are needed for O_2 uptake in developing zebrafish, *Danio rerio*. *J. Exp. Biol.* **205**, 1787–1794 (2002).
13. Rombough, P. J. Ontogenetic changes in the toxicity and efficacy of the anaesthetic MS222 (tricaine methanesulfonate) in zebrafish (*Danio rerio*) larvae. *Comp. Biochem. Physiol. A* **148**, 463–469 (2007).
14. Readman, G. D., Owen, S. F., Murrell, J. C. & Knowles, T. G. Do fish perceive anaesthetics as aversive? *PLoS ONE* **8**, e73773 (2013).

15. Collymore, C., Banks, E. K. & Turner, P. V. Lidocaine hydrochloride compared with MS222 for the euthanasia of zebrafish (*Danio rerio*). *J. Am. Assoc. Lab. Anim. Sci.* **55**, 816–820 (2016).
16. Wilson, J. M., Bunte, R. M. & Carty, A. J. Evaluation of rapid cooling and tricaine methanesulfonate (MS222) as methods of euthanasia in zebrafish (*Danio rerio*). *J. Am. Assoc. Lab. Anim. Sci.* **48**, 785–789 (2009).
17. Wong, D., Keyserlingk, M. A. G., von, Richards, J. G. & Weary, D. M. Conditioned place avoidance of zebrafish (*Danio rerio*) to three chemicals used for euthanasia and anaesthesia. *PLoS ONE* **9**, e88030 (2014).
18. Köhler, A. et al. Report of workshop on euthanasia for zebrafish—a matter of welfare and science. *Zebrafish* **14**, 547–551 (2017).
19. Chen, K. et al. The evaluation of rapid cooling as an anesthetic method for the zebrafish. *Zebrafish* **11**, 71–75 (2014).
20. Mocho, J.-P. et al. A multi-site assessment of anesthetic overdose, hypothermic shock, and electrical stunning as methods of euthanasia for zebrafish (*Danio rerio*) embryos and larvae. *Biology* **11**, 546 (2022).
21. Wallace, C. K. et al. Effectiveness of rapid cooling as a method of euthanasia for young zebrafish (*Danio rerio*). *J. Am. Assoc. Lab. Anim. Sci.* **57**, 58–63 (2018).
22. Leyden, C. et al. Efficacy of tricaine (MS-222) and hypothermia as anesthetic agents for blocking sensorimotor responses in larval zebrafish. *Front. Vet. Sci.* **9**, 864573 (2022).
23. Lines, J. A., Robb, D. H., Kestin, S. C., Crook, S. C. & Benson, T. Electric stunning: a humane slaughter method for trout. *Aquac. Eng.* **28**, 141–154 (2003).
24. Effects of electricity. *Humane Slaughter Association* https://www.hsa.org.uk/humane-harvesting-of-fish-electrical-stunning/effects-of-electricty (2017).
25. Batista Napotnik, T., Polajžer, T. & Miklavčič, D. Cell death due to electroporation—a review. *Bioelectrochemistry* **141**, 107871 (2021).
26. Bohl, R. J., Henry, T. B. & Strange, R. J. Electroshock-induced mortality in freshwater fish embryos increases with embryo diameter: a model based on results from 10 species. *J. Fish Biol.* **76**, 975–986 (2010).
27. Bohl, R. J., Henry, T. B., Strange, R. J. & Rakes, P. L. Effects of electroshock on cyprinid embryos: implications for threatened and endangered fishes. *Trans. Am. Fish. Soc.* **138**, 768–776 (2009).
28. Dwyer, W. P. & Erdahl, D. A. Effects of electroshock voltage, wave form, and pulse rate on survival of cutthroat trout eggs. *North Am. J. Fish. Manag.* **15**, 647–650 (1995).
29. Henry, T. B., Grizzle, J. M., Johnston, C. E. & Osborne, J. A. Susceptibility of ten fish species to electroshock-induced mortality. *Trans. Am. Fish. Soc.* **133**, 649–654 (2004).
30. Hollender, B. A. & Carline, R. F. Injury to wild brook trout by backpack electrofishing. *North Am. J. Fish. Manag.* **14**, 643–649 (1994).
31. Reynolds, J. B. in *Fisheries Techniques* (eds Murphy, B. R. & Willis, D. W.) 221–253 (American Fisheries Society, 1996).
32. Teulier, L., Guillard, L., Leon, C., Romestaing, C. & Voituron, Y. Consequences of electroshock-induced narcosis in fish muscle: from mitochondria to swim performance. *J. Fish Biol.* **92**, 1805–1818 (2018).
33. Nusslein-Volhard, C. & Dahm, R. *Zebrafish* (Oxford Univ. Press, 2002).
34. Meyer, R. E. in *Veterinary Anesthesia and Analgesia* (eds Grimm, K. A. et al.) 130–143 (Wiley, 2015); https://doi.org/10.1002/9781119421375.ch6
35. Parichy, D. M., Elizondo, M. R., Mills, M. G., Gordon, T. N. & Engeszer, R. E. Normal table of postembryonic zebrafish development: staging by externally visible anatomy of the living fish. *Dev. Dyn.* **238**, 2975–3015 (2009).
36. Müller, U. K. & van Leeuwen, J. L. Swimming of larval zebrafish: ontogeny of body waves and implications for locomotory development. *J. Exp. Biol.* **207**, 853–868 (2004).
37. Vibert, R. Neurophysiology of electric fishing. *Trans. Am. Fish. Soc.* **92**, 265–275 (1963).
38. Muto, A., Ohkura, M., Abe, G., Nakai, J. & Kawakami, K. Real-time visualization of neuronal activity during perception. *Curr. Biol.* **23**, 307–311 (2013).
39. Thompson, A. W., Vanwalleghem, G. C., Heap, L. A. & Scott, E. K. Functional profiles of visual-, auditory-, and water flow-responsive neurons in the zebrafish tectum. *Curr. Biol.* **26**, 743–754 (2016).
40. Easter, S. S. Jr. & Nicola, G. N. The development of vision in the zebrafish (*Danio rerio*). *Dev. Biol.* **180**, 646–663 (1996).
41. Niell, C. M. & Smith, S. J. Functional imaging reveals rapid development of visual response properties in the zebrafish tectum. *Neuron* **45**, 941–951 (2005).
42. Nguyen, P. L., Yefimov, B. A., Coffin, A. & Cooper, C. Electroimmobilization as an alternative method to chemical immobilization of larval fish. *Trans. Am. Fish. Soc.* **148**, 725–738 (2019).
43. Lutnesky, M. M. F., Cradock, K. R. & Reynolds, J. B. Immobilization threshold and fish conductivity of two small fishes. *North Am. J. Fish. Manag.* **39**, 788–792 (2019).
44. *AVMA Guidelines for the Euthanasia of Animals: 2020 Edition* (Office of Laboratory Animal Welfare, 2020); https://olaw.nih.gov/policies-laws/avma-guidelines-2020.htm
45. Ferreira, J. M. et al. Anesthesia overdose versus rapid cooling for euthanasia of adult zebrafish. *Zebrafish* **19**, 148–159 (2022).
46. Nordgreen, A. H., Slinde, E., Møller, D. & Roth, B. Effect of various electric field strengths and current durations on stunning and spinal injuries of Atlantic herring. *J. Aquat. Anim. Health* **20**, 110–115 (2008).
47. Robb, D. H. F., O' Callaghan, M., Lines, J. A. & Kestin, S. C. Electrical stunning of rainbow trout (*Oncorhynchus mykiss*): factors that affect stun duration. *Aquaculture* **205**, 359–371 (2002).
48. Snyder, D. E. *Electrofishing and Its Harmful Effects on Fish* (United States Geological Survey USGS, 2003); https://apps.dtic.mil/sti/pdfs/ADA420879.pdf
49. Dolan, C. R. & Miranda, L. E. Injury and mortality of warmwater fishes immobilized by electrofishing. *North Am. J. Fish. Manag.* **24**, 118–127 (2004).
50. Sharber, N. G., Carothers, S. W., Sharber, J. P., De Vos, J. C. & House, D. A. Reducing electrofishing-induced injury of rainbow trout. *North Am. J. Fish. Manag.* **14**, 340–346 (1994).
51. Henry, T. B. & Grizzle, J. M. Survival of largemouth bass, bluegill and channel catfish embryos after electroshocking. *J. Fish Biol.* **64**, 1206–1216 (2004).
52. Halloran, M. C. et al. Laser-induced gene expression in specific cells of transgenic zebrafish. *Development* **127**, 1953–1960 (2000).
53. Ádám, A., Bártfai, R., Lele, Z., Krone, P. H. & Orbán, L. Heat-inducible expression of a reporter gene detected by transient assay in zebrafish. *Exp. Cell. Res.* **256**, 282–290 (2000).
54. Hardy, M. E., Ross, L. V. & Chien, C.-B. Focal gene misexpression in zebrafish embryos induced by local heat shock using a modified soldering iron. *Dev. Dyn.* **236**, 3071–3076 (2007).
55. Murtha, J. M. & Keller, E. T. Characterization of the heat shock response in mature zebrafish (*Danio rerio*). *Exp. Gerontol.* **38**, 683–691 (2003).
56. Cho, M. R., Thatte, H. S., Silvia, M. T. & Golan, D. E. Transmembrane calcium influx induced by ac electric fields. *FASEB J.* **13**, 677–683 (1999).
57. Duchen, M. R. Contributions of mitochondria to animal physiology: from homeostatic sensor to calcium signalling and cell death. *J. Physiol.* **516**, 1–17 (1999).
58. Garcia-Dorado, D., Ruiz-Meana, M., Inserte, J., Rodriguez-Sinovas, A. & Piper, H. M. Calcium-mediated cell death during myocardial

reperfusion. *Cardiovasc. Res.* **94**, 168–180 (2012).
59. Hajnóczky, G., Davies, E. & Madesh, M. Calcium signaling and apoptosis. *Biochem. Biophys. Res. Commun.* **304**, 445–454 (2003).
60. Smaili, S. et al. Calcium and cell death signaling in neurodegeneration and aging. *An. Acad. Bras. Ciênc.* **81**, 467–475 (2009).
61. Xu, D. et al. General anesthetics protects against cardiac arrest-induced brain injury by inhibiting calcium wave propagation in zebrafish. *Mol. Brain* **10**, 44 (2017).
62. Spong, K. E., Andrew, R. D. & Robertson, R. M. Mechanisms of spreading depolarization in vertebrate and insect central nervous systems. *J. Neurophysiol.* **116**, 1117–1127 (2016).
63. Woitzik, J. et al. Propagation of cortical spreading depolarization in the human cortex after malignant stroke. *Neurology* **80**, 1095–1102 (2013).
64. Andreassen, A. H., Hall, P., Khatibzadeh, P., Jutfelt, F. & Kermen, F. Brain dysfunction during warming is linked to oxygen limitation in larval zebrafish. *Proc. Natl Acad. Sci. USA* **119**, e2207052119 (2022).
65. Rijn, C. M., van., Krijnen, H., Menting-Hermeling, S. & Coenen, A. M. L. Decapitation in rats: latency to unconsciousness and the 'wave of death'. *PLoS ONE* **6**, e16514 (2011).
66. Zandt, B.-J., Haken, B., ten, Dijk, J. Gvan & Putten, M. J. A. Mvan Neural dynamics during anoxia and the 'wave of death'. *PLoS ONE* **6**, e22127 (2011).
67. Lambooij, E., Gerritzen, M. A., Reimert, H., Burggraaf, D. & van de Vis, J. W. A humane protocol for electro-stunning and killing of Nile tilapia in fresh water. *Aquaculture* **275**, 88–95 (2008).
68. Lambooij, E., Kloosterboer, R. J., Gerritzen, M. A. & van de Vis, J. W. Assessment of electrical stunning in fresh water of African catfish (*Clarias gariepinus*) and chilling in ice water for loss of consciousness and sensibility. *Aquaculture* **254**, 388–395 (2006).
69. Würbel, H. More than 3Rs: the importance of scientific validity for harm-benefit analysis of animal research. *Lab. Anim.* **46**, 164–166 (2017).

Publisher's note Springer Nature remains neutral with regard to jurisdictional claims in published maps and institutional affiliations.

Open Access This article is licensed under a Creative Commons Attribution 4.0 International License, which permits use, sharing, adaptation, distribution and reproduction in any medium or format, as long as you give appropriate credit to the original author(s) and the source, provide a link to the Creative Commons licence, and indicate if changes were made. The images or other third party material in this article are included in the article's Creative Commons licence, unless indicated otherwise in a credit line to the material. If material is not included in the article's Creative Commons licence and your intended use is not permitted by statutory regulation or exceeds the permitted use, you will need to obtain permission directly from the copyright holder. To view a copy of this licence, visit http://creativecommons.org/licenses/by/4.0/.

© The Author(s) 2025

Methods

Animals

Animal experiments were permitted by the local government authorities (Regierungspraesidium Tuebingen) and conducted in accordance with German federal law and Baden-Württemberg state law. Zebrafish larvae (*Danio rerio*) were reared on a 14/10 h light/dark cycle at 28 °C in E3 medium (5 mM NaCl, 0.17 mM KCl, 0.33 CaCl and 0.33 $MgSO_4$) with 0.01% methylene blue. Wild-type (nacre +/−) larvae were used for the mortality rate and behavioral experiments. Transgenic zebrafish expressing GCaMP6f [*Tg(HuC:H2B-GCaMP6f)jf7Tg*] were used for the two-photon calcium imaging experiments. The top 10–20% of larval zebrafish with high calcium indicator expression levels were selected from all fish at 3 dpf for in vivo calcium imaging experiments using an epifluorescence stereoscope. All behavioral and calcium imaging experiments were performed on 4 dpf zebrafish larvae at room temperature. Supplementary Tables 1–3 contain lists of experimental groups and animals used per group.

Exposure chamber for mortality rate experiments

To determine mortality rates of multiple free-swimming larvae, an exposure chamber covering a volume of 50 × 36 × 15 mm was designed and built out of polystyrene. The internal dimensions of the exposure chamber represent a trade-off between the space needed to safely expose multiple larvae to an electric field and the required voltage gradients. To protect against leakage currents, the programmable power source GW Instek ASR2050R (Good Will Instruments) was connected to the exposure chamber by a residual-current circuit breaker (F200, B Type, ABB Ltd (Asea Brown Boveri)). This guaranteed safe operation for both AC and DC voltages. Two stainless-steel electrodes (36 × 15 mm) with a thickness of 1 mm were placed inside the chamber at a distance of 50 mm. A custom-made 3D-printed electrode holder was used to hold the electrodes in place and to ensure the exact distance of 50 mm. This electrode holder also included a rigid net with an aperture of no more than 405 µm (PA-405/47, Eckert), in which larvae could be placed during exposure. This ensured that larvae were always exposed to the center of the electric field (Supplementary Figs. 4 and 5a). Electrodes were constructed by the precision mechanics workshop of Eberhard Karls University, Tuebingen, Germany. All polymer components were constructed and 3D-printed in the lab (Ultimaker3, Ultimaker B.V., ink: Ultimaker Material PLA Black, diameter 2.85 mm). For safety reasons, operation of the exposure chamber depends on a snap-action switch that requires a closed lid. The lid and bottom of the chamber are transparent to enable diffuse back illumination at 920 nm from below and behavioral recording from above. A light-emitting diode (LED) array containing 48 LEDs with a 50° emission angle and a diffuser (frosted glass) was used for illumination. Recording was done at up to 30 Hz using a camera (DMK23UV024, The Imaging Source Europe GmbH) with a 6 mm objective and an infrared (IR) longpass filter (SCHOTT RG780, Edmund Optics). Both the power source and the camera recording were controlled by the custom-written Python software 'synchASR2000-control'[70]. The software allowed us to individually set voltage type (DC, PDC and AC), overall voltage, maximum current, frequency and exposure duration.

Determining mortality rates

For each experiment, the exposure chamber was filled with 24 mL of room-temperature E3 medium (680 µS/cm conductivity). Five larvae were transferred into the chamber, followed by a 5 min acclimatization period. After that period, the temperature of the E3 medium inside the chamber was measured once using a digital thermometer (GMH 3200 Series, Greisinger) and the lid was closed. An electric field was then applied for a specific exposure duration. In the case of controls, no electric field was applied. During the exposure, larvae were video recorded. The recording was synchronized with the onset of the electric field via the Python software using a timestamp. Immediately after the exposure, the lid was opened and the temperature was measured again. Larvae were then moved into a dish of fresh E3 (room temperature). To determine mortality rates, all larvae were visually examined via a stereo microscope directly after exposure to an electrical field and a second time after a 30 min recovery period in fresh E3 (Fig. 2b). Mortality was defined by the following criteria: no activity of any kind, loss of equilibrium, no operculum movement and no startle response (tested by a strong tactile stimulus in the form of poking with a blunt metal needle). Together with muscle tone and cardiac failure (which were not assessed here), these criteria correspond to the fourth stage of anesthesia in fish, describing overdose[71]. Muscle tone observation was excluded owing to the ability of electrical fields to cause muscle tension. Meanwhile, cardiac arrest is not a suitable criterion for death in larval zebrafish, because their small size ensures that oxygen diffusion into vital tissue is sufficient for survival even after the heart stops beating[11]. Heartbeat may persist for up to 10 min after euthanasia with MS-222 and 40 min after hypothermic shock[11]. Some studies even report that MS-222-treated larvae were able to recover their heartbeat when subsequently transferred to fresh water[11,13]. Also, in our study, cardiac arrest rates (as assessed via visual inspection using a stereoscope) differed from mortality rates for exposure durations between 2 s and 32 s (Supplementary Fig. 6). Larvae were considered dead only if all tested criteria were met at both two observation points (directly after exposure and after the 30 min recovery period) (Fig. 2c). After the second observation point, all larvae were put into ice water for 20 min and were then transferred into a freezer where they were kept for at least 48 h to ensure proper euthanasia for potentially survived fish. In total, 600 fish were used in 30 different groups, with each group containing 4 independent trials with 5 fish each (Supplementary Table 1). Significant differences between different voltage types and between exposure durations within each voltage type were determined by *z*-test for proportions followed by Bonferroni correction. To further minimize potential stress and suffering and to ensure animal welfare, a pilot trial with 20 larvae anesthetized with MS-222 (168 mg/l) and 20 nonanesthetized larvae exposed to 50 V/cm for 32 s (DC) was conducted before all experiments. Because results revealed no increased mortality rates for MS-222 and no visible difference in animal behavior during exposure, all subsequent experiments were carried out without anesthetic (*z*-test for proportions, $P > 0.05$; Supplementary Fig. 7).

Determining loss of equilibrium

Loss of equilibrium was determined by hand using the video recordings from the mortality rate experiments and the image processing package Fiji[72]. The time difference between the exposure onset of electrical stunning and the first frame where larvae departed from the upright position was measured. Not all recorded larvae from the mortality experiments could be analyzed, because they sometimes swam into the shadow cast by the electrode frame, which made it impossible to observe the time point of loss of equilibrium. Therefore, the number of larvae analyzed in this regard differed from the total number of larvae recorded. In total, 295 fish were analyzed.

Setup for simultaneous calcium imaging and electrical stunning

For calcium imaging experiments, a two-photon IR laser (Coherent Chameleon Vision S, Coherent) at a wavelength of 920 nm was used and calcium signals were recorded using a movable-objective microscope (MOM; Sutter Instruments) with GaAs PMTs, C7319 Hamamatsu preamplifiers and the MScan software (2016 version) by Sutter. All recordings were conducted in the optic tectum, scanning a single plane per fish approximately 40–70 µm deep with a 20×/1.0 objective (Zeiss W Plan-Apochromat 421452-9800) at a frequency of 2 Hz and a magnification of 1.8×. To conduct calcium imaging alongside simultaneous visual stimulation and exposure to an electric field, a setup containing a LED ring with 18 × 650 nm LEDs (EVERLIGHT Electronic, EVL 383-2SDRD/S5, 125 mcd) and a centered 50 mm Petri dish with two small stainless-steel electrodes was developed. The electrodes (2 × 3 mm, 0.5 mm thick) were placed at a distance of 3 mm in the Petri dish using a custom-made 3D-printed frame. The frame enclosed the electrodes from

three sides to avoid any unwanted possible contact with the microscope objective (Supplementary Figs. 5c and 8). To connect the electrodes to the power source, a 200-µm-thin copper plate was welded to their back sides to allow soldering of cables. The power source was controlled by the custom-written Python software 'synchASR2000-control'. To present a strong visual on/off stimulus, the LED ring was connected to an Arduino NANO, controlling the power supply of the LEDs. To gate the LEDs during laser scanning, the Arduino NANO considered the fly-back signal provided by the MOM. On/off signals from the LEDs, fly-back signal from the MOM and the onset signal of the electrical field were recorded at 100 Hz via an Arduino UNO and another custom-written Python software called 'recSignals-control'. The whole setup was electrically separated from the microscope objective by a modified SM1L05 lens tube containing an insulating plastic spacer.

Calcium imaging alongside electrical stunning and visual stimulation

For all calcium imaging experiments, the following shock parameters were used: 32 s, 50 V/cm, AC, SIN. For each experiment, a single zebrafish larva was embedded in 1.6% agarose gel (Biozym Sieve GeneticPure Agarose 850080 mixed with E3 medium) between the electrodes (Fig. 4a). The embedding was performed in the absence of any anesthetic drugs. Agarose is electrically neutral, so the electrical conductivity of the gel is determined by the liquid added[73]. Therefore, it can be assumed that the conductivities of E3 medium and agarose gel were approximately the same and it was unlikely to affect the homogeneity of the electric field. Each experiment consisted of three subsequent recordings: baseline recording (6 min, 3 min of which with visual stimulation), shock recording (6 min with visual stimulation) and recovery recording (12 min with visual stimulation) (Fig. 4b). Recordings were done in the optic tectum, which is known to be a hub in visual processing and contains different populations of neurons responding well to on and off flashes[38,39]. In total, seven fish were imaged.

Swimming burst analysis

A high-speed recording (IDT iN8-S1 camera) with a sampling rate of 500 Hz was performed on a single agarose-embedded 4 dpf larva (nacre +/−) using the exposure chamber without the rigid net (Fig. 3a). Agarose was removed around the tail to observe exposure-related movements, as described in Arrenberg[74]. Recording was performed for 10 s (exposure onset was approximately 1 s after the start of recording). Electrical stunning was performed with a sinusoidal AC field, 60 Hz, 50 V/cm, for 32 s.

To analyze the recordings, images were first smoothed using a median filter (filter size 20 × 20 pixels) to remove noise. Afterward, the gray values of all pixels were first inverted and then binarized. Areas smaller than 600 pixels in size were removed to clear the image, leaving only the silhouette of the fish. A skeleton of the silhouette representing the spine of the fish was computed to track tail deflections. Lateral displacement of the tail was defined as the distance (in pixels) of each skeleton pixel to the fish's original rostrocaudal axis, normalized to the mean displacement during the spontaneous swim bout and field exposure. The total tail angle (in degrees) was calculated for each frame by computing the angles between all neighboring pixels on the skeleton and then taking the sum along the entire tail. Tail length was normalized to the shortest skeleton computed using 1D interpolation. In total, two fish were recorded and analyzed.

Transfer experiment

To compare results across experiments on free-swimming and embedded larvae, a transfer experiment was conducted. A single larva was embedded in 1.6% agarose between the small electrodes in the setup for simultaneous calcium imaging and electrical stunning, and a shock (32 s, 50 V/cm, AC) was applied. Directly after shock application, the larva was carefully freed, and mortality was assessed using the behavioral criteria described above. In total, six fish were examined.

Analysis of ROIs and cross-correlation matrices

All data analysis was done in Python. Baseline and recovery recordings were registered to s.d. z projection, and ROIs were segmented using suite2p[75]. The calcium signal ($\Delta F/F_b$, that is, fluorescence changes relative to baseline) at time point t was calculated as in ref. 22. The calcium signal of each ROI was calculated for the second half of the baseline recording (visual stimulus present) and during the period preceding onset of a slow-propagating wave for the recovery recording, which differed across trials. The overall number of ROIs for baseline and recovery recording differed, which could be explained a combination of morphological changes during electrical stunning, the overall decrease in calcium activity and the increase of synchronized activity among ROIs that led to poor segmentation results in the recovery recordings.

Regression-based identification of stimulus-encoding neurons was used in this study to quantify alterations of vision-related activity during and after electrical stunning[76]. For this purpose, an 'on' regressor was computed by first resampling the recorded on/off signals of the visual stimulus to 2 Hz and then convolving them with a calcium impulse response function using an exponential decay time constant of 1.61 s for GCaMP6f. ROIs were then correlated with the on regressor to test how well their activities matched the expected calcium signal of a neuron responding to light onsets. Distributions of correlation coefficients for baseline and recovery recording were analyzed via a Levene test.

To generate cross-correlation matrices, ROIs were sorted by their correlation coefficient (from positive to negative correlation with the stimulus) and a cross-correlation matrix of the 20% best correlated ROIs was computed. Matrices of all fish were brought to the same size (mean size of all matrices) using linear interpolation. A weighted average matrix was then computed, based on the total number of ROIs per fish.

PSD analysis

Welch's PSD method was used for estimating the power density of fluorescence at different frequencies for all recordings (baseline, shock and recovery). Because recordings during exposure to an electrical field were affected by strong spatial drifts of the preparation and image registration and across-frames segmentation of ROIs were therefore not possible, the PSD for each pixel in each recording for all fish was calculated, using the entire recording length of each raw image time series without any preprocessing. Calcium traces for all pixels were first detrended by subtracting the mean, then PSDs were calculated. Finally, the mean PSD spectrum of all pixels was calculated for all recordings. To prove that a large drift in the recording will not affect the mean PSD spectrum in a major way, and that the most prominent frequencies will still be visible, a 100-pixel drift over 720 frames (6 min) was simulated for a stable baseline recording and PSD was calculated subsequently (Supplementary Fig. 3). PSD results were analyzed via two-way repeated-measures ANOVA with Tukey's HSD test.

Reporting summary

Further information on research design is available in the Nature Portfolio Reporting Summary linked to this article.

Data availability

All data from this study are available from the corresponding author upon request.

References

70. Burkhardt, D.-S. & Arrenberg, A. Software synchASRcontrol. *G-Node* https://doi.org/10.12751/g-node.y5pjnv (2024).
71. Sneddon, L. U. Clinical anesthesia and analgesia in fish. *J. Exot. Pet Med.* **21**, 32–43 (2012).
72. Schindelin, J. et al. Fiji: an open-source platform for biological-image analysis. *Nat. Methods* **9**, 676–682 (2012).
73. Walker, P., Lerski, R. A., Mathur-De Vré, R., Binet, J. & Yane, F. VI. Preparation of agarose gels as reference substances for NMR

relaxation time measurement. *Magn. Reson. Imaging* **6**, 215–222 (1988).
74. Arrenberg, A. B. Fiber optic-based photostimulation of larval zebrafish. *Methods Mol. Biol.* **1451**, 343–354 (2016).
75. Pachitariu, M. et al. Suite2p: beyond 10,000 neurons with standard two-photon microscopy. Preprint at *bioRxiv* https://doi.org/10.1101/061507 (2017).
76. Miri, A., Daie, K., Burdine, R. D., Aksay, E. & Tank, D. W. Regression-based identification of behavior-encoding neurons during large-scale optical imaging of neural activity at cellular resolution. *J. Neurophysiol.* **105**, 964–980 (2011).

Acknowledgements
The project on which this Article is based was funded by the German Federal Ministry of Education and Research under grant number 16LW0292. Responsibility for the content of this publication lies with the authors.

Author contributions
The conceptualization of the project was done by A.B.A., D.-S.B. and F.A.D. Experimental setups were designed and constructed by D.-S.B., C.L. and A.B.A. Experiments were conducted by D.-S.B. and C.L.; all data were analyzed by D.-S.B. Resources were provided by A.B.A. Figures were made by D.-S.B., C.T. and A.B.A. The manuscript was written by D.-S.B. and A.B.A. with the help of F.A.D. and C.B. The funding acquisition was done by A.B.A., D.-S.B. and F.A.D.

Funding
Open Access funding enabled and organized by Projekt DEAL.

Competing interests
The authors declare no competing interests.

Additional information
Supplementary information The online version contains supplementary material available at https://doi.org/10.1038/s41684-024-01505-0.

Correspondence and requests for materials should be addressed to Aristides B. Arrenberg.

Peer review information *Lab Animal* thanks Ana Valentim, Kristine von Krogh and the other, anonymous, reviewer(s) for their contribution to the peer review of this work.

Reprints and permissions information is available at www.nature.com/reprints.

nature portfolio

Corresponding author(s): Aristides Arrenberg

Last updated by author(s): Dec 13, 2024

Reporting Summary

Nature Portfolio wishes to improve the reproducibility of the work that we publish. This form provides structure for consistency and transparency in reporting. For further information on Nature Portfolio policies, see our Editorial Policies and the Editorial Policy Checklist.

Statistics

For all statistical analyses, confirm that the following items are present in the figure legend, table legend, main text, or Methods section.

n/a	Confirmed
☐	☒ The exact sample size (*n*) for each experimental group/condition, given as a discrete number and unit of measurement
☐	☒ A statement on whether measurements were taken from distinct samples or whether the same sample was measured repeatedly
☐	☒ The statistical test(s) used AND whether they are one- or two-sided *Only common tests should be described solely by name; describe more complex techniques in the Methods section.*
☒	☐ A description of all covariates tested
☐	☒ A description of any assumptions or corrections, such as tests of normality and adjustment for multiple comparisons
☐	☒ A full description of the statistical parameters including central tendency (e.g. means) or other basic estimates (e.g. regression coefficient) AND variation (e.g. standard deviation) or associated estimates of uncertainty (e.g. confidence intervals)
☐	☒ For null hypothesis testing, the test statistic (e.g. *F*, *t*, *r*) with confidence intervals, effect sizes, degrees of freedom and *P* value noted *Give P values as exact values whenever suitable.*
☒	☐ For Bayesian analysis, information on the choice of priors and Markov chain Monte Carlo settings
☒	☐ For hierarchical and complex designs, identification of the appropriate level for tests and full reporting of outcomes
☒	☐ Estimates of effect sizes (e.g. Cohen's *d*, Pearson's *r*), indicating how they were calculated

Our web collection on statistics for biologists contains articles on many of the points above.

Software and code

Policy information about availability of computer code

Data collection	Behavioral data was collected via imaging source cameras and partly analyzed via ImageJ. 2p-data was collected via the software MScan from Sutter.
Data analysis	Data analysis was performed using Python. All code was custom-written. For registration and segmentation of 2p-data the software suit2p was used.

For manuscripts utilizing custom algorithms or software that are central to the research but not yet described in published literature, software must be made available to editors and reviewers. We strongly encourage code deposition in a community repository (e.g. GitHub). See the Nature Portfolio guidelines for submitting code & software for further information.

Data

Policy information about availability of data

All manuscripts must include a data availability statement. This statement should provide the following information, where applicable:

- Accession codes, unique identifiers, or web links for publicly available datasets
- A description of any restrictions on data availability
- For clinical datasets or third party data, please ensure that the statement adheres to our policy

Data is available upon request. Information on hardware design is provided in the manuscript.

Field-specific reporting

Please select the one below that is the best fit for your research. If you are not sure, read the appropriate sections before making your selection.

☒ Life sciences ☐ Behavioural & social sciences ☐ Ecological, evolutionary & environmental sciences

For a reference copy of the document with all sections, see nature.com/documents/nr-reporting-summary-flat.pdf

Life sciences study design

All studies must disclose on these points even when the disclosure is negative.

Sample size	Each experimental group consisted of 4 trials of 5 animals each
Data exclusions	Any data exclusions are described in the method section.
Replication	no
Randomization	no
Blinding	no

Reporting for specific materials, systems and methods

We require information from authors about some types of materials, experimental systems and methods used in many studies. Here, indicate whether each material, system or method listed is relevant to your study. If you are not sure if a list item applies to your research, read the appropriate section before selecting a response.

Materials & experimental systems

n/a	Involved in the study
☒	☐ Antibodies
☒	☐ Eukaryotic cell lines
☒	☐ Palaeontology and archaeology
☐	☒ Animals and other organisms
☒	☐ Human research participants
☒	☐ Clinical data
☒	☐ Dual use research of concern

Methods

n/a	Involved in the study
☒	☐ ChIP-seq
☒	☐ Flow cytometry
☒	☐ MRI-based neuroimaging

Animals and other organisms

Policy information about studies involving animals; ARRIVE guidelines recommended for reporting animal research

Laboratory animals	Danio Rerio (zebrafish) according to national law and institutional guidelines.
Wild animals	*Provide details on animals observed in or captured in the field; report species, sex and age where possible. Describe how animals were caught and transported and what happened to captive animals after the study (if killed, explain why and describe method; if released, say where and when) OR state that the study did not involve wild animals.*
Field-collected samples	*For laboratory work with field-collected samples, describe all relevant parameters such as housing, maintenance, temperature, photoperiod and end-of-experiment protocol OR state that the study did not involve samples collected from the field.*
Ethics oversight	Experiments were performed according to national law and institutional guidelines.

Note that full information on the approval of the study protocol must also be provided in the manuscript.

7.2 Publication 2

Vertical Optokinetic Eye Movements in the Larval Zebrafish

Burkhardt, D.-S.*, Möller, G.*, Deligand, L., Fichtner, C., Hladnik, T. C., Arrenberg, A. B. (2026). *J Exp Biol*. DOI: https://doi.org/10.1242/jeb.251770

© 2026. Published by The Company of Biologists | Journal of Experimental Biology (2026) 229, jeb251770. doi:10.1242/jeb.251770

RESEARCH ARTICLE

Vertical optokinetic eye movements in the larval zebrafish

David-Samuel Burkhardt[1,*], Gabriel Möller[1,*], Laurian Deligand[1,2], Christiane Fichtner[1,3], Tim C. Hladnik[1,4] and Aristides B. Arrenberg[1,‡]

ABSTRACT

The optokinetic response (OKR), a reflex enabling stable visual processing by minimizing retinal slip, has been well characterized in teleosts over the last decades. Although previous work on teleost OKR mostly focused on its horizontal component, mammals are known to perform vertical and torsional OKR in addition to horizontal OKR. In this study, we characterized the vertical optokinetic response (vOKR) in larval zebrafish and compared it with the horizontal OKR (hOKR) and the vertical vestibulo-ocular reflex (vVOR). Our simultaneous camera-based tracking of vertical and horizontal eye positions revealed a distinct vOKR in larval zebrafish, but with a much smaller dynamic range compared with the hOKR and without any quick phases (resetting saccades). When presented with constant roll-rotating visual stimuli, zebrafish exhibited a brief initial vertical eye rotation in the direction of the stimulus, followed by a period without further slow phase response and interspersed with only spontaneous saccades. This behavior contrasts sharply with the periodical occurrence of resetting saccades (quick phases) during hOKR. The initial vertical response is tuned to similar spatial frequencies and angular velocities as the hOKR. We furthermore showed that the vVOR has a much larger vertical dynamic range than the vOKR, demonstrating that the neuronal circuitry itself – and not the oculomotor plant – is the limiting factor. Although it is unclear whether the observed differences in vertical versus horizontal optokinetic control have an adaptive value for zebrafish, the identified differences are drastic and informative for further studies on visuomotor circuits in teleosts.

KEY WORDS: Vertical optokinetic response, *Danio rerio*, Vertical eye movements, Vertical vestibulo-ocular response, Oculomotor circuits

INTRODUCTION

Eye movements are ubiquitous and essential in vertebrates, enabling animals to stabilize their gaze and process visual information efficiently. Investigation of eye movements provides valuable insights into the neural circuitry underlying sensory perception, motor coordination and behavior. In all vertebrates, eye movements are controlled by six extraocular muscles that enable horizontal, torsional and vertical rotations (Land, 2015), which correspond to yaw, pitch and roll rotations, respectively, in lateral-eyed animals. It is well established in mammals that all three directions of eye movement are used to counteract visual movements based on either vestibular or visual input, thereby stabilizing gaze position and minimizing retinal slip (Erickson and Barmack, 1980; Kitama et al., 2001; Seidman et al., 1995; van den Berg and Collewijn, 1988; Van der Steen and Collewijn, 1984).

Visual gaze stabilization is mediated via the optokinetic response (OKR) to large-field visual motion. This reflex is exhibited across vertebrate species and consists of two components: a slow phase involving relatively slow following of the visual stimulus by the eye, and a resetting quick phase (a type of saccade), which moves the eye in the opposite direction of the stimulus once the maximum eye excursion is reached. The speed during the slow phase can be related to stimulus speed to calculate the gain, where unity corresponds to perfect ocular following (Dehmelt et al., 2021; Glasauer and Straka, 2022; Holm-Jensen and Peitersen, 1979; Rinner et al., 2005). The larval zebrafish is a powerful model system for studying eye movements, their underlying circuitries and development (Brysch et al., 2019; Dowell et al., 2024, 2025; Easter and Nicola, 1997; Matsuda and Kubo, 2021; Orger, 2016). This species combines a fully functional visual system, with the six extraocular eye muscles needed for movement in all directions (Bellegarda et al., 2025; Kasprick et al., 2011), and a vestibular system that enables eye movements in response to acceleration and orientation within a gravitational field (Beck et al., 2004; Lambert et al., 2008; Lim et al., 2024). Previous studies have extensively characterized horizontal eye movements in larval zebrafish (Beck et al., 2004; Dehmelt et al., 2021; Easter and Nicola, 1997; Huang and Neuhauss, 2008; Rinner et al., 2005). Teleosts readily navigate in three dimensions in the water column, which suggests that vertical motion and vertical eye movements are important in these animals as well. Tadokoro et al. (2025) recently investigated the full repertoire of the OKR and VOR in adult goldfish. Furthermore, vertical and torsional eye movements elicited by vestibular – not visual – stimulation have been studied in larval xenopus (Lambert et al., 2008), goldfish (Graf and Meyer, 1983; Tadokoro et al., 2025) and larval zebrafish (Bianco et al., 2012; Sugioka et al., 2023); and in archer fish, 3D motions of eyes, including vertical movements, can be measured with a stereo camera setup (Ben-Simon et al., 2009). However, visually driven vertical eye movements during the optokinetic response (vOKR) have been largely overlooked in the teleost literature, and little is known about their expression and underlying circuitry.

Both optokinetic and optomotor responses stabilize fish gaze and posture based on optic flow mediated self-motion estimation (Britten, 2008; Festl et al., 2012; Kubo et al., 2014; Wang et al., 2019, 2020; Warren and Hannon, 1988). Optic flow is mainly processed in the optic tectum and pretectum by making use of a diverse set of neurons, tuned to different directions and motion patterns. Each direction-selective neuron prefers one out of four

[1]Werner Reichardt Centre for Integrative Neuroscience and Institute for Neurobiology, University of Tuebingen, 72076 Tuebingen, Germany. [2]Biology Department, Ecole Normale Superieure, PSL Universite Paris, 75005 Paris, France. [3]Faculty of Medical and Life Sciences, University of Applied Sciences Furtwangen, 78120 Furtwangen, Germany. [4]Graduate Training Centre of Neuroscience, University of Tuebingen, 72076 Tuebingen, Germany.
*These authors contributed equally to this work

‡Author for correspondence (aristides.arrenberg@uni-tuebingen.de)

D.-S.B., 0009-0001-7829-4913; G.M., 0000-0002-8731-4330; L.D., 0009-0006-8593-7362; C.F., 0009-0005-5208-7456; T.C.H., 0000-0001-9325-2087; A.B.A., 0000-0001-8262-7381

This is an Open Access article distributed under the terms of the Creative Commons Attribution License (https://creativecommons.org/licenses/by/4.0), which permits unrestricted use, distribution and reproduction in any medium provided that the original work is properly attributed.

Received 21 October 2025; Accepted 15 January 2026

local directions: up, down, temporal–nasal (TN) and nasal–temporal (NT) motion (Gabriel et al., 2012; Hunter et al., 2013; Wang et al., 2019; Zhang et al., 2022). Although zebrafish are thought to predominantly experience horizontal motion (TN and NT) owing to their swimming behavior (Ehrlich and Schoppik, 2017), the number of neurons that are direction-selective for vertical up or down visual motion is approximately equal to those encoding horizontal visual motion (Wang et al., 2019; Zhang et al., 2022). Therefore, vertical motion, be it pure up/down translation or roll or pitch rotations, seems to be very relevant for zebrafish.

In this study, we simultaneously recorded horizontal and vertical eye movements in 4-day-old zebrafish larvae (4 days post fertilization, dpf) while eliciting both horizontal and vertical OKR (hOKR and vOKR) by visual stimulation. Further, we quantified the vertical vestibulo-ocular response (vVOR), a reflex that works in concert with the OKR and relies on information from the semicircular canals and otoliths to respond to head acceleration and position. We compared the vVOR dynamics with those of the vOKR. Although we show that the vOKR does exist in larval zebrafish, its characteristics strongly differ from those of the hOKR.

MATERIALS AND METHODS

Animals

Animal experiments were permitted by the local government authorities (Regierungspraesidium Tuebingen) and conducted in accordance with German federal law and Baden-Württemberg state law. Zebrafish [*Danio rerio* (Hamilton 1822)] larvae were reared on a 14 h:10 h light:dark cycle at 28°C in E3 medium (5 mmol l^{-1} NaCl, 0.17 mmol l^{-1} KCl, 0.33 mmol l^{-1} CaCl, 0.33 mmol l^{-1} $MgSO_4$) with 0.01% Methylene Blue. All experiments were performed on 4 dpf zebrafish larvae, which are known to reliably perform hOKR (Easter and Nicola, 1997).

Setup for VOR experiments

To examine vertical eye movements of the VOR, a setup named KEBAB (Kinematic Evaluation of Behavior during Animal Body roll) with the ability of rotating a single larva around its rostral–caudal axis (roll) was developed and built in-house. For the most part, standard Thorlabs components were used to build an examination chamber, infrared (IR) illumination for eye-tracking, visual stimulation and a camera path – all on a single axis using the 30 mm Thorlabs cage system (Fig. S6). A Nema 17 stepper motor (ACT Motor GmbH, Germany) was used to rotate the whole setup. To provide electricity and enable data transfer from the steady world to the rotating camera system, its USB cable was connected via a rotating electrical slip ring (BQLZR 0.48 inch 12 Wire 2A 240V, Amazon). Both IR illumination and visual stimulation consisted of LED diodes (850 nm, white) with a 120-grid diffuser to provide uniform illumination. Recording was performed at ∼20 frames s^{-1} using a monochromatic camera (DMK23UV024, The Imaging Source Europe GmbH). For examination, larvae were embedded on a triangle stage in 1.6% low melting agarose as described in Wang et al. (2020). Agarose around the eyes was removed to allow ocular movements (Fig. S4). The stage was then clipped to a custom-made 3D-printed mount. The whole KEBAB setup was operated via an Arduino Uno with an A4988 RepRap stepper motor driver and the Python library Telemetrix (https://mryslab.github.io/telemetrix/) to enable remote control via a PC. The custom written Python-based software vxPy (https://github.com/thladnik/vxPy) was used to control setup rotation, visual stimulus presentation, camera recording and eye tracking. The noise floor of the setup was measured using anesthetized larvae (168 mg l^{-1} MS222; Fig. S7).

To investigate the vertical VOR, a stimulus protocol consisting of 2×3 stimulation phases, each framed by a 30 s pause phase, was conducted in complete darkness. During the stimulation phases, the KEBAB performed eight full rotations at 90, 45 or 22.5 deg s^{-1} velocity in either the clockwise or counter-clockwise direction. Both directions were performed for each head rotation velocity. During the pause phases, no rotation was performed.

Data analysis of VOR experiments

First, all eye traces of stimulation phases were smoothed using a rolling mean filter with a window size of 2 s and centered around a 0 deg axis to remove noise and outliers. The VOR score was calculated similar to Sun et al. (2018) by Fourier-transforming all eye traces into the power spectrum and then taking the amplitude at the head's rotation frequency (0.25, 0.125 or 0.0625 Hz) in degrees as the corresponding score. For gain and phase lag calculation, a sine function was fitted to the stimulus triggered average (STA) of eye velocity to obtain the full amplitude of eye movements. The gain was then calculated as the ratio between the amplitude of eye velocity and the stimulus velocity. Phase lag was calculated using cross-correlation.

In our vVOR experiments, we only used a single front camera, whereas in our vOKR experiments two cameras (top and front) were used. During vOKR, we noticed that spontaneous horizontal eye movements occurred. Therefore, we carefully inspected the vVOR videos and confirmed that no major horizontal eye movement components occurred. This observation is mainly based on the continuous visibility of the eye lens protruding on the side in the projected front camera recording (see also Movie 1).

Setup for vOKR and hOKR experiments

For recording horizontal and vertical OKR behavior, a modified version of the visual stimulation arena described in Dehmelt et al. (2018) was used. To record horizontal and vertical eye movements simultaneously, the stimulation displays in front and at the back of the fish were removed. Despite the removal of two displays, the visual stimuli of the two remaining displays still covered ∼30% of the zebrafish field of view (Fig. S5, calculated according to Dunn and Fitzgerald, 2020), which should suffice to elicit a reliable OKR (Dehmelt et al., 2021). An additional camera (DMK23UV024, The Imaging Source Europe) was positioned in front of the fish additionally to the camera from the top and the corresponding IR backlight was positioned behind the fish. Fish were positioned in the middle of the arena in a water-filled translucent container, and the cameras were adjusted so that both had a good view of the head and the eyes of the fish. A black lid was placed onto the container, making sure that it had direct contact with the water surface to prevent unwanted reflections at the water-air surface. A similar cover was placed on the bottom of the container for the same reason. Both the lid and bottom cover had a small hole in the middle to allow the IR bottom backlight to reach the fish and the camera from the top to see the fish. The two remaining displays on the left and the right side of the fish were used for OKR stimulus presentation and were sufficient to elicit OKR behavior. For each recording, a single zebrafish larva was embedded into 1.6% agarose. The procedure was similar to that described for the vVOR experiments, but to enable both vertical and horizontal eye movements along with high-quality video recording in the IR spectrum, the agarose around and in front of the eyes was removed, leaving a small triangular portion to stabilize the head (Fig. S4).

Journal of Experimental Biology

Journal of Experimental Biology (2026) 229, jeb251770. doi:10.1242/jeb.251770

vOKR and hOKR stimulus protocols

To assess whether zebrafish larvae exhibit a vOKR and characterize its tuning to different stimulus parameters, a constant rotation OKR stimulus was used. To characterize the vOKR tuning, stimulus parameters known to encompass the range of best hOKR tuning were adapted from Dehmelt et al. (2021). All possible combinations of six different spatial frequencies and five different angular velocities were tested (Table S1). The stimulus protocol consisted of alternating stimulation phases where the stimulus would rotate either clockwise or counter-clockwise, framed by 60 s pause phases with a static grating. The order of spatial frequency and angular velocity pairs was randomized for each recording, as well as the initial direction of rotation, with each parameter pair rotating both clockwise and counter-clockwise.

Because larvae only responded within the first few seconds to a constant rotating stimulus, a second stimulus protocol using sinusoidally modulated rotation was designed with the aim of eliciting a more robust and prolonged vOKR. The number of stimulus periods within 1 s is defined as the repetition rate. First, vOKR tuning to 10 different repetition rates was examined, keeping the angular velocity and spatial frequency constant at 12.5 deg s^{-1} and 0.0611 cycle deg^{-1}, respectively (Table S2). Each repetition rate was displayed twice in a randomized order and with randomized directions, with one stimulation phase consisting of six stimulus periods. Stimulation phases were framed by 20 s pause phases with a static grating.

After characterizing the vOKR tuning to repetition rate, the vOKR tuning to angular velocity and spatial frequency was assessed, using the same parameter range as for the constant rotation stimulus protocol with the sinusoidal modulation at repetition rate of 0.125 Hz (Table S1).

Data analysis of vOKR experiments

All eye traces were filtered with a median filter with a window size of 1 s to remove noise while preserving the velocity profile of the saccadic eye movements. Saccadic eye movements were detected using a multi-step process, including identifying the start and end points of each saccade based on the first and second derivatives of the eye traces laying within a time window of 0.5 s. Thresholds of 1 deg minimal deflection, 30 or 10 deg s^{-1} peak velocity during saccadic movements (for horizontal and vertical eye movements respectively) and 20 or 10 deg s^{-1} average velocity (for horizontal and vertical eye movements respectively) were applied, with the values selected based on visual inspection of the data. If multiple potential start and end time points were detected for a single saccade, amplitude, average velocity, change in direction of eye movements, and peak acceleration were used with different weightings to determine the most appropriate start and end points. This was the same for both recordings using the constant and sinusoidal rotating stimulus. After start and end time points of each saccade had been determined in a last step, the frames before and after both start and end time point were screened for eye deflection differences. If in the frame before or after start or end a more extreme eye deflection was reached that exceeded 0.5 deg, the time point for start or end was shifted to the frame with the eye trace extremum. Saccades were detected individually for each eye and camera.

The gain during the constant rotation stimulus was calculated by taking the ratio of the eye deflection with removed saccades within the first 4 s of each stimulation phase to the corresponding stimulus position. Cumulative average eye positions were calculated by removing all saccades and then averaging all eye traces across all stimulation phases. This same process was applied to the first 15 s, but without removing saccades, to better illustrate the initial vertical response.

Recordings performed alongside the sinusoidal rotating stimulus were often disrupted by spontaneous saccades, although showing an overall sinusoidal pattern. A combined Wiener and median filter were applied to remove high-frequency eye movements, and the signal was detrended afterwards. All further analysis was done using the average response to one stimulus period (stimulus-triggered average, STA). Eye response periods where 50% of all data points exceeded the standard deviation over all other periods within the same stimulation phase were removed from the STA to account for potential distortions by left over saccades. Gain was calculated by taking the ratio of a peak-to-peak sine function plus linear function fitting over the STA and the peak-to-peak stimulus position (similar to Dehmelt et al., 2021). Because the STA of long phases (small repetition rates) exhibited a plateau of maximum eye deflection which would drastically impair the fit of the sine curve, these plateaus were excluded from the fitting process. For vOKR and hOKR (but not vVOR), we fitted the sinusoidal function to the eye position STA instead of the eye velocity STA, because eye position STAs were less noisy. The fitting results were similar (data not shown).

Dynamic range was calculated as the difference between the maximum and minimum eye positions of the STA. The top of descent (ToD), used for analyzing phase lag, was defined as the point at which a rolling mean of the STA gradient decreased by half of the standard deviation after the peak of the sine curve. The phase lag was then calculated as the difference between the ToD of the stimulus and the ToD of the STA.

To analyze different saccade types, all saccades during vOKR and hOKR constant rotation stimuli were sorted corresponding to their apparent direction components into four clusters (Fig. S3A,B). When horizontal and vertical movements were detected on both horizontal and vertical eye traces and occurred within a time window of 5 frames, they were assigned to the same saccade and sorted into the corresponding clusters 3 or 4. If no corresponding saccade was found in the other eye trace, the saccade was characterized as only vertical or horizontal, respectively (clusters 1 or 2). In rare cases, multiple saccades occurred in one camera eye trace within the window and were therefore not assigned to any cluster. To verify the correct detection of pure vertical and pure horizontal saccades, the change of the minor axis length (i.e. the minor axis of the fitted ellipse) was calculated, taking the difference between the axis length before and after the saccade in pixels and dividing it by the major axis length of the eye to normalize it (Fig. S3C). The normalization step was necessary because the overall axis length is in pixels and therefore the overall change also varied between larvae. The difference images of pre- and post-saccade eye positions were calculated using ImageJ (Schindelin et al., 2012).

RESULTS

vVOR has a large dynamic range and is driven by rotational head position

To demonstrate that zebrafish larvae are capable of large vertical eye movements, we first performed vVOR experiments. Animals were mounted in 1.6% agarose in a setup that allowed controlled rotations about the caudo-rostral axis (clockwise and counter-clockwise roll; CW and CCW) alongside tracking of vertical eye movements. Vertical eye movements were recorded in the dark via a camera placed on the same rotation axis (Fig. 1A). Three different angular velocities (22.5, 45 and 90 deg s^{-1}) were tested to examine vertical eye movements elicited by vestibular input. In total, n=9 larvae were used in this experiment. Throughout the experiments, the larvae

Journal of Experimental Biology (2026) 229, jeb251770. doi:10.1242/jeb.251770

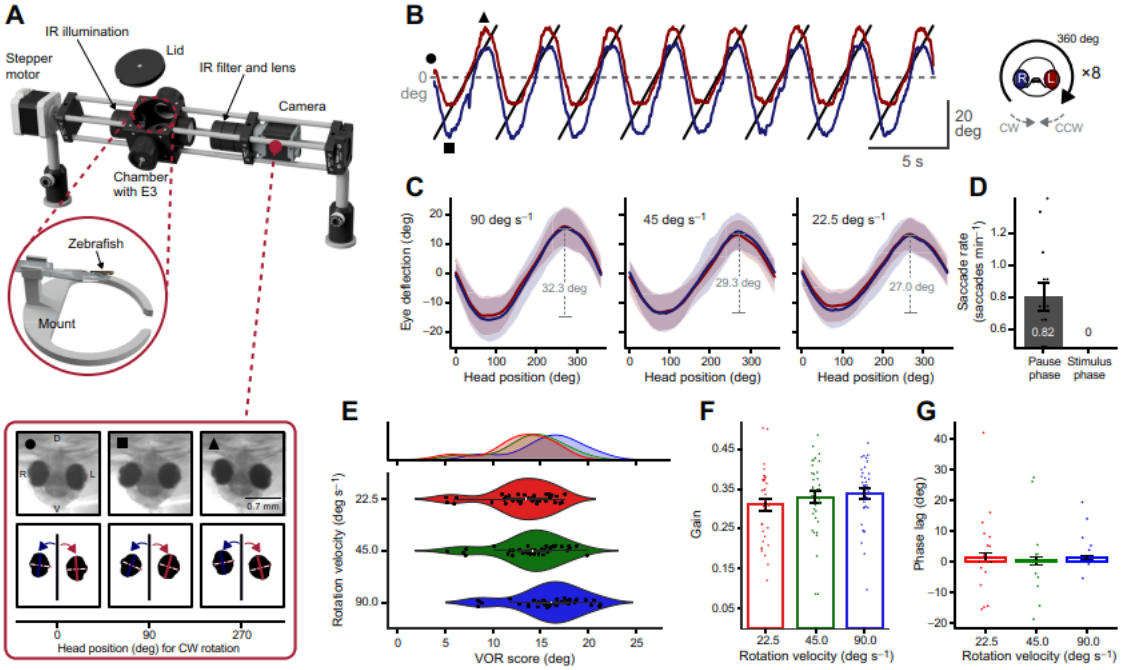

Fig. 1. Vertical vestibulo-ocular reflex in larval zebrafish. (A) Schematic of the experimental setup (KEBAB; Kinematic Evaluation of Behavior during Animal Body roll) used to examine vertical eye movements during constant rotation of the fish. The setup was driven by a stepper motor and controlled via the open-source software vxPy. Bottom: illustration of tracking vertical eye movements. (B) Raw eye traces of the left and right eye during rotation at 90 deg s^{-1}. The symbols (dot, square and triangle) indicate the eye position displayed in A. One stimulation phase contained 8 full rotations, either clockwise or counter-clockwise. (C) Stimulus triggered average (STA) of eye positions during full rotation at 90, 45 and 22.5 deg s^{-1} for all stimulation phases and across all fish (n=9). Envelopes show the standard deviation. Gray dashed lines indicate the dynamic range. (D) Saccade rate during rotation and pause phase. (E) Vestibulo-ocular reflex (VOR) score for 90 deg s^{-1} (blue), 45 deg s^{-1} (green) and 22.5 deg s^{-1} (red). VOR score only contained eye movements at the head rotation frequency. (F) Gain as ratio of sinus-fitted eye velocity to head velocity. (G) Phase lag as temporal difference between sinus-fitted eye velocity to head velocity.

exhibited a nearly perfect sinusoidal pattern of vertical eye position changes in response to the full rotations about the caudo-rostral axis, with the maximal eye deflection occurring at 90 and 270 deg head positions (Fig. 1B; Movie 1). Occasionally, the eye traces contained small outliers, which could be traced back to irregularly occurring vibrations of the stepper motor driving the setup. The average dynamic range of both eyes increased with head velocity, reaching a maximum at 90 deg s^{-1} (32.3±6.4 deg; 29.3±6.2 and 27.0±5.9 deg for 45 and 22.5 deg s^{-1}, respectively; mean±s.d.) (Fig. 1C). Interestingly, the larvae did not perform any saccades during the head rotations, whereas the saccade rate during the pause phases, when no rotation was performed, was 0.82 saccades min^{-1} (Fig. 1D). To analyze only the components of the vertical eye movements related to the stimulus frequency, Fourier analysis was performed to calculate the VOR score. The VOR scores differed with regard to the angular velocities but were nearly normally distributed for all angular velocities, with means±s.d. of 15.9±3.4, 13.9±3.4 and 13.0±3.3 deg for 90, 45 and 22.5 deg s^{-1} angular velocity, respectively (Fig. 1E). The fact that the vVOR score (15.9, 13.9 and 13.0 deg; mean) and the dynamic range half amplitude (16.2, 14.7, 13.5 deg; mean) were close to each other indicates that the eye movements were almost solely driven by the rotational head position. The vVOR gain revealed differences across the angular velocities, peaking at 0.33 for 90 deg s^{-1} (Fig. 1F). The phase lag was small throughout (<2 deg), suggesting that the eyes nearly simultaneously moved together with the head, with almost no delay (Fig. 1G).

vOKR has much smaller dynamic range than hOKR and vertical quick phases are absent

To investigate the existence and functionality of the vOKR in zebrafish, a horizontally striped black and white pattern was rotated vertically around the fish at a constant angular velocity. Eye movements were tracked in two dimensions using top and front cameras to record both horizontal and vertical eye movements (Fig. 2A). Various angular velocities and spatial frequencies were tested to assess the vOKR (Table S1). Each combination of stimulus parameters was presented for 60 s, followed by a 60 s pause phase (Fig. 2B). When presented with a constantly rotating vertical optokinetic stimulus, the zebrafish larvae did not exhibit the typical pattern of slow and quick phases observed in the hOKR. Instead, the eyes followed the visual stimulus for the first 4–5 s, reaching a plateau-like position from which they did not move further. This ‘start response’ was primarily visible in the frontal camera, suggesting it was limited to the vertical component (Fig. 2C). After reaching the plateau, the eyes began performing spontaneous saccades in both clockwise and counter-clockwise (with and against the stimulus direction) directions, which were visible from both the frontal and top cameras, indicating that these saccades might have both vertical and horizontal components (Fig. 2B). Between the spontaneous saccades,

Journal of Experimental Biology (2026) 229, jeb251770. doi:10.1242/jeb.251770

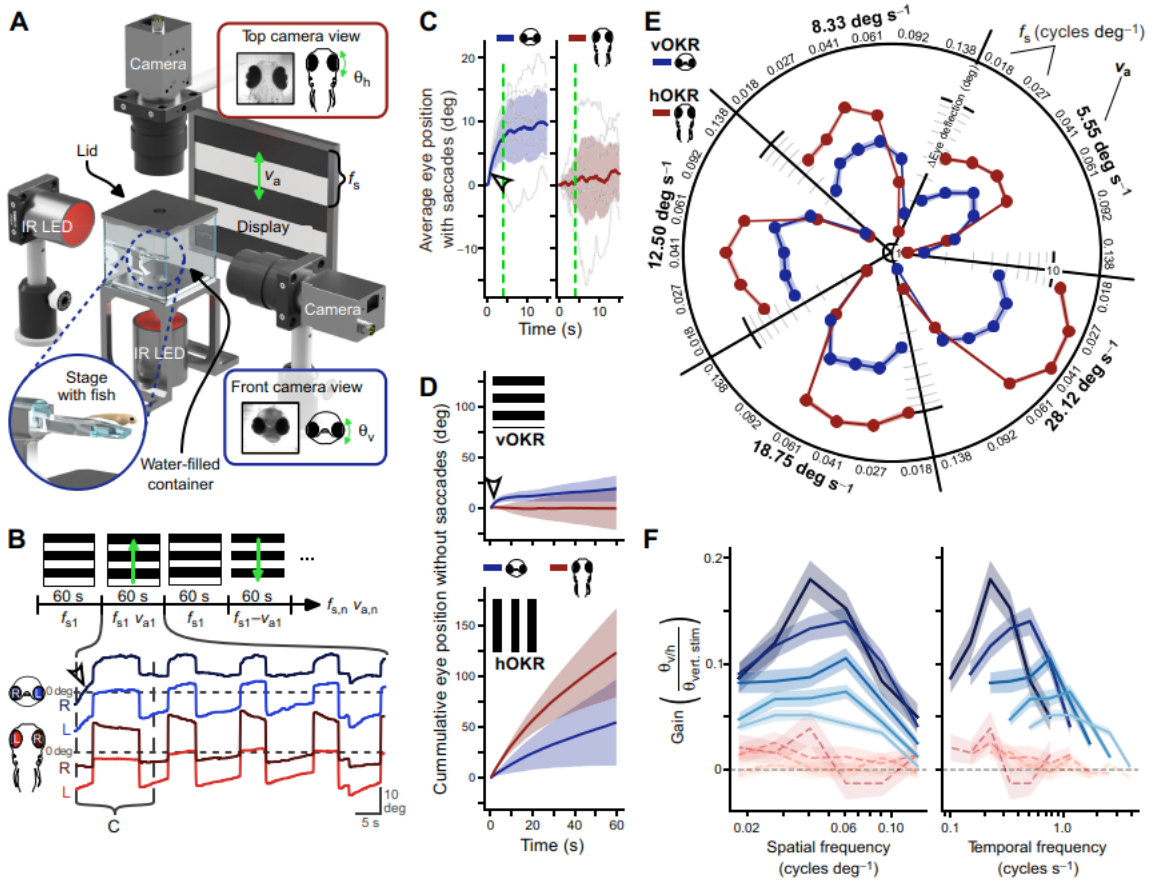

Fig. 2. No vertical quick phases after initial zebrafish vertical optokinetic response (vOKR). (A) Schematic of the setup with two cameras simultaneously recording the horizontal (top) and vertical (front) eye movements. The second display on the right side of the fish is not shown in this illustration. Green arrows indicate the direction of the stimulus rotation and the corresponding eye rotation. (B) Stimulus protocol and example vertical (blue) and horizontal (red) eye traces of one stimulation phase of one fish. Green arrows indicate direction of rotation of the stimulus. A static stimulus with the first spatial frequency (f_{s1}) was followed by the rotational stimulus with the first angular velocity (v_{a1}) after a constant pause, the stimulus rotated in the opposite direction with negative angular velocity, v_{a1}. This pattern was repeated with all the different f_s and v_a combinations until the final stimulus set ($f_{s,n}$ $v_{a,n}$). During the first seconds, only the vertical eye trace shows a deflection (open arrowhead). Vertical dotted lines indicate cutout of C. (C) Average eye position of all fish and all visual stimulations for the first 15 s. Vertical eye trace (blue) shows a distinct rise (open arrowhead) in the first 4 s (green dashed line) whereas the average horizontal eye position (red) does not change during vOKR. (D) Average cumulative eye position with saccades removed for vOKR (top) and horizontal OKR (hOKR; bottom) stimuli. The vertical start response is visible (open arrowhead). Blue lines indicate front camera readings (vertical eye trace), red lines horizontal eye traces. (E) Mean amplitude within first 4 s after stimulus onset and s.e.m. for each stimulus parameter pair. Blue, vertical amplitude for vOKR; red, horizontal amplitude for hOKR. (F) Gain tuning to spatial frequency and temporal frequency for all different angular velocities. Lines show means±s.e.m. Blue, gain for vertical eye trace for vOKR stimulation; red, gain calculated for horizontal eye trace for vOKR stimulation. Dashed horizontal line indicates a gain of 0. n=10 fish.

the eyes remained stationary or slowly drifted back towards a more neutral position. On average, the vertical plateau-like position was held during stimulation with the eyes drifting back to neutral positions in the subsequent pause phase (Fig. S1A). To visualize this surprising start response behavior, we compared the beginning phases of vOKR and hOKR (Fig. 2D). For hOKR, we used the same stimulus protocol but with vertical stripes and horizontal instead of vertical rotation (Fig. 2D). When removing all saccades during vertical and horizontal OKR and calculating the average cumulative eye trace during stimulation, the hOKR revealed the well-known constant slope in the direction of the stimulus, whereas the vOKR flattened out after approximately 4–5 s. Vertical eye movements during the horizontal stimulus protocol were also apparent, as observed in the front camera (Fig. 2D). The presence of larger eye position changes in the front camera during hOKR suggests that larval zebrafish either perform a small vertical component during the hOKR or that the projection of the eye onto the front camera is systematically affected by horizontal eye position changes. For the vOKR, horizontal eye position (measured by the top camera and removing saccades) remained stable around zero during vertical eye movements (Fig. 2D).

To examine the tuning of the start response during vOKR for different spatial frequencies and angular velocities, and to compare it with the tuning of hOKR, the eye position amplitude (half the

Journal of Experimental Biology (2026) 229, jeb251770. doi:10.1242/jeb.251770

dynamic range) and the gain were calculated for the first 4 s of stimulation, after which the eye deflection reached the previously described plateau. The dynamic range tuning was quite similar for vOKR and hOKR (Fig. 2E). For all angular velocities, the dynamic range was around zero for the highest spatial frequency of 0.138 cycles deg^{-1}, then increased with lower spatial frequency until reaching a maximal deflection for either 0.061 or 0.041 cycles deg^{-1} (hOKR and vOKR, respectively) before starting to decline again. Additionally, the dynamic range of eye positions increased with angular velocity, with the dynamic range being more narrowly tuned during hOKR than during vOKR. The maximum amplitude for hOKR after 4 s was 16.92±0.61 deg (at 28.12 deg s^{-1} and 0.041 cycles deg^{-1}), and 5.81±0.38 deg for vOKR (at 28.12 deg s^{-1} and 0.027 cycles deg^{-1}).

The vOKR gain was generally higher for slower angular velocities (Fig. 2F). Within a single angular velocity, the gain showed unimodal tuning in the range from 0.018 to 0.138 cycles deg^{-1} and peaked at medium spatial frequencies around 0.04 to 0.06 cycles deg^{-1}. The same pattern held true when comparing the gain with temporal frequencies, where the slower the angular velocity, the lower the temporal frequency that elicited the highest gain. To further confirm that the eye movements recorded within the first seconds of stimulation only contained a vertical OKR, the gain was also calculated for the horizontal eye movements during vOKR stimulation. The resulting values all lay around zero, indicating that no notable horizontal component was present in the early part of the vOKR.

Periodic vOKR shows phase shifts depending on the time period to stimulus reversal

Because the constant roll-rotating visual stimulus only elicited a transient vOKR within the first 4–5 s, a second sinusoidal rotation stimulus was used to extend the duration for which the eyes would follow the visual motion. The stimulus contained the same striped black and white pattern, but the rotation velocity followed a sinusoidal profile (Fig. 3A). As a result, the stimulus slowly gained speed in one direction until reaching the maximum angular velocity, then decreased again until coming to a full stop before accelerating in the opposite direction. This stimulus introduced a new parameter, the repetition rate, which indicated the frequency of the sinusoidal velocity envelope and provided information on how quickly the maximum velocity was reached. Overall, the sinusoidal stimulus elicited sinusoidal vertical eye movements corresponding to the stimulus position, whereas no stimulus-associated horizontal eye movements were visible in the top camera (Movie 2). During stimulation, larvae showed spontaneous horizontal saccades that also led to deflections in the vertical eye position but did not disrupt the overall sinusoidal pattern. Just as for the constantly rotating stimulus, no vertical resetting quick phases could be observed in response to the sinusoidal stimulus (Fig. 3B).

We tested different repetition rates while keeping the maximum angular velocity constant (12.5 deg s^{-1}) and using only one spatial frequency close to the optimum (0.061 cycles deg^{-1}) (Table S2). The parameters were similar to those used by Dehmelt et al. (2021) for horizontal OKR. For repetition rates between 0.5 and 0.0078 Hz, vertical eye positions followed the stimulus. Repetition rates greater than 0.5 Hz did not elicit any response (Fig. 3C; Fig. S2A). The gain was calculated as the ratio of the amplitude of a fitted sinusoidal function to the eye position and the amplitude of the sinusoidal function of stimulus position. The gain was relatively high for repetition rates between 0.5 and 0.125 Hz (maximum of 0.19 at 0.25 Hz), but started to decrease for lower repetition rates until reaching a value of 0.03 (at 0.0078 Hz) (Fig. 3C). However, the eye traces themselves showed a clear sinusoidal pattern for low repetition rates, and the dynamic range even increased with lower repetition rates. For the highest repetition rates that did not elicit any response, the dynamic range was around zero, but reached around 10 deg for the lowest two repetition rates. Analyzing the STA of eye position for all repetition rates revealed a phase lag with regard to stimulus position, which moved from positive phase angles towards negative ones with decreasing repetition rates (Fig. 3D). For high repetition rates (0.25 and 0.5 Hz), the eyes therefore seemed to lag behind the stimulus, which was expected. However, for lower repetition rates (0.0078 to 0.125 Hz), the eye movement preceded stimulus position change, which is counterintuitive. This negative phase lag meant that the eyes already started moving in the opposite direction during the slow-down of the current stimulus (before the sign of the stimulus velocity would change). For the highest repetition rate with responses (0.5 Hz), the phase lag was 65.76±13.31 deg, whereas for the lowest repetition rate (0.0078 Hz), the phase lag was −59.37±15.69 deg (i.e. a phase advance). When analyzing those phase advances with regard to the eye's acceleration, we found that the sign of eye velocity only changed during slow-down of the stimulus, i.e. after the acceleration turned negative (Fig. 2D, right panel). This phenomenon can potentially be explained by the motion aftereffect or acceleration coding neurons and will be discussed further below.

The vOKR to a repetition rate of 0.125 Hz had the smallest phase lag and was used to investigate the tuning to spatial frequency. The angular velocities and spatial frequencies were varied following the constant rotation stimulus protocol (Table S1). The dynamic range of vertical eye movements during sinusoidal vOKR overall revealed a similar pattern compared with the constant rotating stimulus (Fig. 3E). On average, the dynamic range of eye position was small for high spatial frequencies, then began increasing, and after peaking at 0.041 or 0.061 cycles deg^{-1}, it declined again for lower spatial frequencies. The maximum dynamic range for the slowest angular velocity (5.55 deg s^{-1}) was 3.31±2.44 deg, and the maximum dynamic range for the fastest angular velocity (28.12 deg s^{-1}) was 6.21±3.02 deg. When examining individual fish, much higher dynamic ranges, up to >10 deg (red dashed lines, Fig. 3E) occurred in some fish. Two fish exhibited very distinct dynamic range tuning properties that stood out from the rest (purple and blue dashed lines, Fig. 3E). For high spatial frequencies, their dynamic range was much smaller (<1 deg) than in the other fish. Furthermore, their maximum dynamic range for slower angular velocities was also relatively small, only starting to match the others as angular velocities increased.

The tuning of vOKR to spatial frequency and temporal frequency was similar for sinusoidal and constant rotation stimuli. However, the overall gains were higher for the sinusoidal rotation stimulus, reaching a maximum gain of 0.23±0.03 (at 5.55 deg s^{-1} and 0.041 cycles deg^{-1}; see Fig. 3F).

Zebrafish larvae generate pure vertical and pure horizontal spontaneous saccades

In our recordings, saccadic eye movements were detected during both vOKR and hOKR stimulation. During vVOR, no saccades were visible. Saccadic movements occurred in both the horizontal and vertical planes. Interestingly, the saccade rate during vOKR stimulation was similar to the rate during no stimulation, suggesting that these were purely spontaneous (Fig. 4A). Furthermore, neither the stimulus direction nor the type of stimulation (constant versus sinusoidal) influenced the saccade rate during vOKR stimulation. During hOKR, most saccades occurred against the direction of the stimulus, mirroring

Journal of Experimental Biology

Journal of Experimental Biology (2026) 229, jeb251770. doi:10.1242/jeb.251770

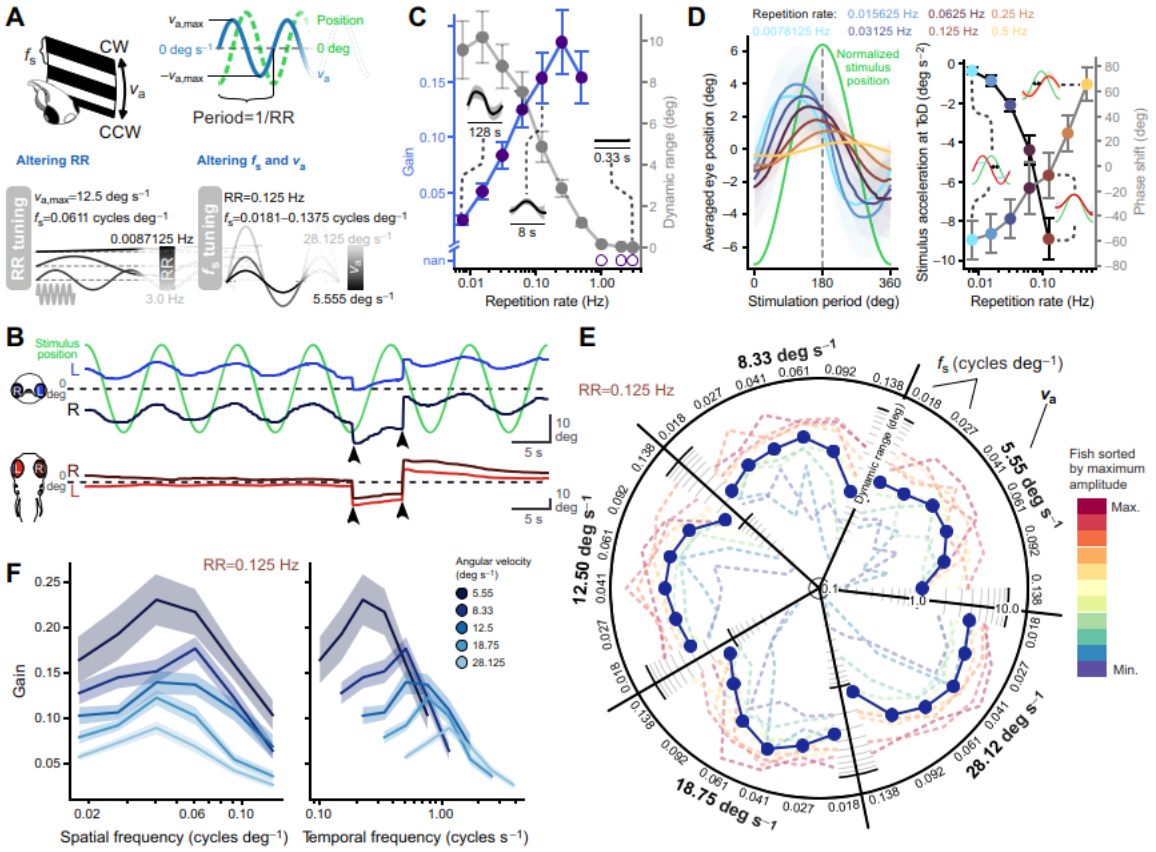

Fig. 3. vOKR tuning to stimuli with sinusoidal velocity envelope. (A) Sinusoidal rotation stimulus scheme. Two different sinusoidal stimuli were used. In the repetition rate tuning stimulus, the maximum angular velocity and the spatial frequency were constant while different repetition rates were tested. In the spatial frequency tuning stimulus, the repetition rate was kept constant while spatial frequency and angular velocity were altered. CW, clockwise; CCW, counterclockwise; v_a, angular velocity; RR, repetition rate; f_s, spatial frequency. (B) Example recording with vertical (blue) and horizontal (red) eye traces. Spontaneous saccades during the sinusoidal response did not disturb the response but shifted it by the amplitude of the saccade (arrowheads). Note the different *y*-axis scales. (C) Mean and standard error of gain (blue) and full dynamic range (gray) over repetition rate. Insets show average response to one stimulus period over all fish for repetition rates 3.0, 0.125 and 0.0078125 Hz (n=8 fish). (D) Left: average response to one stimulus period for different repetition rates. The timescale is normalized to one stimulus period. Vertical dashed line indicates turning point of stimulus position. Right: phase lag of the vOKR (gray lines) for different repetition rates, and acceleration value of the stimulus (black lines) at the time point of eye movement direction change (phase lag). Data points are color-coded with respect to their repetition rate and show mean and standard deviation. Insets show example average responses to one stimulus period of one fish. Green curve indicates stimulus position; red curve shows sine fit to average eye trace. Black arrows indicate the phase lag between stimulus and average response. (E) Dynamic range for each stimulus parameter set. Data points indicate mean of all fish (n=11 fish). Dashed lines show mean dynamic range of single fish, colored according to their mean amplitude. (F) Mean gain with standard error over spatial frequency (left) and temporal frequency (right) for all different angular velocities (see color legend).

the well-known pattern of resetting quick phases during stimulation. To further characterize saccadic eye movements during vOKR stimulation, saccades were sorted into four clusters based on their occurrence with or without corresponding eye movements in the other plane (Fig. S3A,B). A total of 4696 detected saccades were analyzed during vOKR. The first cluster contained saccades with only a vertical component (10.5% of all saccades), whereas saccades with only a horizontal component were sorted into cluster 2 (14.0% of all saccades). Saccades with apparent deflections in both the vertical and horizontal planes were sorted into clusters 3 and 4, depending on their direction (75.5%). Large deflections in the horizontal plane caused a more spherical (less elliptical) appearance of the eye in the frontal camera. This projection artifact often effected false estimates of vertical eye position, as the detected major axis angle was affected by the ellipse fit to the now more spherical shape. Therefore, it was virtually impossible to extract the true vertical and horizontal components of apparently combined eye movements. For this reason, clusters 3 and 4 were not further analyzed, and they likely contain pure horizontal saccades and/or true vertical–horizontal combined eye movements (but no pure vertical saccades).

To ensure that clusters 1 and 2 exclusively contained pure vertical (Movie 3) and pure horizontal (Movie 4) saccades, and that saccadic eye movements within a single plane were not affected by the above-mentioned projection artifact, the change in length of the eye's fitted minor axis was examined (Fig. 4B). For pure vertical movements, the minor axis length was expected to change in the horizontal plane (top view) and stay constant in the vertical plane (front view). Conversely, during pure horizontal eye movements, the minor axis

Journal of Experimental Biology (2026) 229, jeb251770. doi:10.1242/jeb.251770

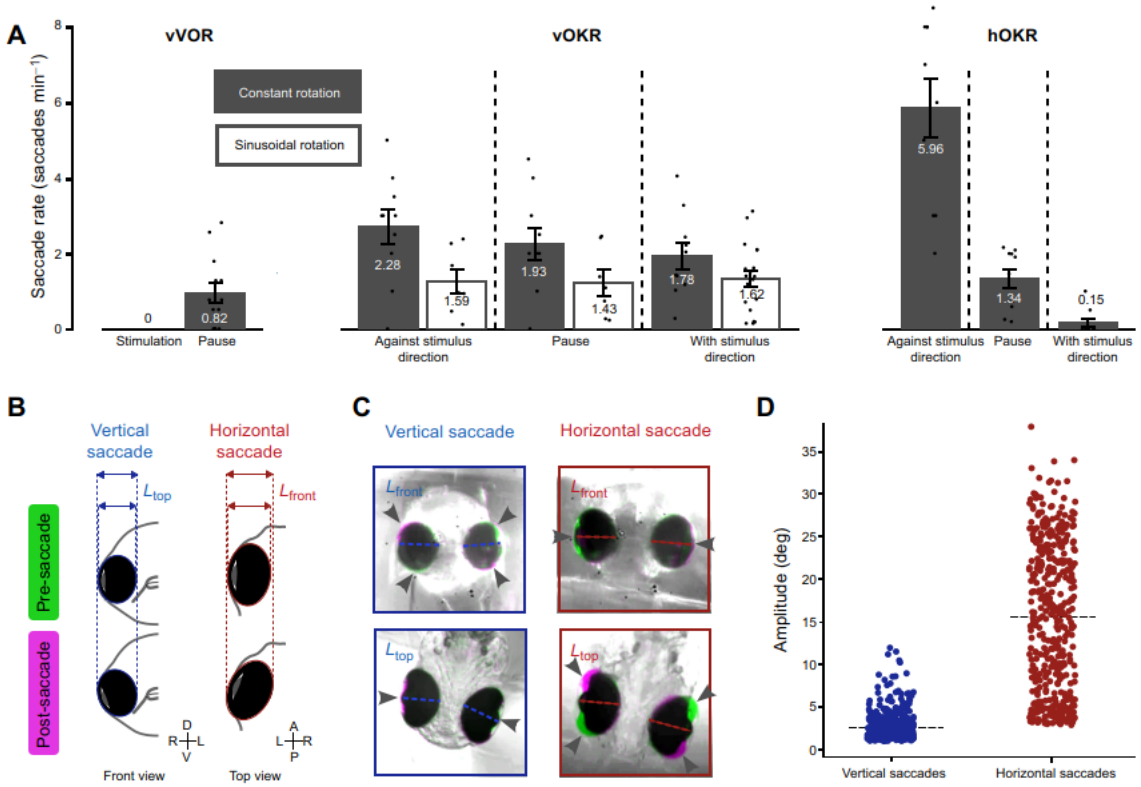

Fig. 4. Characterization of vertical and horizontal saccades. (A) Comparison of the saccade rate (vertical+horizontal saccades) during vertical vestibulo-ocular reflex (vVOR), vOKR and hOKR. For all stimuli, data from the stimulation parameters that elicited the highest number of saccades are shown. (B) Schematic of minor axis length change (ellipse fitting) during vertical and horizontal saccades. During vertical saccades, the minor axis length in the top camera (L_{top}) is expected to change, whereas the minor axis length in the front camera (L_{front}) should remain constant. For horizontal saccades, the expectation is the reverse. These length changes, together with the angle between the major axis and the body axis, were used to detect pure vertical and horizontal eye movements (see also Fig. S3). (C) Difference image of the eyes' pre-saccadic (green) and post-saccadic (magenta) positions for pure vertical and pure horizontal example saccades. Arrowheads indicate the area where position changed. For pure vertical saccades, the top camera showed changes only at the lateral parts of the eyes, whereas the front camera exhibited changes at the dorsal and ventral parts of the eyes. Conversely, during pure horizontal saccades, the image changes were reversed (change at lateral parts of eyes in front camera and at anterior/posterior parts of eyes in the top view camera). (D) Saccade amplitude scatter plot of pure vertical and pure horizontal saccades.

length change was expected to occur in the vertical plane while remaining at zero in the horizontal plane (Fig. S3D). Analysis of the minor axis change distribution during both pure vertical and pure horizontal saccades yielded the expected results, thereby confirming the accurate detection of pure vertical and pure horizontal saccades. To illustrate examples of pure vertical and horizontal eye movements, false color images of pre- and post-saccadic camera recordings were created (Fig. 4C).

Pure vertical saccades almost never exceeded 10 deg in magnitude but frequently exhibited a slight horizontal deflection of a few degrees (Fig. S3B). In contrast, pure horizontal saccades had much larger amplitudes, reaching over 30 deg for some of them (Fig. 4D).

Comparison of vOKR, hOKR and vVOR performance levels

Our findings are summarized in the comparison chart in Fig. 5. Comparing the vOKR and vVOR is especially intriguing, as both involve the same extraocular eye muscles but are driven by different sensory inputs. Although resetting saccades are a characteristic feature of the hOKR, they did not occur during the vOKR or vVOR. Interestingly, spontaneous saccades were regularly observed in both directions (against and with stimulus direction) during the vOKR, whereas no saccades were present during the vVOR, as indicated in Fig. 4A. This suggests that the vestibular roll stimulation or vVOR suppresses spontaneous saccadic eye movements.

To better understand the limits and maximal capabilities of the OKR and VOR, we compared the dynamic range and gain across the different reflexes (Fig. 5A). Although the dynamic range for both constant rotation and sinusoidal vOKR was around 10 deg, the dynamic range for vVOR was about three times larger. This striking difference indicates that the vertical deflection range utilized during vOKR is not limited by the maximum possible vertical oculomotor range of the plant and is consistent with recent findings in adult goldfish (Tadokoro et al., 2025). However, the dynamic range of vVOR and hOKR reached similar levels. The gain values for vOKR were smaller compared with hOKR and vVOR, whereas the gains for hOKR and vVOR were similar (Fig. 5B).

DISCUSSION

This study provides the first characterization of the vOKR in larval zebrafish and compares it with the hOKR and the vVOR. Although

Journal of Experimental Biology (2026) 229, jeb251770. doi:10.1242/jeb.251770

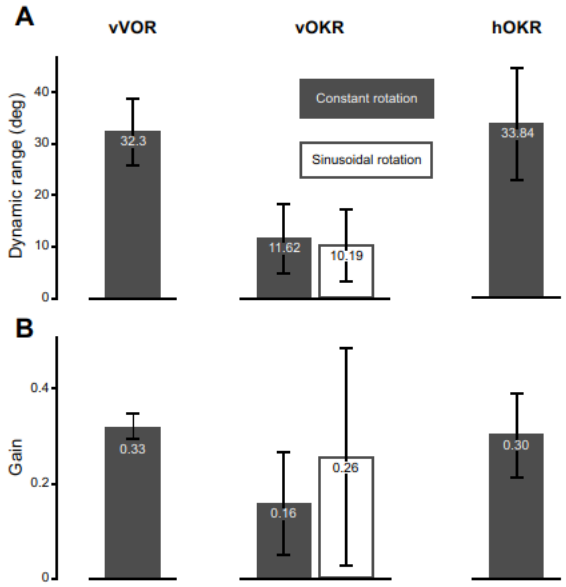

Fig. 5. Performance comparison between vOKR, vVOR and hOKR. (A) Comparison of the dynamic range. For constant rotation (vOKR and hOKR), double the one-directional amplitude was used as the dynamic range. For all stimuli, data of recordings with stimulus parameters that elicited the highest gain are shown. (B) Comparison of the gain (ratio of eye position to stimulus position after 4 s). For all stimuli, data of recordings with stimulus parameters that elicited the highest gain are shown. All bars show means±s.d. For vOKR, filled bars represent values for the constant rotation stimulus whereas open bars represent values for the sinusoidal rotation stimulus.

hOKR has been intensively studied in zebrafish, the vOKR performance remained elusive, even though vertical and torsional OKR have been well described in various species such as primates, cats and even rabbits, which are also lateral-eyed animals and, like zebrafish, do not have foveate vision (Collewijn, 1980; Erickson and Barmack, 1980; Farooq, 2004; Kitama et al., 2001; van den Berg and Collewijn, 1988). As zebrafish serve as a model system for vertebrate visuomotor circuitry, it is essential to know the full behavioral repertoire of the fish. By employing a novel experimental setup, we were able to track both horizontal and vertical eye movements simultaneously while the fish was presented with vertically or horizontally rotating visual stimuli.

Low vOKR performance levels

In mammals, both the hOKR and vOKR consist of slow phases where the eye follows the stimulus, and resetting quick phases during which the eye rapidly moves in the opposite direction to allow for another slow phase (Erickson and Barmack, 1980; Garbutt et al., 2003; Ghasia and Tychsen, 2014; Robinson, 1981). In our vOKR experiment with a constant rotation stimulus, zebrafish revealed a markedly different response pattern. During the first seconds of stimulation, the fish vertically rotated its eyes in the direction of the stimulus. However, after reaching a certain degree of deflection, the eyes did not move further and did not perform any resetting saccades. This contrasts sharply with a recent study in adult goldfish where regularly occurring resetting saccades during vOKR have been reported (Tadokoro et al., 2025). However, the authors mentioned that owing to the minimal generated slow phase components, these resetting saccades were unexpected but had excluded any misdetection. This leaves the question whether the absence of any resetting saccades in larval zebrafish vOKR is a species-specific difference or whether they emerge at later developmental stages. Moreover, the zebrafish performs spontaneous saccades at regular intervals during vOKR stimulation, often with a horizontal component. This lack of suppression of spontaneous saccade generation during vOKR is in striking contrast to the vVOR, where not a single saccade occurred during vestibular stimulation. Although the vOKR is highly robust in humans, in rabbits it appears to be less effective than the hOKR, with fewer and more irregular resetting saccades, where the eyes often remained at their maximum deflection for over 10 s (Erickson and Barmack, 1980).

Generally, the OKR is used to compensate for low-frequency rotations, whereas the vestibulo-ocular reflex is used for high-frequency rotations of the body (Masseck and Hoffmann, 2009; Robinson, 1981). This principle likely also applies to the vertical domain of the zebrafish sensory-motor systems, although we did not explicitly test it in the present study and used different speed regimes for vVOR and vOKR stimulation. We speculate that the vOKR is presumably more relevant for slow and low-frequency roll rotations. Body rotations around this axis probably occur less frequently than for the yaw axis that elicits the hOKR. Such roll rotations are likely quickly adjusted by the gravity-guided posture control mechanisms (Sugioka et al., 2023), which leaves no need for vertical resetting saccades or high dynamic range vOKR responses. Constant visual roll rotation should be very uncommon in healthy fish, which mainly modulate body yaw and – to a lesser extent – body pitch during swimming and navigation (Budick and O'Malley, 2000; Ehrlich and Schoppik, 2017; Mearns et al., 2020).

Saccades during visual stimulation could be classified into four clusters based on their vertical and horizontal components (Fig. S3A,B). Although there are some uncertainties regarding the reliability of the combined horizontal and vertical saccades as large horizontal movements often mask vertical components by projection artifacts in the frontal camera, the presence of pure vertical (Movie 3) and pure horizontal (Movie 4) saccades alone demonstrates that zebrafish larvae can precisely control their eye muscles to generate saccades with specific vertical and horizontal components. Interestingly, both vertical and horizontal saccades were equally observed during both vOKR and hOKR experiments, although OKR performance was much higher for hOKR (Fig. S1B). The vertical saccades during yaw rotation stimuli are likely spontaneous (i.e. not directly driven by the motion stimulus). Further studies are needed to investigate the role of combined versus pure horizontal and vertical saccades for zebrafish task performance and to reveal the ontogenetic performance levels of older larvae and adult zebrafish. Notably, the transient vOKR during constant rotation displayed a spatial frequency and angular velocity tuning that was highly similar to that previously observed for the hOKR (Dehmelt et al., 2021; Rinner et al., 2005).

However, the absolute peak gain values of our hOKR differed from a previous study, with the reported hOKR having approximately three-times higher gain levels than our hOKR at similar angular velocities and spatial frequencies (Rinner et al., 2005), which can potentially be explained by the smaller steradian size of our stimulus arena. Nevertheless, the tuning curve shape of hOKR to velocity and spatial frequency is similar. The dynamic range was significantly different between the vertical and horizontal OKR, with the hOKR reaching much larger eye positions. This is particularly interesting given that during the vVOR, zebrafish were able to achieve three-times absolute higher

vertical eye positions than during vOKR. Together with the high initial vOKR gain and the reported vertical motion sensitivity in the pretectum (Wang et al., 2019), these findings suggest that the limiting factor for vOKR is neither visual motion sensitivity nor the oculomotor plant. Instead, these results point towards the inability of diencephalic direction-selective neurons in recruiting high levels of motoneuron pool activity needed for very peripheral eye positions. This could be caused by motoneurons with high eye position thresholds only being recruited by vestibular and not by visual input (Aksay et al., 2000; Brysch et al., 2019) or by the presence of saccade-type specific motoneuron populations (Brysch et al., 2019; Dowell et al., 2025; Leyden et al., 2021).

Phase advances during low repetition rates might be related to adaptation or acceleration tuning

Using the sinusoidal rotation stimulus, it was possible to evoke a long-lasting sinusoidal vOKR that followed the stimulus position. For low repetition rates that resulted in extended periods of unidirectional stimulus motion, the eyes reached their maximum vertical deflection already after several seconds and remained at that plateau. One might expect the eyes to stay at the plateau until the stimulus changed direction, at which point the eyes would move in the opposite direction away from the plateau. However, the eyes appeared to start rotating in the opposite direction several seconds before the stimulus changed direction, i.e. the stimulus was still moving in the original direction (just slower). This was true for all repetitions during a stimulation phase and did not evolve over time (Fig. S2C), which is why predictive behavior occurring after a training period with a repetitive stimulus can be ruled out (Marsh and Baker, 1997; Miki et al., 2018).

This phenomenon shares some similarities with the motion aftereffect, an illusion of motion in a certain direction caused by prior exposure to motion in the opposite direction (Anstis et al., 1998). The motion aftereffect can reliably be elicited by moving visual stimuli (Braun et al., 2006; Chen et al., 2014; Watamaniuk and Heinen, 2007) and is also known to be present in larval zebrafish with regard to both the optomotor and optokinetic response (Lin et al., 2019; Najafian et al., 2014; Pérez-Schuster et al., 2016; Wu et al., 2020). After prolonged hOKR stimulation, fish exhibit a hOKR in the opposite direction during a stationary stimulus, and the duration of the reversed response depends on the duration of the initial stimulation. At least 200 s of hOKR stimulation is necessary to induce a motion aftereffect according to Pérez-Schuster et al. (2016). Two key differences to the behavior observed in this study are that (1) zebrafish began moving their eyes in the opposite direction while the stimulus was still moving, and (2) our observed phase-advanced vOKR occurred for stimulation periods much shorter than 200 s. For the lowest repetition rate, the duration of stimulus rotation in one direction was over 2 min, whereas for a repetition rate of 0.125 Hz, the stimulus rotated for only 4 s in one direction, and a small phase advance was already visible. One potential explanation for the occurrence of the phase advance could be an interplay between two mutually inhibiting populations of direction-selective neurons coding for opposite velocities. The population coding for the stimulus direction may adapt over time, until the difference between the two population's activities is so small that a deceleration of the stimulus disinhibits the non-stimulated direction-selective population, which induces a vOKR in the opposite direction. However, the fast adaptation (<4 s for 0.125 Hz repetition rate) would be much faster than previously reports on motion aftereffect in zebrafish (Pérez-Schuster et al., 2016; Wu et al., 2020).

An alternative explanation for the occurrence of phase advances is that the direction-selective neurons – in addition to their tuning to velocity – are tuned to acceleration as well (Cao et al., 2004; Thiel et al., 2007), which can be interpreted as a quick form of adaptation, and thus they might lose much of their activity when the stimulus is still running in the same direction but acceleration approaches zero. In this scenario, the occurring eye movements into the opposite direction (back to the null position) would not necessarily be visually driven, but could simply result from passive drift of the eyes back to the resting position (Miri et al., 2022). In line with this hypothesis, centripetal eye movements (which can be interpreted more safely as visually driven) only occurred after the stimulus velocity had switched sign (Fig. 3D), i.e. vOKR towards peripheral positions was always going in the same direction as the stimulus.

Further studies are needed to determine the mechanisms that underlie the observed apparent phase advance of vertical optokinetic responses to slowly repeating sinusoidal rotation stimuli.

Uncertainties associated with projection-based eye tracking

The dual-camera setup used for all recordings enabled simultaneous tracking of horizontal and vertical eye movements in zebrafish larvae. However, many eye movements were visible in both horizontal and vertical eye traces. In particular, saccades with large amplitudes were often visible in both cameras. We tracked horizontal and vertical eye movements in larval zebrafish by fitting an ellipse to the binarized eye image and calculating the angle between the major axis and the body midline. This method should be relatively robust as compared with a previously reported method based on searching the largest distance of 2 pixels within a binarized and segmented eye (Dehmelt et al., 2018) and has also been used to measure vertical eye positions in a previous study (Bianco et al., 2012).

This method can reliably track both pure vertical and pure horizontal eye movements, which can be confirmed by inspecting raw eye traces and measurements such as the change in length of the eye's fitted minor axis during saccadic eye movements and difference images during saccades (see above). However, the method raises some uncertainties regarding combined vertical and horizontal eye movements. Although a large number of eye movements are visible in both the horizontal and vertical planes, the method reaches its limits when attempting to disentangle the vertical and horizontal components of apparently mixed eye movements. Large horizontal eye movements often (but not always) lead to a misdetection of vertical eye position in the frontal camera, caused by an ill-defined ellipse fit with a major/minor axis ratio closer to 1 than for eye positions without horizontal components. This change in projection shape could affect the calculated vertical angle and therefore mask the true vertical component of the movements. The change in projection shape in the frontal camera was especially apparent during hOKR recordings, where the stereotypical slow/quick phase pattern was also observed in the vertical eye trace, albeit with a much smaller amplitude. This even resulted in a small apparent tuning of vertical eye movements to hOKR stimulation (Fig. S1B). If these eye movements were genuine, it would suggest that the hOKR had a constant vertical component, which would be surprising, even considering the potential for small body pitch owing to imprecise embedding of the larva. Nevertheless, combined vertical and horizontal eye movements are found to be present in adult goldfish (Tadokoro et al., 2025) and are most likely also present in zebrafish.

Taken together, our data show that pure horizontal and pure vertical saccades do exist, as well as combined movements, although the true vertical and horizontal components of possible

mixed saccades could not be revealed in this study. The precise measurement of vertical components in apparent horizontal–vertical saccades is hampered by methodological caveats, and a different tracking method of the dual-camera recordings needs to be performed in the future to improve our understanding of the horizontal and vertical components of mixed saccades in larval zebrafish.

Conclusions

In this study, we characterized the vOKR in larval zebrafish and compared its characteristics with the hOKR and the vVOR. Larval zebrafish do perform vOKR, and several basic differences from the hOKR could be identified. One major difference was the absence of resetting vertical saccades during vOKR. The reason for this needs to be explored in future studies. Given that vertical rotation encoding neurons exist (Wang et al., 2019; Zhang et al., 2022), a better understanding of the downstream neuronal processes controlling eye movement and saccade generation could help explain the behavioral differences between vertical and horizontal OKR. Such neurophysiology experiments could also shed light on the differences in dynamic range between vOKR and the vVOR. Additionally, further behavioral experiments are necessary to understand the apparent vOKR phase advance for sinusoidal rotation stimuli in the context of adaptation or acceleration tuning. Our characterization of the vOKR in larval zebrafish provides information on a hitherto elusive behavior and points towards specific questions that will enable a more comprehensive understanding of the neuronal processing of visual information and the control of eye movements.

Acknowledgements

We thank all members of the Arrenberg laboratory for discussions regarding this work and Michael Glaser for excellent fish care.

Competing interests

The authors declare no competing or financial interests.

Author contributions

Conceptualization: D.-S.B., A.B.A.; Data curation: G.M., L.D., C.F.; Formal analysis: G.M., D.-S.B., A.B.A.; Funding acquisition: A.B.A.; Methodology: D.-S.B., G.M., C.F., T.C.H.; Project administration: A.B.A.; Software: D.-S.B., T.C.H.; Supervision: D.-S.B., A.B.A.; Validation: D.-S.B., A.B.A.; Visualization: G.M., D.-S.B.; Writing – original draft: D.-S.B., G.M., A.B.A.; Writing – review & editing: D.-S.B., G.M., A.B.A.

Funding

Open Access funding provided by Eberhard Karls Universität Tübingen. Deposited in PMC for immediate release.

Data and resource availability

Data and Python code used for analysis are available at a G-Node repository (https://gin.g-node.org/Arrenberg_Lab/Data_Analysis_of_vOKR_and_vVOR), DOI:10.12751/g-node.9npkkp.

ECR Spotlight

This article has an associated ECR Spotlight interview with David-Samuel Burkhardt.

References

Aksay, E., Baker, R., Seung, H. S. and Tank, D. W. (2000). Anatomy and discharge properties of pre-motor neurons in the goldfish medulla that have eye-position signals during fixations. *J. Neurophysiol.* **84**, 1035-1049. doi:10.1152/jn.2000.84.2.1035

Anstis, S., Verstraten, F. A. J. and Mather, G. (1998). The motion aftereffect. *Trends Cogn. Sci.* **2**, 111-117. doi:10.1016/S1364-6613(98)01142-5

Beck, J. C., Gilland, E., Tank, D. W. and Baker, R. (2004). Quantifying the ontogeny of optokinetic and vestibuloocular behaviors in zebrafish, medaka, and goldfish. *J. Neurophysiol.* **92**, 3546-3561. doi:10.1152/jn.00311.2004

Bellegarda, C., Auer, F. and Schoppik, D. (2025). Zebrafish as a model to understand extraocular motor neuron diversity. *Curr. Opin. Neurobiol.* **90**, 102964. doi:10.1016/j.conb.2024.102964

Ben-Simon, A., Ben-Shahar, O. and Segev, R. (2009). Measuring and tracking eye movements of a behaving archer fish by real-time stereo vision. *J. Neurosci. Methods* **184**, 235-243. doi:10.1016/j.jneumeth.2009.08.006

Bianco, I. H., Ma, L.-H., Schoppik, D., Robson, D. N., Orger, M. B., Beck, J. C., Li, J. M., Schier, A. F., Engert, F. and Baker, R. (2012). The tangential nucleus controls a gravito-inertial vestibulo-ocular reflex. *Curr. Biol.* **22**, 1285-1295. doi:10.1016/j.cub.2012.05.026

Braun, D. I., Pracejus, L. and Gegenfurtner, K. R. (2006). Motion aftereffect elicits smooth pursuit eye movements. *J. Vis.* **6**, 1. doi:10.1167/6.7.1

Britten, K. H. (2008). Mechanisms of self-motion perception. *Annu. Rev. Neurosci.* **31**, 389-410. doi:10.1146/annurev.neuro.29.051605.112953

Brysch, C., Leyden, C. and Arrenberg, A. B. (2019). Functional architecture underlying binocular coordination of eye position and velocity in the larval zebrafish hindbrain. *BMC Biol.* **17**, 110. doi:10.1186/s12915-019-0720-y

Budick, S. A. and O'Malley, D. M. (2000). Locomotor repertoire of the larval zebrafish: swimming, turning and prey capture. *J. Exp. Biol.* **203**, 2565-2579. doi:10.1242/jeb.203.17.2565

Cao, P., Gu, Y. and Wang, S.-R. (2004). Visual neurons in the pigeon brain encode the acceleration of stimulus motion. *J. Neurosci.* **24**, 7690-7698. doi:10.1523/JNEUROSCI.2384-04.2004

Chen, C.-C., Huang, M. Y.-Y., Weber, K. P., Straumann, D. and Bockisch, C. J. (2014). Afternystagmus in darkness after suppression of optokinetic nystagmus: an interaction of motion aftereffect and retinal afterimages. *Exp. Brain Res.* **232**, 2891-2898. doi:10.1007/s00221-014-3971-4

Collewijn, H. (1980). Sensory control of optokinetic nystagmus in the rabbit. *Trends Neurosci.* **3**, 277-280. doi:10.1016/0166-2236(80)90101-0

Dehmelt, F. A., von Daranyi, A., Leyden, C. and Arrenberg, A. B. (2018). Evoking and tracking zebrafish eye movement in multiple larvae with ZebEyeTrack. *Nat. Protoc.* **13**, 1539-1568. doi:10.1038/s41596-018-0002-0

Dehmelt, F. A., Meier, R., Hinz, J., Yoshimatsu, T., Simacek, C. A., Huang, R., Wang, K., Baden, T. and Arrenberg, A. B. (2021). Spherical arena reveals optokinetic response tuning to stimulus location, size, and frequency across entire visual field of larval zebrafish. *eLife* **10**, e63355. doi:10.7554/eLife.63355

Dowell, C. K., Lau, J. Y. N., Antinucci, P. and Bianco, I. H. (2024). Kinematically distinct saccades are used in a context-dependent manner by larval zebrafish. *Curr. Biol.* **34**, 4382-4396.e5. doi:10.1016/j.cub.2024.08.008

Dowell, C. K., Hawkins, T. and Bianco, I. H. (2025). Subsets of extraocular motoneurons produce kinematically distinct saccades during hunting and exploration. *Curr. Biol.* **35**, 554-573.e6. doi:10.1016/j.cub.2024.12.010

Dunn, T. W. and Fitzgerald, J. E. (2020). Correcting for physical distortions in visual stimuli improves reproducibility in zebrafish neuroscience. *eLife* **9**, e53684. doi:10.7554/eLife.53684

Easter, S. S., Jr and Nicola, G. N. (1997). The development of eye movements in the zebrafish (*Danio rerio*). *Dev. Psychobiol.* **31**, 267-276. doi:10.1002/(SICI)1098-2302(199712)31:4%253C267::AID-DEV4%253E3.0.CO;2-P

Ehrlich, D. E. and Schoppik, D. (2017). Control of movement initiation underlies the development of balance. *Curr. Biol.* **27**, 334-344. doi:10.1016/j.cub.2016.12.003

Erickson, R. G. and Barmack, N. H. (1980). A comparison of the horizontal and vertical optokinetic reflexes of the rabbit. *Exp. Brain Res.* **40**, 448-456. doi:10.1007/BF00236153

Farooq, S. J. (2004). Torsional optokinetic nystagmus: normal response characteristics. *Br. J. Ophthalmol.* **88**, 796-802. doi:10.1136/bjo.2003.028738

Festl, F., Recktenwald, F., Yuan, C. and Mallot, H. A. (2012). Detection of linear ego-acceleration from optic flow. *J. Vis.* **12**, 10. doi:10.1167/12.7.10

Gabriel, J. P., Trivedi, C. A., Maurer, C. M., Ryu, S. and Bollmann, J. H. (2012). Layer-specific targeting of direction-selective neurons in the zebrafish optic tectum. *Neuron* **76**, 1147-1160. doi:10.1016/j.neuron.2012.12.003

Garbutt, S., Han, Y., Kumar, A. N., Harwood, M., Harris, C. M. and Leigh, R. J. (2003). Vertical optokinetic nystagmus and saccades in normal human subjects. *Invest. Ophthalmol. Vis. Sci.* **44**, 3833-3841. doi:10.1167/iovs.03-0066

Ghasia, F. and Tychsen, L. (2014). Horizontal and vertical optokinetic eye movements in macaque monkeys with infantile strabismus: directional bias and crosstalk. *Invest. Ophthalmol. Vis. Sci.* **55**, 265-274. doi:10.1167/iovs.13-12330

Glasauer, S. and Straka, H. (2022). Low gain values of the vestibulo-ocular reflex can optimize retinal image slip. *Front. Neurol.* **13**, 897293. doi:10.3389/fneur.2022.897293

Graf, W. and Meyer, D. L. (1983). Central mechanisms counteract visually induced tonus asymmetries. *J. Comp. Physiol.* **150**, 473-481. doi:10.1007/BF00609573

Holm-Jensen, S. and Peitersen, E. (1979). The significance of the target frequency and the target speed in optokinetic nystagmus (Okn). *Acta Otolaryngol.* **88**, 110-116. doi:10.3109/00016487909137147

Huang, Y.-Y. and Neuhauss, S. C. F. (2008). The optokinetic response in zebrafish and its applications. *Front. Biosci. Landmark* **13**, 1899-1916. doi:10.2741/2810

Hunter, P. R., Lowe, A. S., Thompson, I. D. and Meyer, M. P. (2013). Emergent properties of the optic tectum revealed by population analysis of direction and orientation selectivity. *J. Neurosci.* **33**, 13940-13945. doi:10.1523/JNEUROSCI.1493-13.2013

Kasprick, D. S., Kish, P. E., Junttila, T. L., Ward, L. A., Bohnsack, B. L. and Kahana, A. (2011). Microanatomy of adult zebrafish extraocular muscles. *PLoS ONE* **6**, e27095. doi:10.1371/journal.pone.0027095

Kitama, T., Ishida, M., Luan, H., Kawasaki, T. and Sato, Y. (2001). Difference between horizontal and vertical optokinetic nystagmus in cats at upright position. *Jpn. J. Physiol.* **51**, 463-474. doi:10.2170/jjphysiol.51.463

Kubo, F., Hablitzel, B., Dal Maschio, M., Driever, W., Baier, H. and Arrenberg, A. B. (2014). Functional architecture of an optic flow-responsive area that drives horizontal eye movements in zebrafish. *Neuron* **81**, 1344-1359. doi:10.1016/j.neuron.2014.02.043

Lambert, F. M., Beck, J. C., Baker, R. and Straka, H. (2008). Semicircular canal size determines the developmental onset of angular vestibuloocular reflexes in larval *Xenopus*. *J. Neurosci.* **28**, 8086-8095. doi:10.1523/JNEUROSCI.1288-08.2008

Land, M. F. (2015). Eye movements of vertebrates and their relation to eye form and function. *J. Comp. Physiol. A* **201**, 195-214. doi:10.1007/s00359-014-0964-5

Leyden, C., Brysch, C. and Arrenberg, A. B. (2021). A distributed saccade-associated network encodes high velocity conjugate and monocular eye movements in the zebrafish hindbrain. *Sci. Rep.* **11**, 12644. doi:10.1038/s41598-021-90315-2

Lim, K. H., Kim, H. K., Park, S., Han, E., Song, I., Yoon, H. S., Kim, J., Lee, Y., Jang, Y. H., Rah, Y. C. et al. (2024). Measuring optokinetic reflex and vestibulo-ocular reflex in unilateral vestibular organ damage model of zebrafish. *J. Assoc. Res. Otolaryngol.* **25**, 167-177. doi:10.1007/s10162-024-00936-3

Lin, T.-F., Mohammadi, M., Fathalla, A. M., Pul, D., Lüthi, D., Romano, F., Straumann, D., Cullen, K. E., Chacron, M. J. and Huang, M. Y.-Y. (2019). Negative optokinetic afternystagmus in larval zebrafish demonstrates set-point adaptation. *Sci. Rep.* **9**, 19039. doi:10.1038/s41598-019-55457-4

Marsh, E. and Baker, R. (1997). Normal and adapted visuooculomotor reflexes in goldfish. *J. Neurophysiol.* **77**, 1099-1118. doi:10.1152/jn.1997.77.3.1099

Masseck, O. A. and Hoffmann, K.-P. (2009). Comparative neurobiology of the optokinetic reflex. *Ann. N. Y. Acad. Sci.* **1164**, 430-439. doi:10.1111/j.1749-6632.2009.03854.x

Matsuda, K. and Kubo, F. (2021). Circuit organization underlying optic flow processing in zebrafish. *Front. Neural Circuits* **15**, 709048. doi:10.3389/fncir.2021.709048

Mearns, D. S., Donovan, J. C., Fernandes, A. M., Semmelhack, J. L. and Baier, H. (2020). Deconstructing hunting behavior reveals a tightly coupled stimulus-response loop. *Curr. Biol.* **30**, 54-69.e9. doi:10.1016/j.cub.2019.11.022

Miki, S., Baker, R. and Hirata, Y. (2018). Cerebellar role in predictive control of eye velocity initiation and termination. *J. Neurosci.* **38**, 10371-10383. doi:10.1523/JNEUROSCI.1375-18.2018

Miri, A., Bhasin, B. J., Aksay, E. R. F., Tank, D. W. and Goldman, M. S. (2022). Oculomotor plant and neural dynamics suggest gaze control requires integration on distributed timescales. *J. Physiol.* **600**, 3837-3863. doi:10.1113/JP282496

Najafian, M., Alerasool, N. and Moshtaghian, J. (2014). The effect of motion aftereffect on optomotor response in larva and adult zebrafish. *Neurosci. Lett.* **559**, 179-183. doi:10.1016/j.neulet.2013.05.072

Orger, M. B. (2016). The cellular organization of zebrafish visuomotor circuits. *Curr. Biol.* **26**, R377-R385. doi:10.1016/j.cub.2016.03.054

Pérez-Schuster, V., Kulkarni, A., Nouvian, M., Romano, S. A., Lygdas, K., Jouary, A., Dipoppa, M., Pietri, T., Haudrechy, M., Candat, V. et al. (2016). Sustained rhythmic brain activity underlies visual motion perception in zebrafish. *Cell Rep.* **17**, 1098-1112. doi:10.1016/j.celrep.2016.09.065

Rinner, O., Rick, J. M. and Neuhauss, S. C. F. (2005). Contrast sensitivity, spatial and temporal tuning of the larval zebrafish optokinetic response. *Invest. Ophthalmol. Vis. Sci.* **46**, 137-142. doi:10.1167/iovs.04-0682

Robinson, D. A. (1981). The use of control systems analysis in the neurophysiology of eye movements. *Annu. Rev. Neurosci.* **4**, 463-503. doi:10.1146/annurev.ne.04.030181.002335

Schindelin, J., Arganda-Carreras, I., Frise, E., Kaynig, V., Longair, M., Pietzsch, T., Preibisch, S., Rueden, C., Saalfeld, S., Schmid, B. et al. (2012). Fiji: an open-source platform for biological-image analysis. *Nat. Methods* **9**, 676-682. doi:10.1038/nmeth.2019

Seidman, S. H., Telford, L. and Paige, G. D. (1995). Vertical, horizontal, and torsional eye movement responses to head roll in the squirrel monkey. *Exp. Brain Res.* **104**, 218-226. doi:10.1007/BF00242008

Sugioka, T., Tanimoto, M. and Higashijima, S. (2023). Biomechanics and neural circuits for vestibular-induced fine postural control in larval zebrafish. *Nat. Commun.* **14**, 1217. doi:10.1038/s41467-023-36682-y

Sun, P., Zhang, Y., Zhao, F., Wu, J.-P., Pun, S. H., Peng, C., Du, M., Vai, M. I., Liu, D. and Chen, F. (2018). An assay for systematically quantifying the vestibulo-ocular reflex to assess vestibular function in zebrafish larvae. *Front. Cell. Neurosci.* **12**, 257. doi:10.3389/fncel.2018.00257

Tadokoro, S., Miki, S., Yamanaka, T. and Hirata, Y. (2025). Horizontal, vertical, and torsional optokinetic responses and their adaptations in fish. *J. Neurophysiol.* **133**, 965-986. doi:10.1152/jn.00565.2024

Thiel, A., Greschner, M., Eurich, C. W., Ammermüller, J. and Kretzberg, J. (2007). Contribution of individual retinal ganglion cell responses to velocity and acceleration encoding. *J. Neurophysiol.* **98**, 2285-2296. doi:10.1152/jn.01342.2006

van den Berg, A. V. and Collewijn, H. (1988). Directional asymmetries of human optokinetic nystagmus. *Exp. Brain Res.* **70**, 597-604. doi:10.1007/BF00247608

Van der Steen, J. and Collewijn, H. (1984). Ocular stability in the horizontal, frontal and sagittal planes in the rabbit. *Exp. Brain Res.* **56**, 263-274. doi:10.1007/BF00236282

Wang, K., Hinz, J., Haikala, V., Reiff, D. F. and Arrenberg, A. B. (2019). Selective processing of all rotational and translational optic flow directions in the zebrafish pretectum and tectum. *BMC Biol.* **17**, 29. doi:10.1186/s12915-019-0648-2

Wang, K., Hinz, J., Zhang, Y., Thiele, T. R. and Arrenberg, A. B. (2020). Parallel channels for motion feature extraction in the pretectum and tectum of larval zebrafish. *Cell Rep.* **30**, 442-453.e6. doi:10.1016/j.celrep.2019.12.031

Warren, W. H. and Hannon, D. J. (1988). Direction of self-motion is perceived from optical flow. *Nature* **336**, 162-163. doi:10.1038/336162a0

Watamaniuk, S. N. J. and Heinen, S. J. (2007). Storage of an oculomotor motion aftereffect. *Vision Res.* **47**, 466-473. doi:10.1016/j.visres.2006.09.030

Wu, Y., dal Maschio, M., Kubo, F. and Baier, H. (2020). An optical illusion pinpoints an essential circuit node for global motion processing. *Neuron* **108**, 722-734.e5. doi:10.1016/j.neuron.2020.08.027

Zhang, Y., Huang, R., Nörenberg, W. and Arrenberg, A. B. (2022). A robust receptive field code for optic flow detection and decomposition during self-motion. *Curr. Biol.* **32**, 2505-2516.e8. doi:10.1016/j.cub.2022.04.048